Universidade Federal de Juiz de Fora
Programa de Pós-Graduação em Engenharia Eletrica
Doutorado em Engenharia Elétrica

Mateus de Lima Filomeno

Advances in hybrid power line/wireless systems

Juiz de Fora
2022

Ficha catalográfica elaborada através do Modelo Latex do CDC da UFJF com os dados fornecidos pelo(a) autor(a)

Filomeno, M. de L..
Advances in hybrid power line/wireless systems / Mateus de Lima Filomeno. – 2022.
134 f. : il.

Orientador: Prof. Dr. Moisés Vidal Ribeiro
Coorientador: Prof. Dr. Marcello Luiz Rodrigues de Campos
Tese de Doutorado – Universidade Federal de Juiz de Fora, Doutorado em Engenharia Elétrica. Programa de Pós-Graduação em Engenharia Eletrica, 2022.

1. Hybrid communication systems. 2. Power allocation. 3. Orthogonal chirp-division multiplexing. 4. Orthogonal frequency-division multiplexing. 5. Subcarrier permutation. I. Ribeiro, M. V., orient. II. Campos, M. L. R. de, coorient. III. Título.

Mateus de Lima Filomeno

Advances in hybrid power line/wireless systems

Tese de doutorado apresentada ao Programa de Pós-Graduação em Engenharia Eletrica da Universidade Federal de Juiz de Fora, na área de concentração em sistemas eletrônicos, como requisito parcial à obtenção do título de Doutor em Engenharia Elétrica.

Orientador: Prof. Dr. Moisés Vidal Ribeiro
Coorientador: Prof. Dr. Marcello Luiz Rodrigues de Campos

Juiz de Fora
2022

Mateus de Lima Filomeno

Advances in hybrid power line/wireless systems

Thesis submitted to the Graduated Program
in Electrical Engineering of the Federal University
of Juiz de Fora as a partial requirement for obtaining
a Doctors's degree in Electrical Engineering.
Concentration area: Electronic Systems

Approved on 23 of March of 2022.

EXAMINING BOARD

Prof. Dr. Moisés Vidal Ribeiro –Academic Advisor
Federal University of Juiz de Fora

Prof. Dr. Marcello Luiz Rodrigues de Campos
Federal University of Rio de Janeiro

Prof. Dr. Leonardo de Mello Honório
Federal University of Juiz de Fora

Prof. Dr. Ulysses Roberto Chaves Vitor
Federal University of Juiz de Fora

Prof. Dr. Richard Demo Souza
Federal University of Santa Catarina

Prof. Dr. Cristiano Magalhães Panazio
University of São Paulo

Juiz de Fora, 03/23/2022.

Documento assinado eletronicamente por **Marcello Luiz Rodrigues de Campos Usuário Externo**, em 23/03/2022, às 17:23, conforme horário oficial de Brasília, com fundamento no § 3º do art. 4º do Decreto nº 10.543, de 13 de novembro de 2020

Documento assinado eletronicamente por **Cristiano Magalhães Panazio**, **Usuário Externo**, em 23/03/2022, às 17:24, conforme horário oficial de Brasília, com fundamento no § 3º do art. 4º do Decreto nº 10.543, de 13 de novembro de 2020

Documento assinado eletronicamente por **Leonardo de Mello Honorio**, **Professor(a)**, em 23/03/2022, às 17:24, conforme horário oficial de Brasília, com fundamento no § 3º do art. 4º do Decreto nº 10.543, de 13 de novembro de 2020

Documento assinado eletronicamente por **Richard Demo Souza**, **Usuário Externo**, em 23/03/2022, às 17:24, conforme horário oficial de Brasília, com fundamento no § 3º do art. 4º do Decreto nº 10.543, de 13 de novembro de 2020

Documento assinado eletronicamente por **Moises Vidal Ribeiro**, **Professor(a)**, em 23/03/2022, às 17:24, conforme horário oficial de Brasília, com fundamento no § 3º do art. 4º do Decreto nº 10.543, de 13 de novembro de 2020

Documento assinado eletronicamente por **Ulysses Roberto Chaves Vitor**, **Professor(a)**, em 23/03/2022, às 17:24, conforme horário oficial de Brasília, com fundamento no § 3º do art. 4º do Decreto nº 10.543, de 13 de novembro de 2020

A autenticidade deste documento pode ser conferida no Portal do SEI-Ufjf

To my mother Roseny

To my brother Lucas

To my grandmother Neide

AGRADECIMENTOS

Em primeiro lugar, eu agradeço a Deus por me guiar durante toda a minha vida e, principalmente, por ser meu maior refúgio nos momentos mais difíceis. Como uma das minhas canções favoritas diz: “Eu te agradeço, Senhor. Pelo carinho, pelo amor, pelo cuidado que tens por mim... Cristo te amo. Tu és minha luz. Eu te agradeço, querido Jesus”.

Agradeço a minha mãe, Roseny de Lima Silva, pelo amor e por todo apoio durante toda a minha vida. Sem ela eu certamente não teria concluído esta etapa. Agradeço ao meu irmão, Lucas de Lima Filomeno, e a minha avó, Neide de Araújo Lima, por estarem ao meu lado sempre. Agradeço ao meu pai, Moisés Filomeno, pelo carinho e também pelo sustento. Agradeço ainda a cada um dos meus familiares por me apoiarem sempre que necessário.

Expresso também minha gratidão aos meus irmãos da Igreja Cristã Maranata do Bairro Vale dos Bandeirantes, por todas as orações e por todo carinho ao longo de toda a minha vida.

Agradeço a todos os meus amigos que me acompanharam na jornada do doutorado. Ao meu amigo, Lucas Giroto de Oliveira, eu agradeço pela amizade de longos anos e pela constante parceria no doutorado. De forma especial, agradeço ao amigo Ândrei Camponogara pela troca de experiências e por compartilhar os momentos tristes e alegres, sempre impulsionando o nosso crescimento pessoal. Ao amigo Túlio Fernandes Moreira, eu agradeço pela amizade e momentos de descontração. Agradeço também aos amigos Roberto Massi de Oliveira e Victor Fernandes pela amizade e momentos de aprendizado compartilhados no Laboratório de Comunicações (LCom). Por último, agradeço a todos os colegas de LCom, alunos de iniciação científica, mestrandos, doutorandos e pós-doutorandos, que estiverem comigo ao longo dos últimos anos.

Os meus agradecimentos se estendem ainda a todos os profissionais que direta ou indiretamente contribuíram para a minha formação profissional. Relembro aqui dos Professores Silva (matemática) e Célia (português) que foram fundamentais ainda no ensino fundamental. Eu também sou grato ao Professor H. Vincent Poor por aceitar contribuir com o meu trabalho e fazer parte da minha formação. Estendo também os meus agradecimentos ao Professor Marcello Luiz Rodrigues de Campos, meu coorientador, não apenas por contribuir de forma significativa com meu trabalho, mas também por ser um exemplo de profissional e pessoa para mim. Ao Professor Moisés Vidal Ribeiro, meu orientador, eu agradeço por me acolher no grupo de pesquisa ainda como aluno de iniciação científica, por me levantar nos momentos de desânimo, por enfrentar todos os desafios do doutorado ao meu lado e por mais tantas outras coisas. Muito obrigado por tudo, Professor Moisés.

De forma sincera, agradeço ainda a cada um dos professores que compuseram a banca de avaliação deste trabalho, tanto pela leitura e análise cuidadosa do meu trabalho como pelas valiosas contribuições.

Por fim, mas não menos importante, expresso minha gratidão ao povo brasileiro e mineiro que, direta ou indiretamente, apoiou financeiramente este trabalho por meio da Fapemig, Capes, CNPq e Inerge.

“Commit your way to the Lord; trust in him, and he will act.”
Psalm 37:5.

RESUMO

Nesta tese de doutorado, explora-se o sistema híbrido rede elétrica/ar (do inglês, *hybrid power line/wireless system* - HPWS), que consiste no uso da rede elétrica e do meio de comunicação sem fio em paralelo, para melhorar o desempenho da comunicação de dados ponto-a-ponto. Neste contexto, os tópicos estudados são: alocação de potência e permutação de subportadoras em esquemas de multiplexação ortogonal por divisão em frequência, bem como a aplicação de esquemas de multiplexação ortogonal por divisão em chirp (do inglês, *orthogonal chirp-division multiplexing* - OCDM) ao HPWS. Ao longo do trabalho, considera-se a transmissão simultânea, através da rede elétrica e do ar, de símbolos iguais de forma que a combinação ótima possa ser empregada no receptor. Com relação à alocação de potência, a taxa de dados alcançável e a probabilidade de erro de bit média são otimizadas separadamente sob duas e distintas restrições de potência de transmissão. Independente da restrição de potência, é demonstrado que apenas um meio de comunicação deve ser usado no mesmo índice de subcanal quando objetiva-se maximizar a taxa de dados alcançável ou minimizar a probabilidade de erro de bit média. Consequentemente, soluções conhecidas são adaptadas a algoritmos de alocação de potência que demandam baixo custo computacional. Análises numéricas validam os algoritmos propostos, comprovando sua otimalidade e superioridade em relação a outros algoritmos da literatura. No que diz respeito à permutação de subportadoras, sua otimalidade é analisada tanto para maximizar a taxa de dados alcançável como para minimizar a probabilidade de erro de bit média, levando-se em consideração as alocações de potência uniforme e ótima. Para todos os casos, é demonstrado que as subportadoras utilizadas em um meio devem ser ordenadas de forma crescente com relação às relações sinal-ruído normalizadas e então combinadas com as subportadoras utilizadas no outro meio ordenadas, por sua vez, de forma decrescente com relação às relações sinal-ruído normalizadas. Resultados numéricos mostram que ganhos mais elevados desta permutação de subportadoras são obtidos à medida que a seletividade em frequência aumenta e que a permutação de subportadoras pode ser extremamente útil para aumentar a taxa de dados alcançável ou diminuir a probabilidade de erro de bit média. Acerca da aplicação de esquemas OCDM ao HPWS, processos aleatórios estacionários de sentido amplo são estudados de forma que a técnica de combinação de máxima relação sinal-ruído possa ser derivada no domínio discreto de Fresnel. Além disso, a alocação ótima de potência é analisada. Em seguida, análises numéricas mostram que o HPWS baseado em OCDM pode ser a escolha mais adequada para minimizar a probabilidade de erro de bit quando o transmissor tem pouco conhecimento (um bit de informação) ou nenhum do estado do canal. Por fim, um símbolo piloto que habilita tanto a estimação do canal como a sincronização é derivado para esquemas OCDM operando na rede elétrica e no ar. Resultados numéricos baseados em medições validam o símbolo proposto.

Palavras-chave: Alocação de potência. Sistemas de comunicação híbridos. Multiplexação ortogonal por divisão em chirp. Multiplexação ortogonal por divisão em frequência. Permutação de subportadoras.

ABSTRACT

This dissertation investigates the hybrid power line/wireless system (HPWS), which consist of using power line and wireless media in parallel, to improve point-to-point data communication performance. In this context, the studied topics are: power allocation and subcarrier permutation in orthogonal frequency-division multiplexing schemes, as well as the application of orthogonal chirp-division multiplexing (OCDM) schemes into the HPWS. Throughout the dissertation, the simultaneous transmission of the same symbols through power line and wireless channels is considered so that maximal-ratio combining can be employed at the receiver. Regarding power allocation, the achievable data rate and average bit error probability are individually optimized under two and distinct transmission power constraints. Regardless of the power constraint, it is demonstrated that at most one medium must be used in the same subchannel index when the objective is to maximize the achievable data rate or to minimize the average bit error probability. Consequently, well-known solutions are adapted to provide power allocation algorithms that demand low computational costs. Numerical analyses validate the proposed algorithms, proving their optimality and superiority in relation to other algorithms of the literature. With respect to subcarrier permutation, its optimality is analyzed to either maximize the achievable data rate or minimize the average bit error probability, assuming the optimal or uniform power allocations. For all cases, it is shown that the subcarriers used in one medium must be sorted in ascending order of normalized signal-to-noise ratios (nSNRs) and then combined with the subcarriers used in the other medium sorted, in its turn, in descending order of nSNRs. Numerical results show that higher gains of this subcarrier permutation are obtained as frequency selectivity increases and that subcarrier permutation can be extremely useful for increasing the achievable data rate or decreasing the average bit error probability. Regarding the application of OCDM schemes into the HPWS, wide-sense stationary random processes in the discrete-Fresnel domain are studied so that the maximal-ratio combining technique can be derived. In addition, the optimal power allocation is analyzed. Numerical analyses then show that the OCDM-based HPWS may be a suitable choice if the aim is to minimize the bit error probability and the transmitter has partial (one bit of information) or no knowledge of the channel state. Finally, a pilot symbol that enables joint channel estimation and synchronization is derived for power line and wireless OCDM schemes. Numerical results based on measurements validate the proposed symbol

Key-words: Hybrid communication systems. Power allocation. Orthogonal chirp-division multiplexing. Orthogonal frequency-division multiplexing. Subcarrier permutation.

LIST OF FIGURES

LIST OF TABLES

LIST OF ABBREVIATIONS AND ACRONYMS

ACGN	additive colored Gaussian noise
AMI	advanced metering infrastructure
AWGN	additive white Gaussian noise
BEP	bit error probability
CDF	cumulative distribution function
CFO	carrier frequency offset
CFR	channel frequency response
CIR	channel impulse response
CLT	central limit theorem
CP	cyclic prefix
CSI	channel state information
DFT	discrete Fourier transform
DFnT	discrete Fresnel transform
EGC	equal gain combining
FFT	fast Fourier transform
HIS	hybrid independent system
HPWS	hybrid power line/wireless system
IoT	Internet of Things
IP	interior point
ISI	intersymbol interference
ISM	industrial, scientific and medical
KKT	Karush-Kuhn-Tucker
LOS	line-of-sight
LPTV	linear periodically time-variant
LTI	linear time-invariant
MRC	maximal-ratio combining
MIMO	multiple-input multiple-output
MSE	mean squared error
NLOS	non-line-of-sight
NOMA	non-orthogonal multiple access

NP	nondeterministic polynomial-time
nSNR	normalized signal-to-noise ratio
OC	optimum combining
OCDM	orthogonal chirp-division multiplexing
OFDM	orthogonal frequency-division multiplexing
OTFDM	orthogonal time-frequency division multiplexing
PAM	pulse amplitude modulation
PLC	power line communication
PSD	power spectral density
PSK	phase-shift keying
QAM	quadrature amplitude modulation
QoE	quality of experience
QoS	quality of service
QPSK	quadrature phase-shift keying
RF	radio frequency
SC	selection combining
SC-CP	single carrier with cyclic prefix
SG	Smart Grid
SMC	saturated metric combining
SIMO	single-input multiple-output
SNR	signal-to-noise ratio
SPC	sum power constraints
SPCC	sum power-channel constraints
UA	uniform allocation
VLC	visible light communication
WSS	wide-sense stationary

CONTENTS

1 INTRODUCTION

Telecommunication systems play a pivotal role in modern society, impacting the social, cultural, and economic life of people. Hence, astonishing and increasing demands for connectivity among people and things have prompted research efforts toward the development of effective data communication technologies that meet the requirements of emerging applications, such as those of Smart Homes, Smart Cities, Smart Grid (SG), Internet of Things (IoT), and Industry 4.0 [1–6]. Those applications are expected to require massive telecommunication infrastructures to support the connectivity among a large number of users and machines demanding distinct quality of service (QoS) or quality of experience (QoE). Indeed, a recent global forecast predicts over 5.3 billion total Internet users by 2023, compared to approximately 3.9 billion in 2018 [7]. Moreover, there is an expectation of 29.3 billion networked devices by 2023, which significantly contrasts with the 18.4 billion in 2018.

Motivated by those explosive demands for connectivity, the telecommunications industry and R&D institutions have been examining different media and frequency bandwidths to introduce new generations of efficient and effective data communication technologies, which can include wireless communication, power line communication (PLC), visible light communication (VLC), as well as their combination [8–13]. In this context, wireless media and electric power grids have been recognized as two among the most important media, due to their ubiquity, implementation feasibility, and low cost. These media, however, present unique characteristics related to signal propagation and, as a consequence, inherent distinct challenges to be overcome.

Regarding electric power grids, the main challenges are the impedance mismatching and time-varying behavior of loads that result in time-varying frequency selectivity; the increasing signal attenuation along with frequency and distance; high-power impulsive noise presence due to load dynamics; the use of unshielded power cables; the power cable degradation due to aging effects; and the restrictive regulatory constraints, see [1, 11] and references therein. On the other hand, wireless communication has to deal with the lack of line-of-sight (LOS); the increasing signal attenuation along with distance and frequency; the susceptibility to co-channel interference; the stochastic time-varying behavior of channel conditions; the adoption of restrictive constraint on the total transmission power; and scarcity of spectrum, see [8–10] and references therein.

In the literature, there are several attempts to mitigate the negative impacts of the aforementioned drawbacks and, at the same time, to maximize the channel resource usage. Among them, cooperative communication was introduced to increase the transmit diversity not only in wireless communication systems [10], but also in other scenarios, such as the PLC ones [14–16]. The idea behind this strategy is the use of intermediate nodes (called relays) between transmitter and receiver nodes to emulate a multiple-input multiple-output (MIMO) communication system. Nonetheless, a relay node is not always available and therefore new strategies have to be pursued. In this regard, advanced digital signal processing techniques have been continuously exploited to improve data communication, for instance, by mitigating impulsive noise effects [17, 18] or in-

troducing advanced data transmission schemes, such as the orthogonal time-frequency division multiplexing (OTFDM) [19], the orthogonal chirp-division multiplexing (OCDM) [20–22], and the classic orthogonal frequency-division multiplexing (OFDM) [23, 24]. Another often-used strategy refers to the use of frequency-domain power allocation techniques, which consists of optimally distributing the available total transmission power along with the frequency [24–26]. In the case of the OFDM scheme, for instance, the waterfilling-based algorithm is well-known as the optimal power allocation solution for maximizing the achievable data rate [24, 27].

The aforementioned discussion shows that exists several research directions to advance digital communication systems for either PLC or wireless communication technologies. However, the limitations associated with power line and wireless media have driven research efforts not only into their individual improvements but also into the design of new technologies and standards that use both media jointly [28–44]. In this context, power line and wireless communication interfaces can be used individually or simultaneously, just as illustrated in Figures 1 and 2. Figure 1(a) shows the power line and wireless communication interfaces being used individually and operating within different frequency bands. In this type of hybrid communication system, an intermediate node must have an up-converter to retransmit through the wireless channel the signal that was received from the power line channel, and a down-converter to retransmit through the power line channel the signal that was received from the wireless channel [28–30]. Figure 1(b) depicts the use of power line and wireless communication interfaces individually that does not require intermediate nodes due to the use of the same frequency band for PLC and wireless communication [31–34]. In this system, the transceivers are connected to either power line or wireless media and can communicate with each other because electric power grids are composed of unshielded power cables. On the other hand, Figure 2(a) shows the use of power line and wireless communication interfaces simultaneously and within different frequency bands [35–38], whereas Figure 2(b) illustrates power line and wireless communication interfaces simultaneously and within the same frequency band [41–44]. Note that a cross-talk between both channels appears in the last as the same frequency band is used for both data communication interfaces.

Figure 1 – Hybrid communications systems in which power line and wireless communication interfaces are used individually

(a) Different frequency band (b) Same frequency band

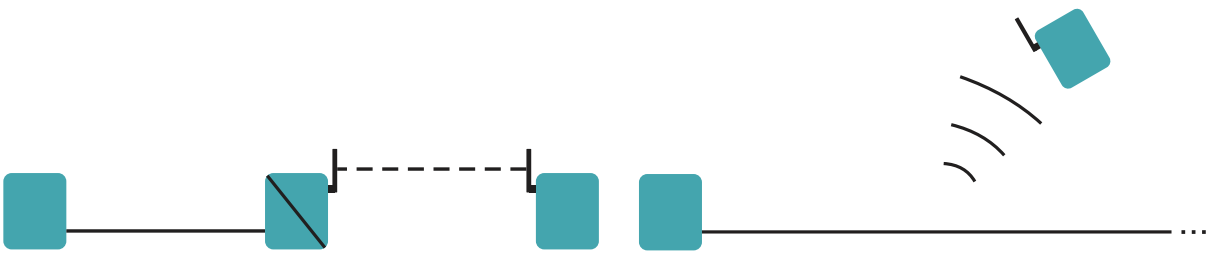

Source: Personal collection.

Figure 2 – Hybrid communication systems in which power line and wireless communication interfaces are used simultaneously

Source: Personal collection.

Of the four types aforementioned, the hybrid communication system in which power line and wireless communication interfaces are used simultaneously and within different frequency bands - named as hybrid power line/wireless system (HPWS) or hybrid PLC/radio frequency (RF) system - has been more studied since the complementary characteristics/diversity of power line and wireless media can be better exploited to minimize existing impairments that degrade the QoS between two nodes. Furthermore, an HPWS has a large number of applications as it does not rely on efficient antennas within the frequency band regulated for PLC systems, i.e., below 86 MHz. For example, in the context of Smart Homes, many devices are connected to the electric power grids and, with the advancement of technologies focused on the IoT [45], more and more devices are manufactured with wireless communication technologies. Therefore, if new generations of smart home devices will be connected to both wireless media and electric power grids, why not jointly exploit both channel resources to make more efficient and effective data communication systems? Turning to the context of SGs and/or Smart Cities, such kind of hybrid communication system could also be used for assisting advanced metering infrastructure (AMI) to implement smart metering technologies, as pointed out in [4]. Wherever two wireless communication devices are powered by the same electric power circuit, the HPWS can be employed. There are hence numerous applications in which the HPWS can be useful to improve the QoS of a data communication system. For this reason, the HPWS - the hybrid communication system displayed in Figure 2(a) - will be the focus of this dissertation henceforth.

In the context of HPWSs, there is a number of important aspects that can provide further improvements to the data communication performance and that are still unexplored in the literature. For instance, power allocation techniques have not been studied to improve the HPWS performance in terms of either achievable data rate or average bit error probability (BEP). Regarding HPWSs, the literature has already studied the simultaneous transmission of equal symbols that are later combined using maximal-ratio combining (MRC) at the receiver. Still, the power allocation of this hybrid system has not been addressed yet. Power allocation in HPWSs is quite different from that of PLC and wireless communication due to the characteristics of each media and the application of combining techniques to the received symbols. From a practical perspective, power allocation is essential to show how to optimally design HPWSs transceivers. However, it is also extremely important from a theoretical perspective to quantify the optimal

performance of the hybrid system. Therefore, power allocation must be precisely formulated and examined for HPWSs, despite being well established for non-hybrid communication systems.

Furthermore, subcarrier permutation has been studied only to maximize the achievable data rate under uniform power allocation [46]. This technique considers an OFDM scheme in which the information transmitted through a specific subcarrier of the power line medium is transmitted through a different subcarrier of the wireless medium. This permutation is undone at the receiver and then the power line and wireless received symbols are combined. This technique allows a better use of the diversity between two media and therefore it needs to be investigate not only to maximize the achievable data rate but also to minimize the average BEP. Also, subcarrier permutation and power allocation have to be jointly analyzed.

Finally, the investigation of the OCDM scheme in HPWSs has not been addressed in the literature yet. Recently, the OCDM scheme has attracted interest from researchers as a promising alternative to the well-known OFDM scheme. In non-hybrid contexts, OCDM-based systems have presented higher robustness against multipath propagation, intersymbol interference (ISI), and impulsive noise. Hence, the combination of HPWS and OCDM must be discussed as well. Moreover, timing and frequency synchronization for OCDM-based systems have not been investigated and therefore these subjects need to be addressed so that the OCDM scheme can be used in HPWSs.

1.1 OBJECTIVES

Given the aforementioned discussion, the current dissertation has its main objectives described as follows:

- To investigate the optimal power allocation for maximizing the achievable data rate in hybrid power line/wireless systems under two different approaches for limiting the transmission power, which are based on the sum power constraints (SPC) and the sum power-channel constraints (SPCC). To do so, the same symbols are simultaneously transmitted through parallel media to be later combined using MRC technique and frequency-selective channels are taken into account.

- To provide a complete discussion on power allocation in hybrid power line/wireless system by also studying it with the aim of minimizing the average BEP. To this end, the investigation also encompasses the two approaches for bounding the transmission power and considers the simultaneous transmission of equal symbols through parallel and frequency-selective channels. Also, OFDM scheme and MRC technique are employed and the same modulation is considered in all subcarriers.

- To study the optimal subcarrier permutation in hybrid power line/wireless system to better exploit the frequency selectivity of power line and wireless media. In particular, the subcarrier permutation is optimized to improve the data communication performance in

terms of both achievable data rate and average BEP. Also, the subcarrier permutation is analyzed for uniform power allocation and optimal power allocation under the two approaches for bounding the transmission power.

- To propose an OCDM-based HPWS, i.e., an HPWS in which power line and wireless transmitted data are equal and modulated onto orthogonal subchirps based on the discrete Fresnel transform (DFnT). In this regard, the combining weights to perform the MRC technique are derived based on the assumption of wide-sense stationary (WSS) random processes in the discrete-Fresnel domain. Also, the investigation of the optimal power allocation in OCDM-based HPWSs is aimed.

- To solve synchronization issues in the OCDM scheme with Schmidl & Cox synchronization technique [47]. The Schmidl & Cox technique, widely used in OFDM schemes, relies on a pilot symbol with two equal halves in the time domain. Therefore, the aim is to provide an OCDM pilot symbol in the discrete-Fresnel domain (considered in OCDM schemes) that has two equal halves in the time domain, enabling the application of the Schmidl & Cox technique into OCDM schemes.

1.2 DISSERTATION OUTLINE

The remainder of this document is organized as follows:

- Chapter 2 presents the hybrid power line/wireless system considered throughout this document. In this regard, this chapter presents the state-of-the-art research on the HPWS as well as its major fundamentals and associated definitions. Also, a general model that covers the hybrid communication systems used in subsequent chapters is mathematically described and the major assumptions are clearly stated.

- Chapter 3 formulates the optimization problems associated with the optimal power allocation in hybrid power line/wireless system for maximizing the achievable data rate under SPC and SPCC. Then it shows analytical solutions to each of them and proposes power allocation algorithms to obtain such solutions. Based on numerical results, this chapter also compares the proposed solutions with alternative ones from the literature.

- Chapter 4 describes the problem formulation of the power allocation for minimizing the average BEP in hybrid power line/wireless systems. In sequel, it proposes power allocation algorithms to this problem, considering both SPC and SPCC. Again, a comparative analysis between the proposed and previous solutions is discussed based on numerical results.

- Chapter 5 discuss the subcarrier permutation in hybrid power line/wireless systems. In this sense, this chapter formulates optimization problems related to the maximization of the achievable data rate and minimization of the average BEP. Solutions are then presented

when uniform and optimal power allocation (under SPC and SPCC) are taken into account. Finally, numerical analyses validate the presented solutions.

- Chapter 6 introduces the OCDM-based HPWS. In this context, the behavior of wide-sense stationary random processes are investigated in the discrete-Fresnel domain and the power allocation of the previous chapters is extended to the OCDM-based HPWS. The OCDM-based HPWS is then numerically compared to the OFDM-based HPWS in terms of achievable data rate and average BEP.

- Chapter 7 models the effect of non-perfect synchronization in OCDM schemes and then provide a discrete-Fresnel domain pilot symbol that can be used for enabling Schmidl & Cox synchronization in OCDM-based systems. Then a comb OCDM symbol structure that can be adopted for joint channel estimation and Schmidl & Cox synchronization is presented. Numerical analyses based on effective measurements validate the obtained findings.

- Chapter 8 ends this Doctoral dissertation by stating its concluding remarks.

2 HYBRID POWER LINE/WIRELESS SYSTEM

In the early 2000s, a data concentrator equipped with both PLC and wireless communication interfaces was presented as a solution to provide a reliable and wide-range data communication infrastructure [48, 49]. At that time, a simple measure of the channel quality was carried out to decide which interface to use and, although both channels were not used simultaneously, the parallel implementation of the two technologies already characterized the so-called HPWS. In fact, any parallel (and usually simultaneous) use of power line and wireless channels defines the HPWS.

Currently, the HPWS is undoubtedly the most investigated hybrid system based on PLC and wireless communication technologies since there are several applications for its usage (e.g., smart metering and smart home applications). The use of different frequency bands in power line and wireless transmissions make it possible to adapt the existing technologies for these media, enabling a faster implementation of the HPWS. Furthermore, due to the intrinsic physical differences, power line and wireless media have distinct characteristics that complement each other when both are used in parallel.

In order to maximize the resources available in an HPWS, however, it is necessary to understand its behavior, which means e.g. knowledge of the state-of-the-art research as well as channel and noise characteristics. In addition, a suitable modeling of the HPWS has to be adopted for achieving realistic findings and conclusions. In this context, the main contributions of this chapter are stated as follows:

- The detailed description of hybrid systems in which power line and wireless media are connected in parallel, i.e., the HPWS. In this sense, the major fundamentals, definitions, and the state-of-the-art research of the HPWS are discussed. Also, the main effects that influence channel and noise characteristics in power line and wireless are presented.
- The introduction of the HPWS model that is considered in the next chapters. In this sense, a hybrid communication system with a general number of parallel channels is described in order to be able to draw more general conclusions. In other words, the number of considered media is not always assigned as two (i.e., power line and wireless media). Also, the considered assumptions are clearly stated.

The remainder of this chapter is presented as follows: Section 2.1 provides an historical evolution of the HPWS; Section 2.2 discusses channel and noise characteristics in HPWSs; Section 2.3 describes a general hybrid communication systems model that encompasses the HPWS.

2.1 FUNDAMENTALS, DEFINITIONS, AND STATE-OF-THE-ART RESEARCH

HPWSs were firstly proposed with the aim of increasing the data communication reliability. According to [4, 50], PLC and wireless communication are subjected to distinct

environmental influences and effects of signal propagation; hence, both channels must be simultaneously harmed for data communication to be interrupted, which considerably increases the robustness of the data communication system. In particular, [4] interestingly pointed out how PLC and wireless communication characteristics complement each other in the context of IoT and SG, presenting numerically a continuous achievable data rate, even when the uptime of one channel is not constant.

In order to benefit from the HPWS, however, it is required that the SNRs of the two media fall within similar ranges. Otherwise, the two media cannot support the same application requirements. In this regard, prior investigation is needed to assess whether the use of the HPWS is advantageous or not. To illustrate it, [36, 51] carried out SNR indoor and broadband measurements for house and office environments, concluding that the average SNRs of power line and wireless channels are within similar and wide ranges. Based on this result, the authors stated the existing diversity between power line and wireless channels could be exploited in benefit of indoor data communication as the SNR of either power line or wireless channels is not dominant over the other.

Once power line and wireless channels are available and their SNRs fall within similar ranges, the major constraint that remains is related to the hardware resources. In this regard, focusing on narrowband applications, [52–54] implemented and discussed relevant issues on HPWS transceivers design. For instance, [53] highlighted the difficulties in either creating a hybrid standard or using two different standards (one per interface) and then concluded that using a PLC standard can be an adequate choice since a wireless one would not be able to deal with the hardness of the power line medium. In addition, [53] showed that HPWS transceivers may consume only 12% more energy and require 50% more hardware resources than a conventional PLC transceiver, which is quite low compared to the reliability benefits that they can provided. On the other hand, [52] revealed a high power consumption if separated hardware and standards are assumed for PLC and wireless communications. Yet, it presented a robust HPWS transceiver capable of meeting the demands of SG communications.

Over the years, besides justifying and motivating the use of HPWSs, several studies aimed to efficiently explore the existing diversity between power line and wireless channels. In the vast majority of such studies, OFDM scheme was applied over power line and wireless channels regardless of considering broadband or narrowband transmissions. Since power line channels are mostly frequency selective, this seams to be the most suitable choice. In addition, the contributions often considered the unlicensed industrial, scientific and medical (ISM) band (900 MHz, 2.4 GHz, or 5.8 GHz) for wireless transmission, whereas narrowband ($3 - 500$ kHz) or broadband transmissions ($1.7 - 86$ MHz) were taken into account for the power line operation. Due to the existence of more mature technologies, these frequency bands have been preferred in the study of HPWSs. Moreover, the HPWS has already been investigated in outdoor and indoor scenarios. Figure 3(a) shows the use of HPWS in an outdoor scenario, whereas Figure 3(b) illustrates a typical application of HPWS in an indoor scenario.

Based on the given frameworks, there are a number of diversity strategies to explore the availability of power line and wireless channels. In the literature, the most prominent are:

- Source diversity: this strategy assumes the transmission of different information through power line and wireless channels [51]. The two branches defined by power line and wireless media work as independent systems, with the major objective being to increase the data rate.
- Transmit diversity: this strategy also assumes the transmission of different information through power line and wireless channels, but the received symbols are combined at the receiver side (see [55] for further details). To correctly decode the information, two

Figure 3 – Typical scenarios for the use of the hybrid power line/wireless system

(a) outdoor scenario

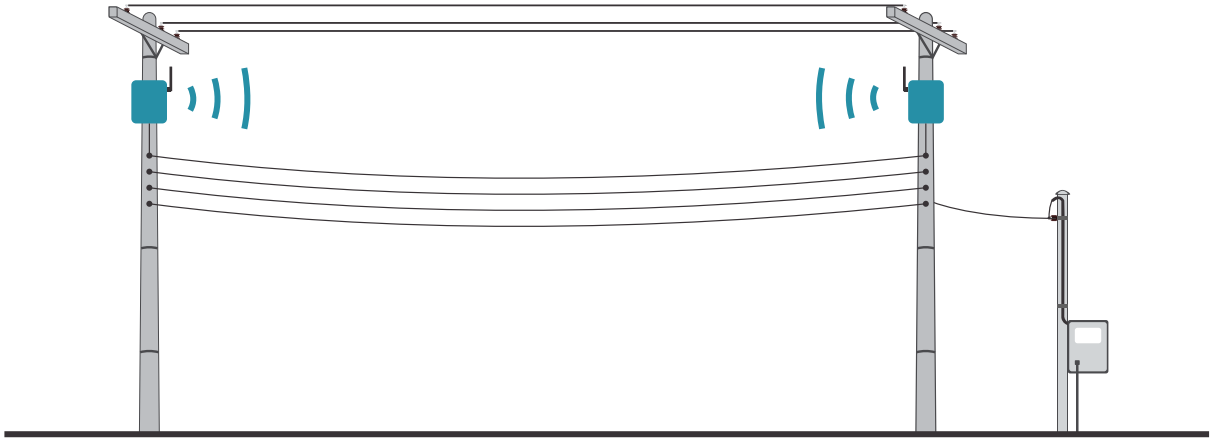

(b) indoor scenario

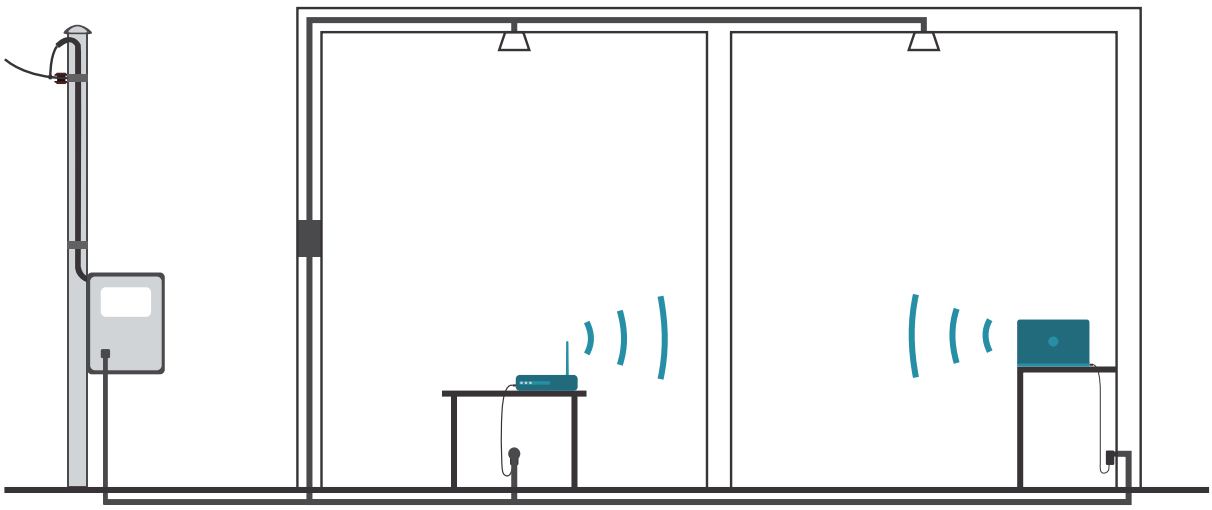

Source: Personal collection.

time slots are required and, for this reason, it has been investigated only in a cooperative scenario.

- Selection diversity: this strategy considers that the transmitter chooses the best channel (or subchannels in OFDM scheme) to use while the other channel is put on standby. The major objective is to yield an improved performance and save total transmission power [56].

- Receive diversity: this strategy, also called modulation diversity, assumes the transmission of equal data symbols through power line and wireless channels and later the received signals copies are combined [51].

Among the diversity strategies, receive diversity is the most employed because it enables a significantly improvement of data communication reliability at a low cost w.r.t computational complexity. For this reason, there are several investigations that analyzed the performance of well-known combining techniques for receive diversity in the HPWS context, such as equal gain combining (EGC), selection combining (SC), and MRC [37, 38, 57–62]. There are other investigations, however, that proposed new combining techniques focused on the specific characteristics of PLC and wireless communication [36, 62–64]. In this context, [36] introduced the optimum combining (OC) and saturated metric combining (SMC) techniques for dealing with the additive white Gaussian noise (AWGN) noise model in the wireless medium and the Middleton Class-A noise model in the power line medium [65]. By comparing them with the MRC technique, the authors showed improved performances once the receiver knows the instantaneous (in case of OC technique) or statistical (in case of SMC technique) parameters of the power line noise. In [36], the authors also showed the MRC technique is suitable for several in-home scenarios, where the power line noise is not severely impulsive. A few years later, [62–64] investigated combining techniques for a different HPWS, more precisely, narrowband transmission was considered and then the power line noise was modeled differently. Assuming coherent modulation, [62, 63] proposed two combining techniques based on the knowledge of the instantaneous or average noise power. Similar to [36], the MRC technique was used as a benchmark and then analogous conclusions were drawn. Also, in [62, 64], the authors proposed combining techniques for differential modulation based on the PLC noise characteristics and proved the superiority of the proposals over conventional combining techniques.

In the past decade, some works addressed different ways of exploiting the existing diversity between power line and wireless channels. For example, based on OFDM scheme, [46] proposed a subcarrier permutation strategy to increase the capacity in HPWS. In summary, the same information is transmitted through power line and wireless channels but in distinct subchannels; at the receiver side, subcarrier permutation is carried out before symbol combining, enabling the capacity increase. By assuming uniform power allocation, [46] demonstrated that the subcarrier of a medium should be sorted in ascending order of their SNRs and then combined with the subcarrier of the other medium sorted in descending order of their SNRs. Another interesting idea was presented in [66–68]. The authors proposed an advanced framework to

estimate and then cancel the impulsive noise (in the power line branch) and the narrowband interference (in the wireless branch) based on their sparsity in time and frequency domains, respectively. In other words, it was assumed the narrowband interference affected few subcarriers and, likewise, the impulsive noise degraded few samples of the same OFDM block; afterwards, it was shown different ways to estimate their values using the compressive sensing theory. Following, [56] demonstrated that transmitting only through the best channel provides a gain of 3 dB in the received SNR compared to the SC at the receiver due to the power saved.

In the meantime, HPWSs were also investigated to increase the receiving SNR in cooperative scenarios [35, 55, 69–72]. Data communication between source and destination nodes could be therefore aided by relay nodes besides exploiting the power line and wireless channels diversity. On this subject, [55, 69, 70] assumed hybrid dual-hop channel models and showed improvements in terms of end-to-end capacity, bit error rate, and outage probability. First, [69] presented improved capacity and error rate performances for in-home data communication systems by selecting the adequate route between power line source-destination link and wireless source-relay-destination link. In [70], closed-form expressions were derived to evaluate the benefits that a relay node can offer when it is able to select the signal which is received with higher SNR. In other words, a dual-interface relay node that can apply SC technique was investigated. On the other hand, [55] studied a receive diversity scheme in which equal symbols are transmitted through power line and wireless channels and the received symbols are then combined with MRC technique at the relay and destination nodes. Also, [55] proposed a transmit diversity scheme that achieves higher capacity if a specific condition of the power line and wireless SNRs is met. In such scheme, different symbols are transmitted through power line and wireless channels and yet they are combined at the relay node to exploit channel diversity.

Also regarding cooperative scenarios, [35, 71, 72] did not assumed the dual-hop channel model in the HPWS, but rather the single-relay channel model. In this case, the destination node receives four signals, which originate from: power line and wireless source-relay-destination links, and power line and wireless source-destination links. Hence, further improvements can be yielded based on two distinct diversities. Within this context, [35] compared the ergodic achievable data rate and outage probabilities of the hybrid single-relay channel model with its non-hybrid versions. Based on analytical and numerical results, the authors pointed out the outstanding performance of HPWSs regardless of relay position and cooperative protocol (e.g., amplify-and-forward and decode-and-forward). In its turn, [71] carried out a performance analysis of the incomplete version of the hybrid single-relay channel model, i.e., by taking into account the absence of any link or communication interface. Again, the advantages of the HPWS were stated. At last, [72] demonstrated SNR gains in the context of non-orthogonal multiple access (NOMA) networks even applying the HPWS only between relay and destination nodes.

In 2013, [73] suggested the parallel exploitation of power line and wireless channels to increase security of data communication systems. In a SG scenario, it showed that such a hybrid system is more robust to jamming attack than non-hybrid systems. A few years

later, eavesdropping attacks were also addressed in the literature [74–76]. In this regard, [74] investigated the ergodic achievable secrecy rate and the secrecy outage probability of the HPWS in the presence of one eavesdropper. The study considered the complete and incomplete versions of the HPWS, proving that both are beneficial to security, especially when the eavesdropper has only one data communication interface. On the other hand, [75] analyzed the application of the HPWS in a dual-hop channel model and then derived closed-form expressions for the average secrecy capacity in case of one eavesdropping attack. Numerical results then showed the advantageous of the hybrid system once again. Finally, [76] introduced an artificial noise scheme to improve the physical layer security. It proposed to use the best channel for data plus artificial noise transmission (legitimate transmitter to legitimate receiver) and the worse channel for artificial noise transmission (legitimate receiver to legitimate transmitter). In this way, if the eavesdropper does not have access to both communication channels simultaneously (power line and wireless), its SNR is null or severely degraded, and then the secrecy capacity is increased significantly. Overall, HPWSs were proved to have great potential to increase the physical layer security.

More recently, [77] applied the HPWS to a cooperative scenario focusing on energy harvesting. Although PLC devices (and also HPWS ones) are directly connected to the electric power network, energy harvesting enables the capture of the energy received out of the main frequency in PLC systems. In this context, [77] showed the most efficient way of exploiting the HPWS is to use both power line and wireless channels for data transmission and energy harvesting simultaneously, based on power splitting, instead of selecting one channel for data transmission and other for energy harvesting.

2.2 CHANNEL AND NOISE CHARACTERISTICS IN THE HPWS

By considering the HPWS in which power line and wireless communications operate in different frequency bands, it is straightforward that both channel and noise characteristics are independent in power line and wireless media. As a consequence, HPWSs face distinct dynamics of power line and wireless media, which creates a unique type of diversity between these media. In order to understand the origin of this diversity, the following paragraphs discuss the basic characteristics of channel and noise in power line and wireless media.

Power line channels originate from the multipath propagation scenario created by the multiple reflections in loads connected to the electric power grid [78]. These loads have an impedance mismatch with the electric power grid, which creates a frequency-selective channel regarding both narrowband ($3 - 500$ kHz [1]) and broadband ($1.7 - 86$ MHz [79]) applications. In addition, the electronic loads connected to the electric power grid are usually characterized by high-frequency parameters that change with the voltage amplitude of mains frequency and, therefore, a linear periodically time-variant (LPTV) behavior is observed in power line channels [80, 81]. This effect, however, is usually slow and can be disregarded for short symbol time intervals. Moreover, the attenuation of power line channels increases with the distance and

frequency. Note that power lines are primarily designed to maximize power transfer at the mains frequency (50 or 60 Hz). Hence, there is a natural physical constraint associated with high frequency usage in electric power cables, which is observed through the attenuation levels.

Wireless propagation is also characterized by several reflections that the transmitted signal suffers before arriving at the receiver. There are, however, some scenarios in which the LOS component is stronger than the non-line-of-sight (NLOS) ones and hence the multiple reflections can be disregarded. The existence of NLOS components typically varies significantly with the scenario and frequency bands that are considered. In addition, the presence and absence of those components respectively define a wireless channel with flat and selective behavior in the frequency domain. Within the so-called ISM bands, wireless channels can be usually considered flat if a narrow frequency bandwidth is assumed or frequency selective if broadband communication is considered [8]. Therefore, wireless channels are usually less frequency selective than power line channels, which is associated with the smaller delay spread of wireless channels compared to power line ones. In addition, the path loss is usually more intense on wireless than on power line channels.

The noise effect in wireless communication, on the other hand, can be considered less severe than in PLC. In wireless communication, interference from different communication systems and thermal noise are often assumed as the main sources of noise. Interference occurs when two or more RF devices of distinct communication systems use the same frequency band; hence, the signal transmitted in one communication system is captured as noise in the other and vice versa. This kind of noise is not always present and is more observed in wireless communication systems that use unlicensed frequency bands, such as the ISM bands. Thermal noise instead is unavoidable and present in every RF device. It is generated by the agitation of electric charges in any conductor, i.e., it does not depend on either material or shape of the conductor [82–84]. The power density of the thermal noise is naturally proportional to the temperature and does not vary with frequency (except at extremely high frequencies). Also, it follows a Gaussian distribution, which enables the proper modeling of thermal noise by the well-known WSS random process AWGN.

Regarding the PLC, the noise is considerably more complex. The literature describes five components that form the additive noise in the power line medium [85, 86]: colored background noise, narrowband noise, periodic impulsive noise asynchronous to the mains frequency, periodic impulsive noise synchronous to the mains frequency, and asynchronous impulsive noise. Each of these components has a different source, except for the periodic impulsive noise components since both originate from switched power supplies. Based on this mix of noise components, the time-domain additive noise on power line systems is classified as a non-Gaussian random process with non-stationary behavior. However, the asynchronous components can be disregarded due to low amplitude and/or rate of occurrence. As a consequence, the power line noise can be modeled by a cyclostationary random process (with respect to the mains frequency). Under this assumption, it can be also modeled as an additive colored Gaussian noise (ACGN) in the

frequency domain. According to [87, 88], since the Fourier transform performs a sum of several phase-shifted variables, the central limit theorem (CLT) shows that the resulting variable is Gaussian distributed.

Note that channel and noise characteristics of power line and wireless media are influenced by different factors. Furthermore, the distance between two HPWS devices, the chosen ISM frequency band for the RF transmission, and the constraints on the transmitted signal power spectral density (PSD) impact the HPWS performance. As a consequence, power line and wireless SNRs may be within different or similar ranges. In the former case, hybrid communication systems are rarely recommended because the worst communication channel cannot support the same applications that the best can. Hence the performance of the hybrid communication system is equal to the performance of the best communication channel. In the latter case, however, the loss of one communication channel can be overcome by the other and the difference in frequency selectivity of both media can be exploited, using combining techniques, to obtain an advanced data communication system. Based on the assumption that power line and wireless SNRs are within similar ranges, the mathematical model of the HPWS considered in part of this dissertation is presented in the next section.

2.3 HYBRID COMMUNICATION SYSTEM MODEL

This section describes a hybrid communication system that can be used to represent the HPWS in several scenarios, such as indoor and outdoor, narrow and broadband, etc. In this system, the preamble symbols (used e.g. for synchronization and channel state acquisition) are designed individually for each medium, whereas the data symbols are equally transmitted over all channels. The discrete baseband representation of the HPWS model is depicted in Figure 4. In this figure, dashed lines stand for the wireless medium (subscript "1"), whereas continuous lines indicate the power line medium (subscript "2"). Moreover, the transmitter (denoted by Tx) and the receiver (denoted by Rx) can perform data communication over both power line and wireless media. The other variables in Figure 4 will be described throughout this section. Furthermore, a general hybrid communication system model is assumed in order to cover a wider range of scenarios, i.e., a higher number of involved media.

Let a hybrid communication system composed of N_{C} channels in parallel operate in a frequency bandwidth equal to B_{w}. As $N_{\mathrm{C}} = 2$ is considered, one has the HPWS. In such a system, the transmission of each symbol occurs during a symbol time interval equal to T_{symb}. In particular, wireless channels are considered static depending on the application, whereas power line channels are usually classified as a LPTV system [81]. Hence, the hybrid communication system should be classified as LPTV as well. However, it is common to assume that $T_{\mathrm{symb}} \ll T_{\mathrm{c}}^{\mathrm{H}}$, in which $T_{\mathrm{c}}^{\mathrm{H}}$ is the hybrid coherence time such that $T_{\mathrm{c}}^{\mathrm{H}} = \min_{m}\{T_{\mathrm{c}}^{m}\}$, with T_{c}^{m} denoting the coherence time of the m^{th} channel[1]. Under this condition, the hybrid communication system

[1] The coherence time of a channel can be defined as the time interval within which variations are irrelevant

Figure 4 – Hybrid power line/wireless system model

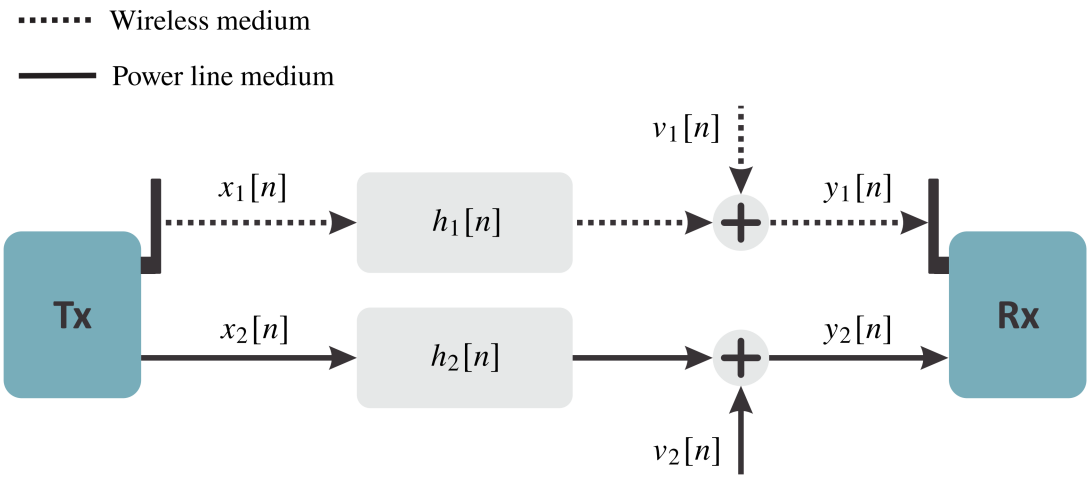

Source: Personal collection.

can be considered linear time-invariant (LTI) within each symbol time interval. Therefore, the CIR of the m^{th} medium can be represented by the L_m-length sequence $\{h_m[n]\}_{n=1}^{L_m}$, $m \in \{1, 2\}$, then the time-domain signal received in the m^{th} medium can be expressed as

$$y_m[n] = x_m[n] \star h_m[n] + v_m[n], \tag{2.1}$$

where $\{x_m[n]\}$ and $\{v_m[n]\}$ are time-domain sequences that stand for, respectively, transmitted signal and additive noise in the m^{th} medium, which are modeled as stationary random processes, and $\star$ denotes the linear convolution operator.

In addition to the sequence representation used in (2.1), the CIR of the m^{th} medium can be expressed as a vector $\mathbf{h}_m = [h_m[1]\ h_m[2]\ \ldots\ h_m[L_m]]^T$. In the discrete-frequency domain, the vector of length N_S that represents the channel frequency response (CFR) of each medium is then expressed as $\mathbf{H}_m = \mathbf{W}[\mathbf{h}_m^T\ \mathbf{0}_{1\times N_S - L_m}]^T$, in which $\mathbf{W}$ is the N_S-size discrete Fourier transform (DFT) matrix and $\mathbf{0}_{1\times(N_S-L_m)}$ is a null row vector of length $N_S - L_m$. Each channel is therefore divided into N_S subchannels through which N_S subcarriers are used. Furthermore, CFRs can be rewritten as $\mathbf{H}_m = [H_{m,1}\ H_{m,2}\ \ldots\ H_{m,N_S}]^T$, such that $H_{m,k}$ denotes its k^{th} element and $k \in \{1, 2, \ldots, N_S\}$. If no ISI is experienced, the frequency-domain representation of a symbol received in the k^{th} subchannel and m^{th} medium can be expressed as

$$Y_{m,k} = \sqrt{p_{m,k}}\, H_{m,k}\, X_{m,k} + V_{m,k}. \tag{2.2}$$

With respect to (2.2), $X_{m,k}$ is a random variable with zero mean, i.e., $\mathbb{E}\{X_{m,k}\} = 0, \forall m, k$ and unit variance, i.e., $\mathbb{E}\{|X_{m,k}|^2\} = 1, \forall m, k$ that represents the frequency-domain transmitted symbol at the k^{th} subcarrier and m^{th} medium, whereas $p_{m,k} \in \mathbb{R}^+$ is the transmission power allocated to that subcarrier. In its turn, the noise on the k^{th} subchannel and m^{th} medium is represented by a Gaussian random variable $V_{m,k} \in \mathbb{C}$, with $\mathbb{E}\{V_{m,k}\} = 0$, $\forall m, k$.

and therefore it can be considered LTI.

Note that the power line noise can be modeled as an ACGN in the frequency domain due to application of the Fourier transform - see [87] - and the wireless noise follows an AWGN random process. Nonetheless, the AWGN can be seen as a special case of ACGN where the noise variance is the same along with the entire frequency band. Moreover, the additive noise at the output of different media can be assumed to be independent from each other, whereas at the output of different subchannels it can be modeled by uncorrelated random variables [87]. Mathematically, $\mathbb{E}\{V_{m,k}V_{p,k}^*\} = 0, \forall m \neq p$, as well as $\mathbb{E}\{V_{m,k}V_{m,j}^*\} = \mathbb{E}\{V_{m,k}\}\mathbb{E}\{V_{m,j}^*\}, \forall k \neq j$, with $(\cdot)^*$ denoting the complex conjugate operator. Nonetheless, if $m = p$ and $k = j$, then $\mathbb{E}\{V_{m,k}V_{m,k}^*\} = p_{V_{m,k}}$, such that $p_{V_{m,k}} \in \mathbb{R}^+$ refers to the noise power on the k^{th} subchannel associated with the m^{th} medium.

Following, the normalized signal-to-noise ratio (nSNR) - or channel-to-noise gain - can be defined as

$$\overline{\gamma}_{m,k} \triangleq \frac{|H_{m,k}|^2}{p_{V_{m,k}}}, \forall\, m,\ k. \tag{2.3}$$

The nSNR is different from the conventional SNR [89]. The nSNR considers unit transmission power in each subchannel, whereas the SNR assumes a different transmission power and therefore it is given by

$$\gamma_{m,k} = p_{m,k}\overline{\gamma}_{m,k}, \forall\, m,\ k. \tag{2.4}$$

Notice that the nSNR depends only on the immutable characteristics of the media, such as channel and noise, and thus it cannot be changed. The SNR, on the other hand, may be controlled by changing the transmission power.

The nSNR is also relevant to determine the total number of subcarriers N_{S} in a multicarrier system. In this study, it is considered that each subcarrier occupies a frequency bandwidth narrower than the nSNR hybrid coherence bandwidth, i.e., the smallest nSNR coherence bandwidth[2] among the N_{C} media [89]. In other words, it is assumed $\Delta_f \ll B_{\text{c}}^{\text{H}}$, with $\Delta_f = B_{\text{w}}/N_{\text{S}}$ indicating the frequency spacing between adjacent subcarriers and $B_{\text{c}}^{\text{H}} = \min_m\{B_{\text{c}}^m\}$ representing the nSNR hybrid coherence bandwidth, in which B_{c}^m is the nSNR coherence bandwidth associated with the m^{th} medium. Since the nSNR coherence bandwidth is different over each of the considered media, distinct numbers of subcarriers could be assumed over different channels. However, the amount of information transmitted over the channels with fewer subcarriers would be smaller and a zero-padding would be require to combine the received symbols in the frequency domain [90].

Furthermore, two sets of transmission power constraints are regarded along the current study. They are as follows:

- Sum power constraint (SPC): The transmitter node has a total transmission power, $P_{\text{T}} \in \mathbb{R}^+$, to be shared among all transmitters; therefore it can be mathematically expressed as $\sum_{m,k} p_{m,k} \leq P_{\text{T}}$. Moreover, $p_{m,k} \geq 0, \forall m, k$.

[2] The nSNR coherence bandwidth is defined as the bandwidth within which the nSNR associated with a medium can be considered flat.

- Sum power-channel constraint (SPCC): The transmitter node has a maximum transmission power to be used to transmit data through each channel. In other words, there are N_{C} constraints described by $\sum\limits_{k} p_{m,k} \leq P_m$, $m \in \{1, 2, \ldots, N_{\mathrm{C}}\}$, in which $P_m \in \mathbb{R}^+$ is the transmission power to be used in the m^{th} medium. Also, $p_{m,k} \geq 0, \forall m, k$.

Note that the former set of constraints defines a theoretical approach that intends to yield the highest performance possible, whereas the latter is a practical and useful set of constraints for designing and implementing a hybrid communication system that exploit parallel channels. The term practical here means that the SPCC takes into account the existing power constraints associated with all channels (e.g., the distinct power constraints applied to power line and wireless communication systems).

2.3.1 MRC Signal-to-Noise Ratio

In this dissertation, distinct information is assumed to be initially transmitted over subcarriers with different indices, while the same information is sent through subcarriers with the same index but in different media, i.e., $X_{1,k} = X_{2,k} = \ldots = X_{N_{\mathrm{C}},k}, \forall k$. Note that different power can be transmitted over distinct subchannels and media in a hybrid communication system such as the HPWS. This characteristic makes those systems differ from single-input multiple-output (SIMO) systems, where $p_{1,k} = p_{2,k} = \ldots = p_{N_{\mathrm{C}},k}, \forall k$. At the receiver side, the MRC technique is applied to combine the N_{C} copies of received data symbols from different media. This combining technique is optimal for a stationary process and is here carried out in the frequency domain for every subcarrier index.

In order to understand the combining technique, the k^{th} subchannel of the N_{C} media in parallel can be analyzed (see Figure 5). Observe that applying a combining technique corresponds to compute a weighted sum of the symbols received from the considered media. Therefore, by using the weight factor $\alpha_{m,k} \in \mathbb{C}$ for the k^{th} subchannel and the m^{th} medium, the resulting symbol after using the combining technique is expressed as

$$Y_k = \sum_{m} \alpha_{m,k} Y_{m,k}, \forall k \tag{2.5}$$

$$= \left(\sum_{m} \alpha_{m,k} \sqrt{p_{m,k}} H_{m,k} \right) X_k + \sum_{m} \alpha_{m,k} V_{m,k}, \forall k. \tag{2.6}$$

At this point, the frequency-domain additive noise is a weighted sum of the noise in each of the considered media. Since those noise components are modeled by independent Gaussian random variables, the resulting noise can be modeled by a Gaussian random variable as well [91].

From (2.6), it is clear that Y_k is the sum of the transmitted symbol weighted by power and channel terms as well as a noise term. As the transmitted symbol, X_k, has unit variance and

Figure 5 – Parallel subchannels combined with MRC technique

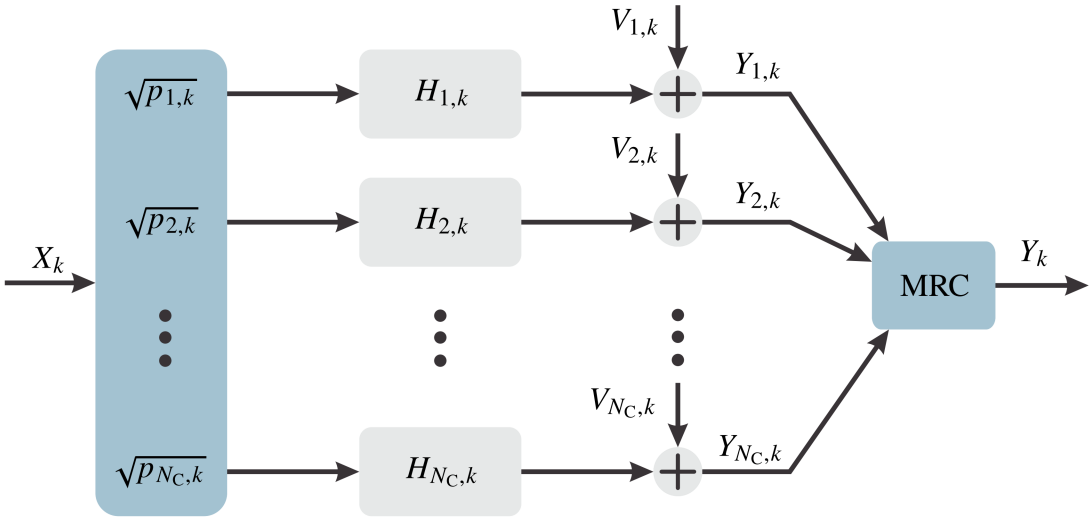

Source: Personal collection.

zero mean, the SNR of the received symbol after combination can be expressed as

$$\gamma_k = \frac{\mathbb{E}\left\{\left|\sum_m \alpha_{m,k}\sqrt{p_{m,k}}H_{m,k}\right|^2\right\}}{\mathbb{E}\left\{\left|\sum_m \alpha_{m,k}V_{m,k}\right|^2\right\}} = \frac{\left|\sum_m \alpha_{m,k}\sqrt{p_{m,k}}H_{m,k}\right|^2}{\sum_m |\alpha_{m,k}|^2 p_{V_{m,k}}} \tag{2.7}$$

$$= \frac{\left|\sum_m \alpha_{m,k}\sqrt{p_{V_{m,k}}}p_{V_{m,k}}^{-1/2}\sqrt{p_{m,k}}H_{m,k}\right|^2}{\sum_m |\alpha_{m,k}\sqrt{p_{V_{m,k}}}|^2}. \tag{2.8}$$

With the purpose of finding the maximum value of the above SNR, (2.8) can be rewritten as

$$\gamma_k = \frac{\left|\sum_m A_k B_k\right|^2}{\sum_m |A_k|^2}, \tag{2.9}$$

where $A_k = \alpha_{m,k}\sqrt{p_{V_{m,k}}}$ and $B_k = H_{m,k}\sqrt{p_{m,k}/p_{V_{m,k}}}$. Then the use of the Cauchy-Schwarz inequality results in

$$\frac{\left|\sum_m A_k B_k\right|^2}{\sum_m |A_k|^2} \leq \frac{\sum_m |A_k|^2 \sum_m |B_k|^2}{\sum_m |A_k|^2} = \sum_m |B_k|^2 \tag{2.10}$$

$$= \sum_m p_{m,k}\overline{\gamma}_{m,k}. \tag{2.11}$$

Therefore, by applying the MRC technique, the SNR of the resulting symbol is equal to the sum of the SNRs of the combined ones. In addition, the equality holds if $A_k/B_k^* = 1$ and then $\alpha_{m,k} = \sqrt{p_{m,k}}H_{m,k}^*/p_{V_{m,k}}, \forall m, k$.

3 POWER ALLOCATION FOR MAXIMIZING THE ACHIEVABLE DATA RATE

Power allocation is a classic topic for data communication researches that has already been very studied in non-hybrid contexts. Focusing on maximizing the achievable data rate, it is well-known that the waterfilling yields the optimal power allocation solution for non-hybrid communication systems. Depending on the type of hybrid communication system, the power allocation can be easily derived from non-hybrid solutions. For instance, the optimal power allocation for hybrid independent system (HIS)[1] is obtained by concatenating the normalized signal-to-noise ratio of power line and wireless media, then running the waterfilling algorithm. Regarding the HPWS, on the other hand, the power allocation problem is considerably different from that for non-hybrid systems due to the characteristics of each media and the use of combining techniques. To the best of the authors' knowledge, no study reports how to compute the optimal performance of the HPWS in terms of achievable data rate, which requires its power allocation technique.

Moreover, [53] discussed and designed a prototype of a narrowband HPWS transceiver and concluded that the hardware resources required by such data communication system can be significantly low. Recently, [51] showed that the maximum data rate of the so-called HIS is higher than the one achieved by HPWS. However, hardware complexity of an HIS transceiver is similar to the hardware complexity associated with two transceivers (one for power line and another for wireless communication). According to [53], this hardware complexity is considerably higher than the hardware complexity offered by a HPWS transceiver.

Based on the achievements related to HPWSs discussed in [51, 53], this hybrid system appears as an attractive alternative for improving the achievable data rate in comparison to HIS when a constraint on hardware resource availability is taken into account. In this context, power allocation algorithms that aim to maximize the data rate of an HPWS must be investigated (e.g., to demonstrate how to achieve the optimal performance of this hybrid system). Focused on power allocation for maximizing the achievable data rate in HPWS, this chapter look into the optimal power allocation in this type of hybrid communication system by pointing out the circumstances in which the usage of channels resources can be optimally exploited, assuming the combining technique most adopted in the literature (i.e., MRC). In this regard, the main contributions of this chapter are summarized as follows:

- The investigation of the optimal power allocation in HPWS by assuming two different constraints on the transmission power (i.e., the sum power and the sum power-channel constraints). To this end, this chapter formulates the optimization problems that encompasses the achievable data rates of both power constraints and discusses their mathematical solutions. Moreover, it proposes power allocation algorithms for both power constraints.

[1] Hybrid independent system refers to the use of independent power line and wireless channels for data communication between transmitter and receiver nodes, i.e., the transmission of distinct information through power line and wireless channels. It is also referred as hybrid system with source coding diversity [51].

- The comparative analysis among the proposed power allocation algorithms and previous power allocation algorithms that are well-established for non-hybrid systems, such as waterfilling [24] and uniform power allocation. In this regard, interior point (IP)-based algorithms are also used in order to validate the proposed power allocation algorithms.

The remainder of this chapter is organized as follows: Section 3.1 addresses the formulation of the optimization problems; Section 3.2 discusses the sum power constraint and its associated power allocation algorithm, whereas Section 3.3 does the same for the sum power-channel constraint; Section 3.4 focuses on numerical results and their analyses, whereas Section 3.5 summarizes the most important findings.

3.1 PROBLEM FORMULATION

In this chapter, it is assumed that the frequency representation of the symbols transmitted through each medium is equal. Therefore, $X_{1,k} = X_{2,k} = \ldots = X_{N_C,k}, \forall k$. Hence, symbols simultaneously received from subchannels with the same index in different media can be combined with the MRC technique. Thus the resulting symbols have SNRs equal to the sum of SNRs of the combined symbols. In other words, the resulting SNR for the k^{th} subchannel can be expressed as

$$\gamma_k = \sum_{m=1}^{N_C} p_{m,k}\overline{\gamma}_{m,k}, \forall k. \tag{3.1}$$

As mentioned in Chapter 2, the information transmitted over each subchannel occupies a frequency bandwidth equal to Δ_f and thus the total frequency bandwidth is $B_w = \Delta_f \times N_S$. Hence, assuming a sampling frequency equal to $2B_w$ and transmitted symbols modeled by a Gaussian random variable, the data rate of the hybrid data communication system in which the signals received from N_C parallel media are combined with the MRC technique is given by [27]

$$R = \frac{B_w}{N_S} \sum_{k=1}^{N_S} \log_2 (1 + \gamma_k) . \tag{3.2}$$

Given this data rate, an intriguing challenge is to come up with an achievable data rate denoted by $C = \max\{R\}$. In other words, it is necessary to find out the values of $p_{m,k}, \forall m, k$, that maximize the data rate and hence the formulation of an optimization problem is required.

The optimization problem that defines the achievable data rates of the HPWS can be written as

$$C = \max_{p_{m,k}} \frac{B_w}{N_S} \sum_{k=1}^{N_S} \log_2 \left(1 + \sum_{m=1}^{N_C} p_{m,k}\overline{\gamma}_{m,k} \right), \tag{3.3}$$

subject to either

$$\text{SPC} \begin{cases} \sum\limits_{m,k} p_{m,k} \leq P_T \\ p_{m,k} \geq 0, \ \forall \ k, m \end{cases} \tag{3.4}$$

or

$$\text{SPCC} \begin{cases} \sum\limits_{k} p_{m,k} \leq P_m, \ \forall m \\ p_{m,k} \geq 0, \ \forall \ k, m. \end{cases} \tag{3.5}$$

Following [53], the current formulation assumes the transmission of the same information through all N_C media and the application of the MRC technique to the received symbols per subchannel. As a consequence, a significant part of the data and signal processing performed at the link and physical layers, respectively, can be unified, as seen in [39, 53]. Therefore, the HPWS can increase data rate in comparison to non-hybrid systems at a lower hardware complexity than HIS [53]. In this regard, the following research question arises: *"How could the total transmission power be allocated in HPWS for maximizing data rates under the sum power or sum power-channel set of constraints?"* Answers to this question are presented in Section 3.2 and Section 3.3 for the SPC and the SPCC, respectively.

3.2 OPTIMAL POWER ALLOCATION FOR HYBRID POWER LINE/WIRELESS SYSTEMS: SUM POWER CONSTRAINT

This section presents the solution of the optimization problem related to the SPC and the algorithm to obtain it. For this purpose, a new optimization problem $C' = \frac{N_\text{S}}{B_\text{w} \log_2 \text{e}} C$ is introduced, since solving the optimization problem C' is equivalent to solving C, but with the advantage of dealing with a smaller number of variables. Afterwards, a simple division by the factor given above is enough to obtain C. The optimization problem comprising the SPC can be then described by

$$C' = \min_{p_{m,k}} - \sum_{k=1}^{N_\text{S}} \ln \left(1 + \sum_{m=1}^{N_\text{C}} p_{m,k} \overline{\gamma}_{m,k} \right), \tag{3.6}$$

subject to

$$\text{SPC} \begin{cases} \sum\limits_{m,k} p_{m,k} \leq P_\text{T} \\ p_{m,k} \geq 0, \ \forall \ k, m. \end{cases} \tag{3.7}$$

Note that the inequality constraints are linear and therefore convex functions, thus Slater's condition holds [92]. Hence, if the objective function is positive semidefinite on the considered set of transmission powers, then satisfying the Karush-Kuhn-Tucker (KKT) conditions is sufficient for a solution to be unique and optimal [92].

A possible alternative to verify the convexity of the objective function is to evaluate whether its Hessian matrix is positive semidefinite or not. To do so, let the objective function be given by

$$R' = - \sum_{k=1}^{N_\text{S}} \ln \left(1 + \sum_{m=1}^{N_\text{C}} p_{m,k} \overline{\gamma}_{m,k} \right). \tag{3.8}$$

By deriving the above equation with respect to p_{m_1,k_1}, all terms from the external summation (in k) can be regarded as constants but the term $k = k_1$. As a consequence, one has

$$\frac{\partial R'}{\partial p_{m_1,k_1}} = -\frac{\overline{\gamma}_{m_1,k_1}}{1 + \sum\limits_{m} p_{m,k_1}\overline{\gamma}_{m,k_1}}, \tag{3.9}$$

$\forall m_1 \in \{1, 2, \ldots, N_{\mathrm{C}}\}$ and $k_1 \in \{1, 2, \ldots, N_{\mathrm{S}}\}$.

The second derivative of R' with respect to p_{m_2,k_2} can be then expressed as

$$\frac{\partial^2 R'}{\partial p_{m_2,k_2}\partial p_{m_1,k_1}} = -\overline{\gamma}_{m_1,k_1}\frac{\partial}{\partial p_{m_2,k_2}}\left[\frac{1}{1 + \sum\limits_{m} p_{m,k_1}\overline{\gamma}_{m,k_1}}\right]. \tag{3.10}$$

Note that $\partial^2 R'/\partial p_{m_2,k_2}\partial p_{m_1,k_1} = 0$ if $k_1 \neq k_2$. On the other hand, if $k_1 = k_2$, then

$$\frac{\partial^2 R'}{\partial p_{m_2,k_2}\partial p_{m_1,k_1}} = \underbrace{\overline{\gamma}_{m_1,k_1}\overline{\gamma}_{m_2,k_1}}_{\in \mathbb{R}^+}\underbrace{\left(\frac{1}{1 + \sum\limits_{m} p_{m,k_1}\overline{\gamma}_{m,k_1}}\right)^2}_{\in \mathbb{R}^+}. \tag{3.11}$$

All terms of (3.11) are real and positive numbers. As a consequence, the Hessian matrix of the objective function is positive semi-definite within the considered domain of $p_{m,k}$ and thus the objective function defined by (3.8) is convex [92].

As the optimization problem defined in (3.6) is convex, the system of equations formed by the KKT conditions can be solved to find the optimal solution. In this regard, let the *Lagrangian* for the SPC optimization problem and its derivative with respect to $p_{q,i}$ be, respectively, given by

$$\mathcal{L} \triangleq -\sum_{k} \ln\left(1 + \sum_{m} p_{m,k}\overline{\gamma}_{m,k}\right) + \lambda\left(\sum_{m,k} p_{m,k} - P_{\mathrm{T}}\right) + \sum_{m,k}\mu_{m,k}(-p_{m,k}) \tag{3.12}$$

and

$$\frac{\partial \mathcal{L}}{\partial p_{q,i}} = \frac{-\overline{\gamma}_{q,i}}{1 + \sum\limits_{m} p_{m,i}\overline{\gamma}_{m,i}} + \lambda - \mu_{q,i}, \tag{3.13}$$

$\forall q \in \{1, 2, \ldots, N_{\mathrm{C}}\}$ and $i \in \{1, 2, \ldots, N_{\mathrm{S}}\}$; where $\lambda \in \mathbb{R}^+$ and $\mu_{q,i} \in \mathbb{R}^+$ are *Lagrange* multipliers. In sequel, the KKT conditions can be used for obtaining the following system of equations:

$$\frac{-\overline{\gamma}_{q,i}}{1 + \sum\limits_{m} p_{m,i}\overline{\gamma}_{m,i}} + \lambda - \mu_{q,i} = 0, \forall q, i \tag{3.14}$$

$$\lambda\left(\sum_{q,i} p_{q,i} - P_{\mathrm{T}}\right) = 0 \tag{3.15}$$

$$\mu_{q,i}(-p_{q,i}) = 0, \forall q, i \tag{3.16}$$

Based on a mathematical analysis of the system of equations given above, the following theorem can be written:

Theorem 1*: If a hybrid system operates over $N_C \in \mathbb{N}^*$ parallel and linear channels, the additive noise is a Gaussian (white or colored) random process, the receiver makes use of the MRC technique, and the SPC applies, then achieving the maximum data rate imposes that transmission of information must be through the subchannels offering the highest nSNRs. Therefore, the equivalent nSNR for the k^{th} subchannel, from transmitter to receiver, is defined by*

$$\overline{\gamma}_k \triangleq \max_m \{\overline{\gamma}_{m,k}\}, \forall k. \tag{3.17}$$

Proof. The proof of Theorem 1 is a consequence of Lemma 1 and Lemma 2. □

Lemma 1*: Two or more media cannot be used to transmit data through the same subchannel in order to maximize the achievable data rate of hybrid systems that operate over parallel channels and additive noise that is a stationary random process, that use MRC, and that are subject to the sum power constraint.*

Proof. Let us assume that a portion of the total transmission power is allocated to any two or more media at a same subchannel. If q_1 and q_2 represent these media and I indicates the chosen subchannel, then $p_{q_1,I} \neq 0$ and $p_{q_2,I} \neq 0$, which imply $\mu_{q_1,I} = \mu_{q_2,I} = 0$, see (3.16). Thus, by applying these values to (3.14), the following equations are obtained:

$$1 + \sum_m p_{m,I}\overline{\gamma}_{m,I} = \frac{\overline{\gamma}_{q_1,I}}{\lambda} \tag{3.18}$$

and

$$1 + \sum_m p_{m,I}\overline{\gamma}_{m,I} = \frac{\overline{\gamma}_{q_2,I}}{\lambda}. \tag{3.19}$$

Only $\lambda \to \infty$ solves the system of equations formed by (3.18) and (3.19) and also satisfies $\lambda \geq 0$ regardless of the values of $\overline{\gamma}_{q_1,I}$ and $\overline{\gamma}_{q_2,I}$. Thus, one has

$$1 + \sum_m p_{m,I}\overline{\gamma}_{m,I} = 0 \tag{3.20}$$

$$\sum_m p_{m,I}\overline{\gamma}_{m,I} = -1. \tag{3.21}$$

Since $\overline{\gamma}_{m,I} \in \mathbb{R}^+$, $\forall m$, there must be a value of $m \in \{1, 2, \ldots, N_C\}$ such that $p_{m,I} < 0$ to ensure (3.20) is true. However, it violates a constraint of the optimization problem and, as a consequence, provides the reader with the following result: for a given subchannel, I, the assumption of the existence of any two media, q_1 and q_2, such that $p_{q_1,I} \neq 0$ and $p_{q_2,I} \neq 0$, disagree with a constraint defined by the KKT conditions. Therefore, two or more media should not transmit data through the same subchannel for maximizing the data rate. □

Lemma 2*: The maximization of the achievable data rate of a hybrid system that operates over parallel channels and additive noise (stationary random process) and that uses MRC and is subject to the SPC implies that a given subcarrier might transmit a portion of the total transmission power through a subchannel associated with a given medium if, and only if, its nSNR is the highest among all media in the chosen subchannel index.*

Proof. Let q_1 indicates a medium such that $p_{q_1,I} \neq 0$ and q_2 represents any of the $N_C - 1$ media with $p_{q_2,I} = 0$. Once more using (3.14) and (3.16), one has

$$1 + p_{q_1,I}\overline{\gamma}_{q_1,I} = \frac{\overline{\gamma}_{q_1,I}}{\lambda} \tag{3.22}$$

and

$$1 + p_{q_1,I}\overline{\gamma}_{q_1,I} = \frac{\overline{\gamma}_{q_2,I}}{\lambda - \mu_{q_2,I}}. \tag{3.23}$$

As a consequence,

$$\lambda = -\mu_{q_2,I}\frac{\overline{\gamma}_{q_1,I}}{\overline{\gamma}_{q_2,I} - \overline{\gamma}_{q_1,I}}. \tag{3.24}$$

Since $\mu_{q,i} \geq 0, \forall q, i$ and $\lambda \geq 0$, one can conclude that $\overline{\gamma}_{q_1,I}$ must be greater than $\overline{\gamma}_{q_2,I}$ to guarantee (3.24) is true and, as a consequence, not violate the KKT conditions. As a result, the subcarrier that might transmit a portion of the available transmission power in a specific subchannel is the one with the highest nSNR among all media.

If more than one media has the maximum value of nSNR for a given subchannel index k, then the transmission power allocated to the k^{th} subcarrier can be arbitrarily distributed among them. □

Corollary 1*: The optimal power allocation of the total transmission power based on the sum power constraint and parallel channels implies in hybrid systems that make use of the MRC technique attaining the same achievable data rate as the hybrid systems with the SC technique [61].*

3.2.1 Proposed Power Allocation Algorithm

Based on Theorem 1, there is a definition of an equivalent data communication channel formed by the subchannels with the highest nSNRs among all media. It means that the resulting nSNR associated with the k^{th} subchannel (index) is given by $\max_m\{\overline{\gamma}_{m,k}\}, \forall k$. Based on that, the power allocated to the subcarrier index of distinct media showing nSNR lower than the maximum is null. Thus, it is necessary to define how to allocate the total transmission power among the media with the highest nSNR for a given subchannel index. Nonetheless, in case of existing only one medium per subchannel, the computation of the achievable data rate is well-known from the literature and it is accomplished by using the waterfilling algorithm, which is concisely presented in Appendix A. Therefore, a proper and straightforward solution can be conceived by running the waterfilling algorithm and taking into account only the subchannels with the highest nSNR among the media, i.e., using the equivalent nSNRs, $\max_m\{\overline{\gamma}_{m,k}\}, \forall k$, as its input parameters (see Algorithm #1 for the HPWS).

Note that Algorithm #1 is organized into two steps. First, it defines the maximum nSNR value per subchannel, and second, it performs the conventional waterfilling algorithm. In the case of the HPWS, the computational complexity associated with the first step is proportional to N_S (i.e., $O(N_S)$) since only one comparison operation is required per subchannel. Similarly, it has been already shown that the conventional waterfilling algorithm may have a computational

Algorithm #1: Power allocation algorithm for maximizing the achievable data rate in HPWS under the SPC

Input :

$\overline{\gamma}_{1,k}$ is the nSNR of the 1st medium ($m = 1$) and k^{th} subchannel, $k \in \{1, 2, \ldots, N_{\text{S}}\}$

$\overline{\gamma}_{2,k}$ is the nSNR of the 2nd medium ($m = 2$) and k^{th} subchannel, $k \in \{1, 2, \ldots, N_{\text{S}}\}$

P_{T} is the total transmission power.

Output :

$p_{1,k}$ is the power allocated to the 1st medium and k^{th} subchannel, $k \in \{1, 2, \ldots, N_{\text{S}}\}$

$p_{2,k}$ is the power allocated to the 2nd medium and k^{th} subchannel, $k \in \{1, 2, \ldots, N_{\text{S}}\}$

begin

$\mathcal{K} = \{1, 2, \ldots, N_{\text{S}}\}$;

$p_{1,k} = 0, \forall k \in \mathcal{K}$;

$p_{2,k} = 0, \forall k \in \mathcal{K}$;

$\{\overline{\gamma}_k\} = \max\{\overline{\gamma}_{1,k}, \overline{\gamma}_{2,k}\}, \forall k \in \mathcal{K}$;

$\{q\} = \arg\max\{\overline{\gamma}_{1,k}, \overline{\gamma}_{2,k}\}, \forall k \in \mathcal{K}$;

$[\{p_k\}, \lambda] = \text{waterfilling}(\{\overline{\gamma}_k\}, P_{\text{T}}), \forall k \in \mathcal{K}$;

$\{p_{q,k}\} = \{p_k\}$;

end

complexity of order $O(N_{\text{S}})$ [93] and therefore the computational complexity of Algorithm #1 is also of order $O(N_{\text{S}})$. Note that the cyclostationary behavior of the power line characteristics (channel and noise statistics) can be also used to reduce the computational complexity associated with power allocation algorithms, as carried out in [81]. Finally, the use of a greedy algorithm for allocating integer number of bits can be easily adapted from the literature [93] to accomplish a feasible power allocation.

3.3 OPTIMAL POWER ALLOCATION FOR HYBRID POWER LINE/WIRELESS SYSTEMS: SUM POWER-CHANNEL CONSTRAINT

This section outlines the solution of the optimization problem related to the SPCC. Similar to the previous section, a new optimization problem $C'' = \frac{N_{\text{S}}}{B_{\text{w}} \log_2 \text{e}} C$ is introduced. The optimization problem originating from the SPCC is then given by

$$C'' = \min_{p_{m,k}} - \sum_{k=1}^{N_{\text{S}}} \ln\left(1 + \sum_{m=1}^{N_{\text{C}}} p_{m,k} \overline{\gamma}_{m,k}\right), \tag{3.25}$$

subject to

$$\text{SPCC} \begin{cases} \sum\limits_{k} p_{m,k} \leq P_m, \ \forall m \\ p_{m,k} \geq 0, \ \forall\, k, m. \end{cases} \tag{3.26}$$

Observe that the objective function is the same as the one in the previous section and thus it is convex on the considered set. Also, the inequality constraints are linear and convex functions.

Therefore, meeting the KKT conditions yields the optimal solution.

By applying the KKT conditions to this optimization problem, the following system of equations is obtained:

$$\frac{-\overline{\gamma}_{q,i}}{1+\sum\limits_{m} p_{m,i}\overline{\gamma}_{m,i}} + \lambda_q - \mu_{q,i} = 0, \forall q, i \tag{3.27}$$

$$\lambda_q \left(\sum_i p_{q,i} - P_q \right) = 0, \forall q \tag{3.28}$$

$$\mu_{q,i}(-p_{q,i}) = 0, \forall q, i \tag{3.29}$$

Now, consider $a \in \{1, 2, \ldots, N_C\}$ and $b \in \{1, 2, \ldots, N_C\}$, with $a \neq b$. From (3.27), the following equation arises:

$$\frac{\overline{\gamma}_{a,i}}{\overline{\gamma}_{b,i}} = \frac{\lambda_a - \mu_{a,i}}{\lambda_b - \mu_{b,i}}, \forall i, \tag{3.30}$$

A careful analysis of (3.30) for a given subchannel $I \in \{1, 2, \ldots, N_S\}$ can be helpful. First, consider $\overline{\gamma}_{a,I}/\overline{\gamma}_{b,I} > \lambda_a/\lambda_b$, with $\lambda_b > 0$, and then apply it to (3.30). The following inequality is obtained:

$$\frac{\lambda_a}{\lambda_b} < \frac{\lambda_a - \mu_{a,I}}{\lambda_b - \mu_{b,I}}. \tag{3.31}$$

By contradiction, one can show that $\mu_{b,I} \neq 0$. Assuming that $\mu_{b,I} = 0$, one can obtain

$$\frac{\lambda_a}{\lambda_b} < \frac{\lambda_a - \mu_{a,I}}{\lambda_b} \Rightarrow \tag{3.32}$$

$$\Rightarrow \lambda_a < \lambda_a - \mu_{a,I}, \tag{3.33}$$

which is evidently false since $\lambda_a \geq 0$ and $\mu_{a,I} \geq 0$. As a consequence, $\mu_{b,I}$ cannot be equal to zero if $\overline{\gamma}_{a,I}/\overline{\gamma}_{b,I} > \lambda_a/\lambda_b$. Similarly, one can find that $\mu_{a,I} \neq 0$ if $\overline{\gamma}_{a,I}/\overline{\gamma}_{b,I} < \lambda_a/\lambda_b$. Based on the fact that either $\mu_{q,i}$ or $p_{q,i}$ has to be equal to zero - see (3.16) - one has:

- If $\frac{\overline{\gamma}_{a,I}}{\overline{\gamma}_{b,I}} > \frac{\lambda_a}{\lambda_b}$, then $p_{b,I} = 0$.
- If $\frac{\overline{\gamma}_{a,I}}{\overline{\gamma}_{b,I}} < \frac{\lambda_a}{\lambda_b}$, then $p_{a,I} = 0$.

Notice that a and b can be any combination of N_C taken two at a time and therefore interesting conclusions can be drawn. First, an amount of power will be allocated in both media a and b if, and only if, $\frac{\overline{\gamma}_{a,I}}{\overline{\gamma}_{b,I}} = \frac{\lambda_a}{\lambda_b}$. However, this is likely to happen only if a and b have precisely the same nSNR value or the total power intended to one of them is too low in relation to that intended for the other. Also, it can be extended to a higher number of media by taking different combinations of a and b and then, when dealing with media with completely different selectivities, i.e., curves of nSNR that have considerably different behaviors, the probability of two or more media transmitting information through the same subcarrier in order to maximize data rate is extremely small.

Still based on the above remarks, if $\overline{\gamma}_{a,i}/\overline{\gamma}_{b,i} > \lambda_a/\lambda_b$, $\forall i$, then the portion of the total transmission power assigned to the second medium would be null. On the other hand, if

$\overline{\gamma}_{a,i}/\overline{\gamma}_{b,i} < \lambda_a/\lambda_b$, $\forall i$, then the first medium would have null power. Therefore, assuming that $P_a \neq 0$ and $P_b \neq 0$, one has

$$\min_i \left\{ \frac{\overline{\gamma}_{a,i}}{\overline{\gamma}_{b,i}} \right\} \leq \frac{\lambda_a}{\lambda_b} \leq \max_i \left\{ \frac{\overline{\gamma}_{a,i}}{\overline{\gamma}_{b,i}} \right\}. \tag{3.34}$$

As the focus of this dissertation is on the HPWS, only two parallel channels ($N_{\mathrm{C}} = 2$) are considered henceforth. In this context, Figure 6 illustrates the aforementioned achievements for a decreasing nSNR ratio curve (the same could be obtained for a sorted version of a non-decreasing nSNR ratio curve). Observe that subchannels whose nSNR ratio values are above the λ_1/λ_2 ratio have null power allocated to the second medium, whereas the first medium has null power allocated to subchannels that present nSNR ratio values below the λ_1/λ_2 ratio. Therefore, the nSNR ratio values above and below the λ_1/λ_2 ratio are characterized by having $p_{2,i} = 0$ and $p_{1,i} = 0$, respectively. By applying such values to a system of equations formed by the KKT conditions, the following equations are obtained and used as the basis of the proposed algorithm:

- $p_{1,i} = 0$:

$$1 + p_{2,i}\overline{\gamma}_{2,i} = \frac{\overline{\gamma}_{2,i}}{\lambda_2 - \mu_{2,i}} \tag{3.35}$$

and

$$p_{2,i} \geq \frac{\overline{\gamma}_{1,i}}{\lambda_1 \overline{\gamma}_{2,i}} - \frac{1}{\overline{\gamma}_{2,i}}. \tag{3.36}$$

- $p_{2,i} = 0$:

$$1 + p_{1,i}\overline{\gamma}_{1,i} = \frac{\overline{\gamma}_{1,i}}{\lambda_1 - \mu_{1,i}} \tag{3.37}$$

and

$$p_{1,i} \geq \frac{\overline{\gamma}_{2,i}}{\lambda_2 \overline{\gamma}_{1,i}} - \frac{1}{\overline{\gamma}_{1,i}}. \tag{3.38}$$

3.3.1 Proposed Power Allocation Algorithm

First of all, it is worth mentioning that the i^{th} subcarrier has a transmission power different from zero allocated to both first and second media if, and only if, $\overline{\gamma}_{1,i}/\overline{\gamma}_{2,i} = \lambda_1/\lambda_2$. However, the probability of occurring such situation is quite low (mainly for high values of N_{S}) and therefore its occurrence can be disregarded. As a result, one obtains a suboptimal power allocation algorithm that yields a solution quite close to the optimal and, most importantly, it is feasible.

Note that (3.35) and (3.37) are equal to the equations of the conventional waterfilling algorithm [24], indicating that such algorithm may be helpful for determining the power allocation among subcarriers. Based on that, subchannels in which $\overline{\gamma}_{1,i}/\overline{\gamma}_{2,i} > \lambda_1/\lambda_2$ constitute the set of inputs to the conventional waterfilling algorithm related to the first medium ($p_{2,i} = 0$), whereas the remainder of the subchannels feeds the conventional waterfilling algorithm associated with the second medium ($p_{1,i} = 0$). In addition, the lower bound established by (3.36) and (3.38)

Figure 6 – An example of subchannel indices associated with their corresponding null subcarriers for a decreasing nSNR ratio curve

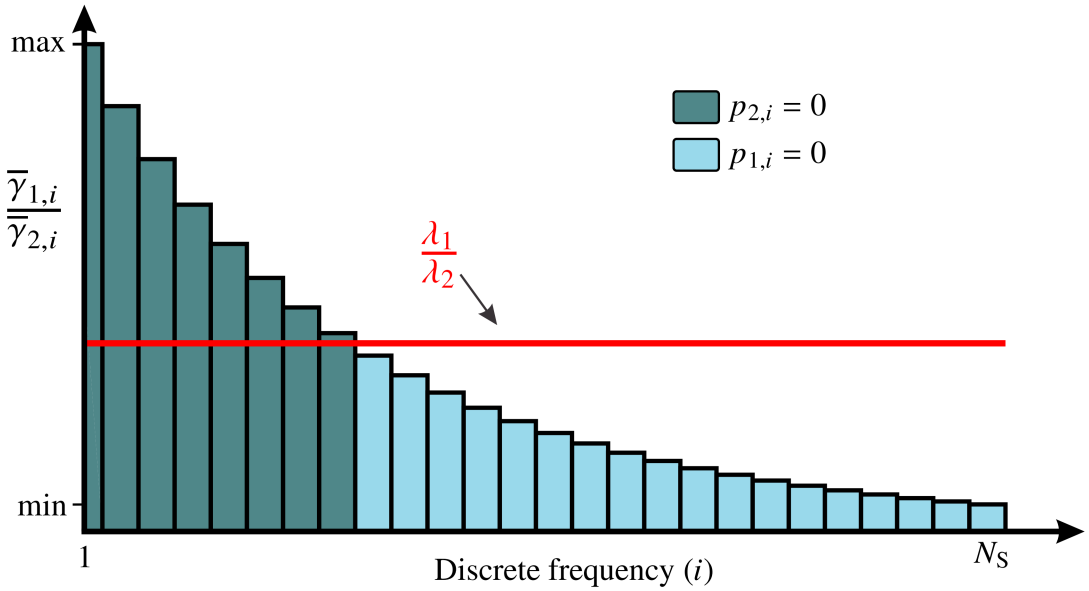

Source: Personal collection.

must be obeyed for the transmission power allocated to each subcarrier. Therefore, the main task accomplished by the proposed algorithm is to find λ_1 and λ_2 that satisfy the waterfilling equations, (3.35) and (3.37), and the constraints established by (3.36) and (3.38). In fact, from the conventional waterfilling algorithm, finding λ_1 and λ_2 results in also finding $p_{1,i}$ and $p_{2,i}$, $\forall i$.

Algorithm #2 is proposed to find the values of λ_1 and λ_2 and hence $p_{1,i}$ and $p_{2,i}$, $\forall i$. The main idea is to exchange the λ_1/λ_2 ratio within the range imposed by (3.34) until reaching its suboptimal value, i.e., the one in which either few or no subchannels violate the constraints defined by (3.36) and (3.38). In such algorithm, $\mathcal{A}$ and $\mathcal{B}$ are sets composed of subchannels that are, respectively, above and below the λ_1/λ_2 ratio. Also, $\mathcal{A}_\text{v}$ and $\mathcal{B}_\text{v}$ represent, respectively, subchannels that are above and below the λ_1/λ_2 ratio and violate the lower bound for the transmission power.

After initialization, Algorithm #2 starts a loop considering that the λ_1/λ_2 ratio is only above the subchannel with smaller $\overline{\gamma}_{1,i}/\overline{\gamma}_{2,i}$. Two waterfilling algorithms (described in Appendix A) are then performed for subchannels that are above and below the λ_1/λ_2 ratio and, after that, the lower bound for the allocated transmission power is checked for all subchannels. Next, the *if* statement is just to retain the transmission power values of the iteration in which the number of violated constraints is the smallest. In sequel, if there are no subchannels that violate equations (3.36) and (3.38), i.e., $\mathcal{A}_\text{v} \cup \mathcal{B}_\text{v} \neq \varnothing$, then the transmission powers allocated to the subchannels will be those defined by the current iteration. Otherwise, the loop is again performed but now removing the subchannel with smallest $\overline{\gamma}_{1,i}/\overline{\gamma}_{2,i}$ from those which are above the λ_1/λ_2 ratio and moving it to those that are below such ratio. This procedure is repeated until either there is no subchannel that violates the constraints established by (3.36) and (3.38) or only one subchannel remains above the λ_1/λ_2 ratio, i.e., $\text{Card}\{\mathcal{B}\} = N_\text{S} - 1$, where $\text{Card}\{\cdot\}$ denotes the cardinality

Algorithm #2: Power allocation algorithm for maximizing the achievable data rate in HPWS under the SPCC

Input :

$\overline{\gamma}_{1,k}$ is the nSNR of the 1st medium ($m = 1$) and k^{th} subchannel, $k \in \{1, 2, \ldots, N_{\text{S}}\}$

$\overline{\gamma}_{2,k}$ is the nSNR of the 2nd medium ($m = 2$) and k^{th} subchannel, $k \in \{1, 2, \ldots, N_{\text{S}}\}$

P_1 is the maximum transmission power to be distributed in the first medium

P_2 is the maximum transmission power to be distributed in the second medium

Output :

$p_{1,k}$ is the power allocated to the 1st medium and k^{th} subchannel, $k \in \{1, 2, \ldots, N_{\text{S}}\}$

$p_{2,k}$ is the power allocated to the 2nd medium and k^{th} subchannel, $k \in \{1, 2, \ldots, N_{\text{S}}\}$

begin

$p_{1,k} = 0, \forall k$;

$p_{2,k} = 0, \forall k$;

$\mathcal{A} = \{1, 2, \ldots, N_{\text{S}}\}$;

$\mathcal{B} = \varnothing$;

$\mathcal{A}_{\text{v}} = \mathcal{A}$;

$\mathcal{B}_{\text{v}} = \mathcal{B}$;

$N_{\text{v}} = N_{\text{S}}$;

while $[(\mathcal{A}_{\text{v}} \cup \mathcal{B}_{\text{v}}) \neq \varnothing]$ & $[\text{Card}\{\mathcal{B}\} \neq N_{\text{S}} - 1]$ **do**

$q = \arg\min_{\mathcal{A}} \{\overline{\gamma}_{1,a}/\overline{\gamma}_{2,a}\}, \forall a \in \mathcal{A}$;

$\mathcal{A} = \mathcal{A} - q$;

$\mathcal{B} = \mathcal{B} \cup q$;

$[\{p_{1,a}\}, \lambda_1] = \text{waterfilling}(\{\overline{\gamma}_{1,a}\}, P_1), \forall a \in \mathcal{A}$;

$[\{p_{1,b}\}, \lambda_2] = \text{waterfilling}(\{\overline{\gamma}_{2,b}\}, P_2), \forall b \in \mathcal{B}$;

$\mathcal{A}_{\text{v}} = \{a \in \mathcal{A} | p_{1,a}\overline{\gamma}_{1,a} < (\overline{\gamma}_{2,a}/\lambda_2) - 1\}$;

$\mathcal{B}_{\text{v}} = \{b \in \mathcal{B} | p_{2,b}\overline{\gamma}_{2,b} < (\overline{\gamma}_{1,b}/\lambda_1) - 1\}$;

if $\text{Card}\{\mathcal{A}_{\text{v}} \cup \mathcal{B}_{\text{v}}\} \leq N_{\text{v}}$ **then**

$\mathcal{X} = \mathcal{A}$;

$\mathcal{Y} = \mathcal{B}$;

$p_{1,x} = p_{1,a}, \forall x \in \mathcal{X}$;

$p_{2,y} = p_{2,b}, \forall y \in \mathcal{Y}$;

$N_{\text{v}} = \text{Card}\{\mathcal{A}_{\text{v}} \cup \mathcal{B}_{\text{v}}\}$;

end

end

$p_{1,k} = p_{1,x}, \forall k \in \mathcal{X}$;

$p_{2,k} = p_{2,y}, \forall k \in \mathcal{Y}$;

end

of a set. In case there is no combination of subchanels such that $\mathcal{A}_{\mathrm{v}} \cup \mathcal{B}_{\mathrm{v}} \neq \varnothing$, the transmission power allocated to each subchannel will be defined by the loop iteration in which the violation of fewer constraints are observed.

In order to analyze the computational complexity of Algorithm #2, observe that before and after the *while* loop there are only assignment operations and thus the associated complexity is of order $O(1)$. In addition, the *if* statement within the *while* loop also demands a computational complexity $O(1)$. Among the remaining parts, the most expensive in terms of computational complexity are the conventional waterfilling algorithm and the search for the minimum argument, which individually require a complexity of order $O(N_{\mathrm{S}})$. Since both iterates at most $N_{\mathrm{S}} - 1$ times (i.e., the maximum number of iterations in the *while* loop), Algorithm #2 has a computational complexity $O({N_{\mathrm{S}}}^2)$. Note that in this case there is one less degree of freedom in comparison to the SPC, which further restricts the problem and therefore makes its solution more complex. It is worth mentioning that due to the fact that Algorithm #2 is based on the well-known waterfilling algorithm, its practical implementation for allocating power and also bits is perfectly feasible. This means that the waterfilling algorithm used in Algorithm #2 may be replaced by the Levin-Campello algorithm [93], allowing the discretization of the available power and, as a consequence, the allocation of an integer number of bits per subcarrier. In summary, the proposed power allocation algorithms can be eventually implemented at a usual hardware cost.

3.4 NUMERICAL ANALYSES

This section discusses numerical results for evaluating the effectiveness of the proposed power allocation algorithms. To do so, the transmitter node has knowledge of the CSI of the media and two are considered ($N_{\mathrm{C}} = 2$), i.e., the HPWS. CFR and additive noise PSD of the measured broadband and in-home PLC define the first medium, whereas wireless CFR and circularly symmetric complex AWGN models define the second medium. In addition, the considered frequency bandwidth is $B_{\mathrm{w}} = 80$ MHz, which comply with the wireless local area network standard IEEE 802.11ac [94] and also with the PLC regulations [79]. In this sense, there are three frequency bands most considered by the regulations, which are $1.7 - 30$ MHz, $1.7 - 50$ MHz, and $1.7 - 86$ MHz. Taking the broadest frequency bandwidth as a reference, the considered frequency bandwidth can be employed. Since realistic data based on measurement campaigns are considered, the total frequency bandwidth is divided into $N_{\mathrm{S}} = 128$ subchannels, each subchannel frequency bandwidth is equal to $\Delta_f \cong 658.6$ kHz, which is smaller than the average coherence bandwidth of broadband and in-home power line channels [95].

The analysis of the proposed power allocation algorithms includes comparisons with previous power allocation algorithms (such as the conventional waterfilling and the uniform allocation (UA)). Furthermore, algorithms based on the interior-point method [96], which it is here named as IP algorithms, are used as benchmarks. This method is used as a reference because it provides the optimal solution for convex optimization problems and the problems considered in this dissertation have such characteristic.

Figure 7 – nSNRs for power line and wireless media in the considered frequency bandwidth

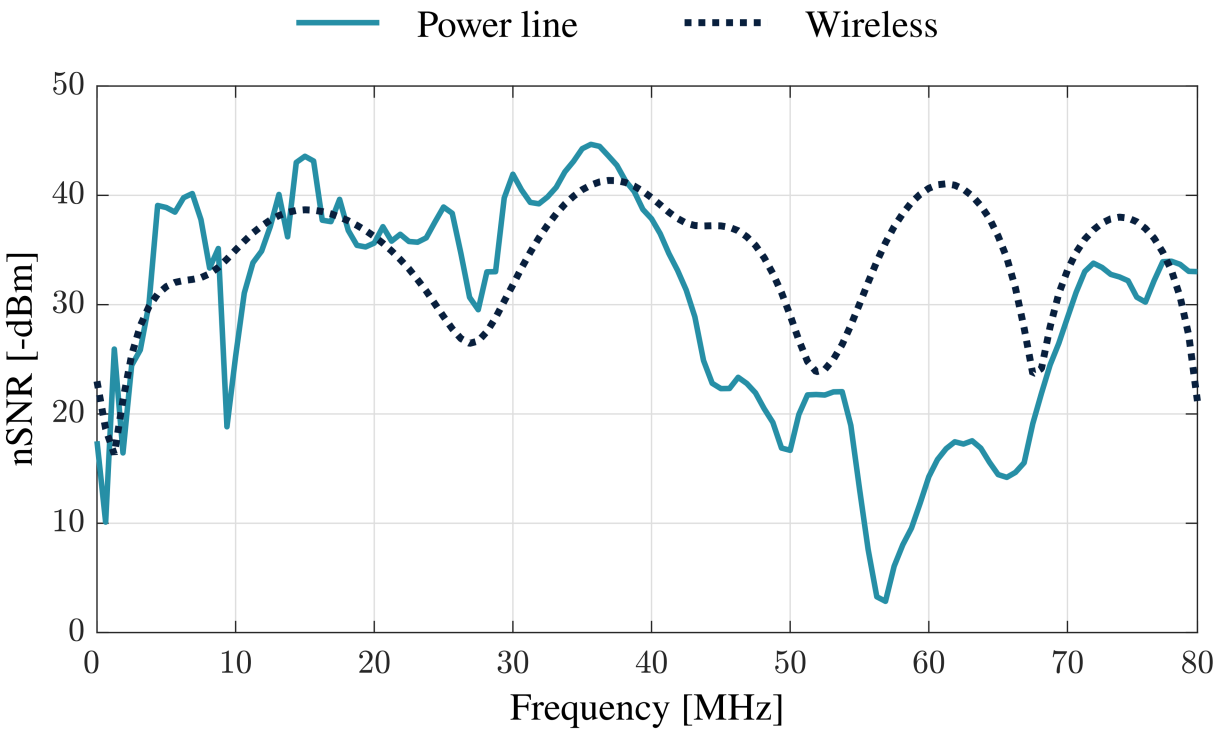

Source: Personal collection.

Regarding the total transmission power, the following range applies for the majority of the results $P_{\mathrm{T}} \in \{-30, 5, \ldots, 30\}$ dBm. For the results related to the SPCC, $P_1 = \alpha P_{\mathrm{T}}$ and $P_2 = (1-\alpha)P_{\mathrm{T}}$, $0 \leq \alpha \leq 1$. Therefore, the parameter α determines the percentage of the total transmission power that is allocated to each medium. Note that for an optimal α value SPC and SPCC are equivalent, otherwise SPC outperforms SPCC.

3.4.1 Channel Impulse Response and Additive Noise

With respect to the first medium, CFR and additive noise PSD are those obtained from a measurement campaign carried out to characterize broadband and in-home power line channels, see [15] for details. To attain the noise power, which is necessary for obtaining γ_m, the multiplication of the discrete additive noise PSD by the subchannel frequency bandwidth Δ_f applies. Regarding the second medium, the wideband wireless channel model (non-line-of-sight residential scenario), reported in [97], provides samples of CFR. To select the considered frequency bandwidth, B_{w}, the original channel undergoes a digital bandpass filtering with a center frequency equal to 5.8 GHz. Also, the wireless additive noise is assumed to be circularly symmetric complex AWGN.

To have a fair comparison between power line and wireless media and evaluate only the existing diversity between them, the noise power on the wireless medium is computed to make the average value of the nSNR equal in both power line and wireless media [36, 51]. In other words, it is assumed that $\sum_k |\overline{\gamma}_{1,k}| = \sum_k |\overline{\gamma}_{2,k}|$. The obtained nSNRs for power line and wireless media are depicted in Figure 7 for the considered frequency bandwidth.

3.4.2 Achievable Data Rate Analysis

The first achievable data rate analysis refers to the comparison between the proposed and IP-based power allocation algorithms. The use of the IP power allocation algorithm aims just to validate the proposed ones. Figure 8 shows the achievable data rate in this comparison for $\alpha = 0.1$ in order to highlight the difference between SPC and SPCC. Note that the performances of the proposed power allocation algorithms match the ones of the IP-based power allocation algorithm even for Algorithm #2, which is a suboptimal solution. It proves that the proposed algorithms are suitable for power allocation purposes as well as Algorithm #2 yields a negligible performance degradation compared to the optimal solution.

Turning to Figure 9, a new parameter is analyzed to compare SPC and SPCC. It is here called achievable data rate ratio and can be expressed as follows:

$$\rho_{\beta}(\alpha) \triangleq \frac{C_{\beta}(\alpha)}{C_{\text{SPC}}(\alpha)}, \tag{3.39}$$

with $\beta \in \{\text{SPC,SPCC}\}$ and $C_{\text{SPC}}(\alpha)$ and $C_{\text{SPCC}}(\alpha)$ being respectively obtained from Algorithms #1 and #2. Observe that ρ_{β} and the achievable data rate, C_{β}, suffer the influence of α. From the analysis of $\rho_{\beta}(\alpha)$, it is possible to see the upper bound established by SPC for SPCC and also to infer the optimal value of α. In fact, the optimal α will be the one in which $\rho_{\text{SPC}}(\alpha) = \rho_{\text{SPCC}}(\alpha)$; however, it may vary according to the total transmission power due to the different frequency selectivity of both channels. For instance, the optimal value of α is 0.35 for $P_{\text{T}} = -15$ dBm and approximately 0.45 for $P_{\text{T}} = 15$ dBm. Figures 9(a) and 9(b) also show a

Figure 8 – Achievable data rate as a function of P_{T} for Algorithms #1 and #2 and IP-based algorithms ($\alpha = 0.1$)

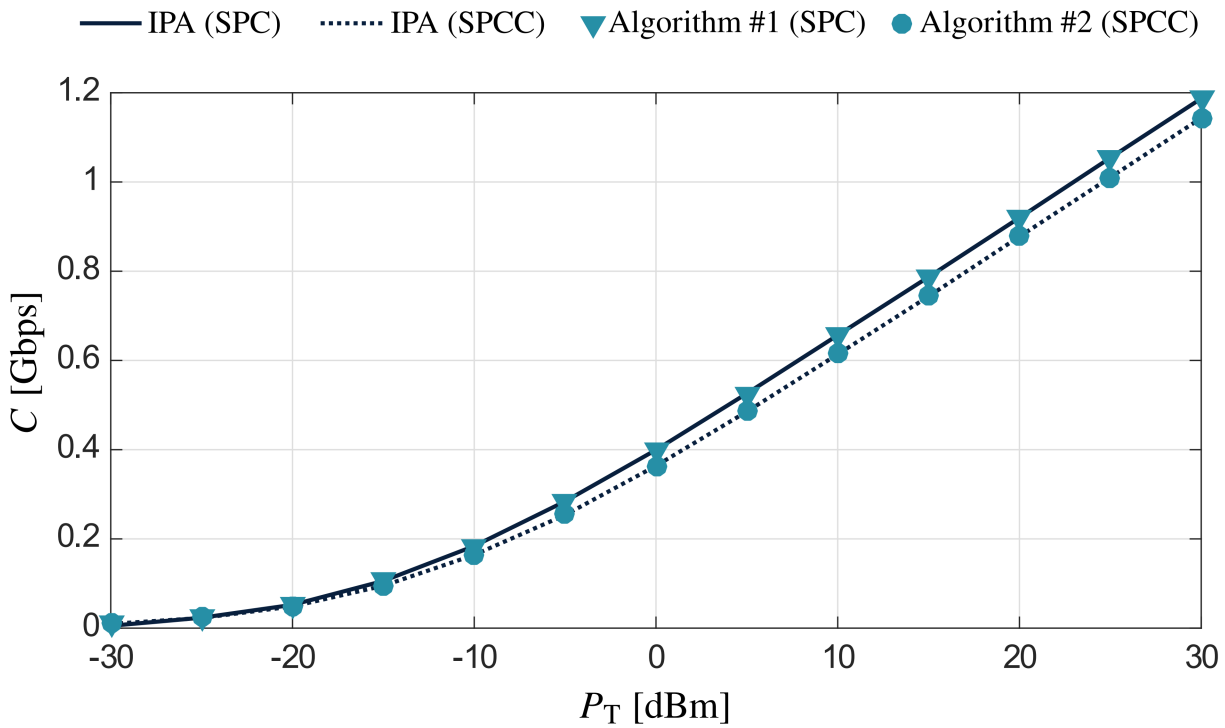

Source: Personal collection.

Figure 9 – Achievable data rate ratio versus α for different total transmission powers

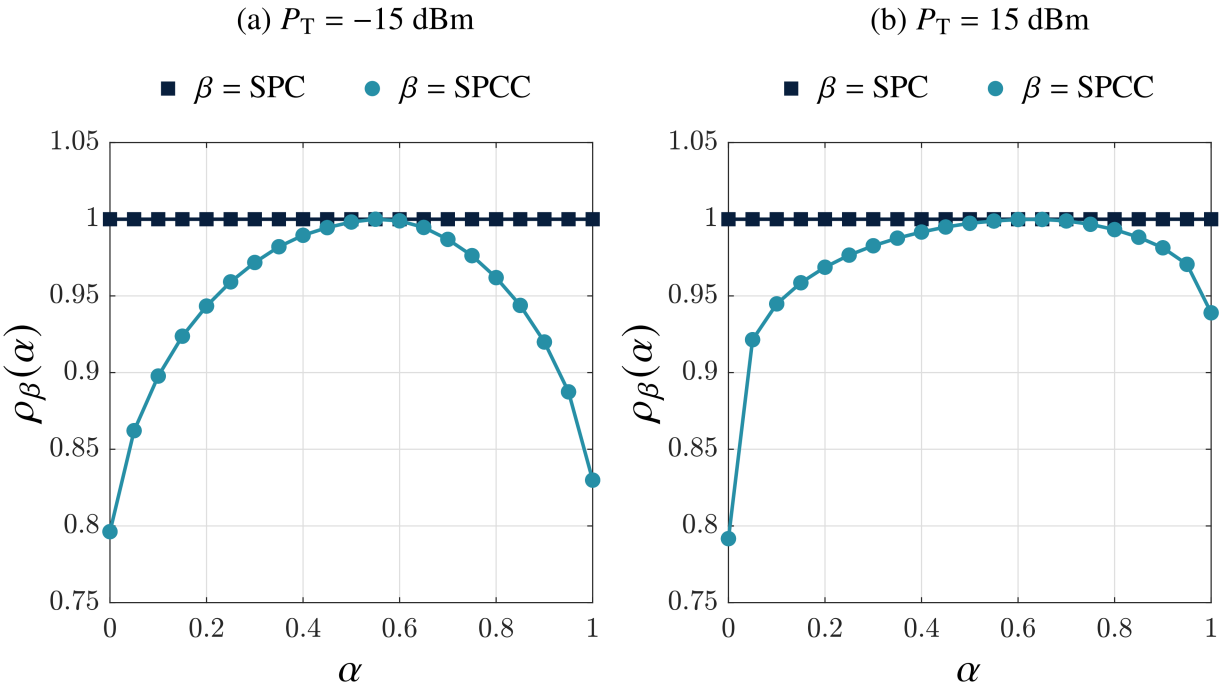

Source: Personal collection.

comparison between hybrid and non-hybrid systems, proving that the former outperforms the later in terms of achievable data rate. Note that if $\alpha = 1$, then all the available power is allocated to the first medium and therefore it is the same as considering only the wireless channel. On the other hand, $\alpha = 0$ implies in allocating the total transmission power to only the power line medium. For $P_T = -15$ dBm, to use only the first ($\alpha = 1$) or the second ($\alpha = 0$) media results in achievable data rates around to, respectively, 83% and 79% of the achievable data rate yielded by the optimal hybrid communication. For $P_T = 15$ dBm, these values are respectively 93% and 78%. Note that such percentages vary depending on the total transmission power due to the frequency selectivity of the considered channels as well. A final performance comparison between hybrid and non-hybrid systems is presented in Figure 10, where the achievable data rates obtained by Algorithm #2 is displayed for distinct α values. In this figure, the dominance of the HPWS over power line and wireless systems is clearly portrayed.

Now, a comparison among the proposed power allocation algorithms and other power allocation algorithms for HPWS is shown in Figure 11. In this figure, for comparison purpose, the conventional waterfilling and UA are considered as the previous power allocation algorithms. This comparison uses $\alpha = 0.6$, which is assumed to be as close as possible to the optimal when P_T ranges from -30 to 30 dBm. Due to such choice, Algorithms #1 and #2 yield equal performances, matching their achievable data rate results in the analyzed P_T range. By comparing the proposed power allocation algorithms with the previous ones, one can see that uniform power allocation yields the worst performance since it allocates power to subcarriers regardless of their nSNR values (i.e., subchannels with high or low nSNR values receive the same amount of power). In addition, the use of waterfilling results in the same performance as the proposed algorithms

Figure 10 – Achievable data rate as a function of P_{T} for Algorithm #2 with different α values

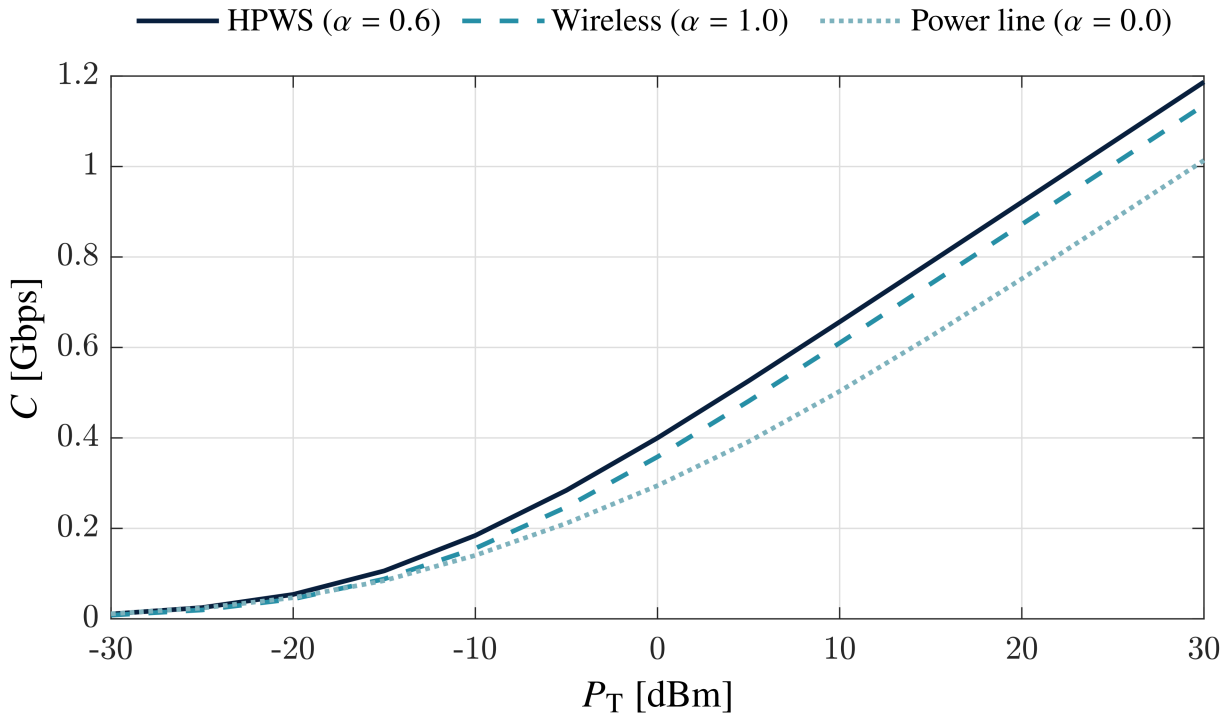

Source: Personal collection.

when low values of P_{T} are applied (e.g., $P_{\mathrm{T}} \leq -10$ dBm). In other words, the use of low values of the total transmission power shows that waterfilling allocates power only to the best subcarriers of each medium. Notwithstanding, there is a trend to the best subchannels of each medium to be at opposite sides in the $\overline{\gamma}_{1,i}/\overline{\gamma}_{2,i}$ curve (see Figure 6) and therefore the proposed power allocation algorithms tend to allocate the available power to the same subcarriers as the conventional waterfilling does. As P_{T} increases, the conventional waterfilling starts to allocate power to subcarriers of a medium that are already supplied by the other and, as a consequence, its performance decays until it matches the UA performance. The proposed power allocation algorithms, however, continue on their upward trajectories, offering achievable data rates greater than those of UA and waterfilling. It is worth mentioning that for $P_{\mathrm{T}} \to \infty$ or $P_{\mathrm{T}} \to 0$, all power allocation algorithms tend to be equal.

3.4.3 Transmission Power Benchmarks

This subsection aims to give benchmarks for transmission powers obtained from Algorithms #1 and #2 in order to make their reproducibility feasible. For this reason, simple and synthetic data are taken into account so that one can implement the proposed power allocation algorithms and check the obtained results based only on the information contained in this subsection. In this regard, it is considered that $\overline{\gamma}_{1,k} = 35$ dB and $\overline{\gamma}_{2,k} = 70 - 4k$ dB, $\forall k \in \{1, 2, \ldots, N_{\mathrm{S}}\}$, with $N_{\mathrm{S}} = 16$. Note that synthetic nSNR values are considered in this section only to make comparisons easier. In addition, the same frequency bandwidth as the previous results are assumed, i.e., $B_{\mathrm{w}} = 80$ MHz. Also, $P_1 = 0.5P_{\mathrm{T}}$ and $P_2 = 0.5P_{\mathrm{T}}$, therefore

Figure 11 – Performance comparison among the proposals, waterfilling, and uniform power allocation ($\alpha = 0.6$)

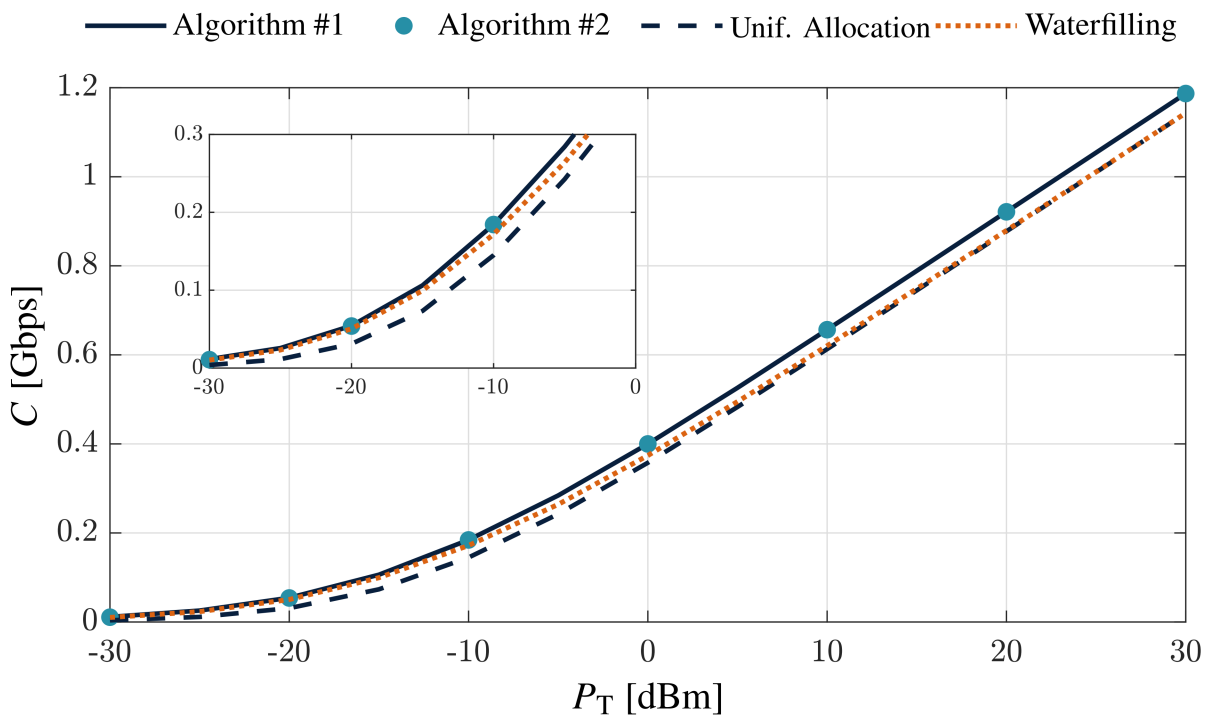

Source: Personal collection.

$\alpha = 0.5$.

Based on the given simulation environment, the transmission powers outputted by Algorithms #1 and #2 for $P_T = 10$ dBm are listed in Table 1. Observe that for $k \geq 9$ Algorithms #1 and #2 allocate the same power to all subcarriers. This occurs because the first medium becomes dominant and its nSNRs values are constant, being optimally used with constant power as well. In addition, Figure 12 shows the obtained achievable data rates for $P_T \in \{0, 2, \ldots, 30\}$ under the same conditions.

3.5 SUMMARY

This chapter has studied the optimal power allocation for hybrid power line/wireless systems when MRC and frequency-selective channels are considered and the additive noise is a colored Gaussian random process. Based on the achievable data rate, optimization problems dealing with two different situations have been formulated and solved. The former applied the sum power constraint, which consists of limiting the total transmission power, whereas the latter considered the sum power-channel constraint and therefore it limits not only the total transmission power but also the given power to each medium. Both constraints have been deeply analyzed and power allocation algorithms have been presented for them.

Table 1 – Transmission powers obtained from Algorithm #1 and #2 (P_T = 10 dBm)

k	Transmission power (μW)			
	Algorithm #1		Algorithm #2	
	$p_{1,k}$	$p_{2,k}$	$p_{1,k}$	$p_{2,k}$
1	0.0	799.3	0.0	657.6
2	0.0	798.9	0.0	657.2
3	0.0	798.0	0.0	656.3
4	0.0	795.6	0.0	653.9
5	0.0	789.6	0.0	647.9
6	0.0	774.4	0.0	632.8
7	0.0	736.5	0.0	594.8
8	0.0	641.1	0.0	499.4
9	483.3	0.0	625.0	0.0
10	483.3	0.0	625.0	0.0
11	483.3	0.0	625.0	0.0
12	483.3	0.0	625.0	0.0
13	483.3	0.0	625.0	0.0
14	483.3	0.0	625.0	0.0
15	483.3	0.0	625.0	0.0
16	483.3	0.0	625.0	0.0

Source: Personal collection.

Figure 12 – Achievable data rate as a function of P_T

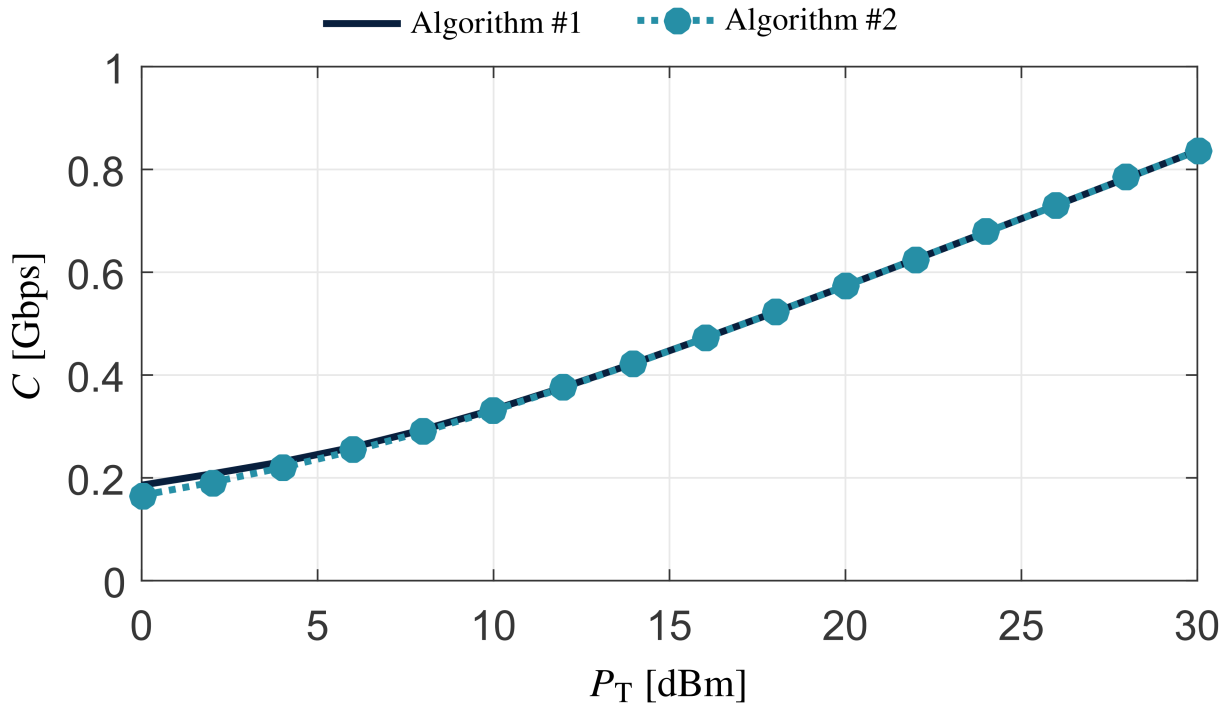

Source: Personal collection.

4 POWER ALLOCATION FOR MINIMIZING THE AVERAGE BIT ERROR PROBABILITY

Chapter 3 discussed the power allocation for maximizing the achievable data rate of HPWSs and showed that at most one medium should be used in the same subchannel index to maximize this parameter if MRC is used. Despite this advance, the investigation of power allocation techniques for minimizing the average BEP in the HPWS is an open problem as well. Motivated by recent findings on HPWS [36, 53], it was previously stated that HPWS is an appealing alternative for increasing the achievable data rate of a data communication system at a low computational cost; however, it can also be employed for improving the average BEP under similar constraints on hardware resource availability.

In [25], the optimal power allocation for minimizing the average BEP of OFDM schemes applied to a SIMO system was investigated. As the number of received antennas is equal to unity, the algorithm proposed by [25] does for the average BEP the same as waterfilling does for the achievable data rate. Such an algorithm, however, cannot be directly applied to HPWS due to less control of the transmission powers in a SIMO system than in a hybrid one. For this reason, power allocation for minimizing the average BEP of HPWS must be also investigated. Aiming to provide a comprehensive discussion on power allocation in HPWS and precisely fill this gap in the literature, this chapter investigates the power allocation for minimizing the average BEP in hybrid communication systems, by taken into account the OFDM scheme and the MRC technique. In this context, the major contributions of this chapter are stated as follows:

- The introduction of power allocation for minimizing the average BEP in hybrid communication system. In this regard, this chapter formulates the optimization problems under sum power and sum power-channel constraints. Their mathematical solutions are then provided for frequency-selective channels and ACGN. Consequently, it can be used to deal with flat channels and AWGN as well.

- The proposal of feasible power allocation algorithms for minimizing the average BEP in HPWSs for coherent modulations under sum power and sum power-channel constraints. The introduced power allocation algorithms based on an upper bound of the Q-function to achieve the minimal average BEP at low computational cost. Also, the proposed power allocation algorithms are validated and compared with other power allocation algorithms.

The rest of this chapter is presented as follows: Section 4.1 formulates the optimization problems associated with the minimization of the average BEP in hybrid communications systems, whereas Section 4.2 discusses their optimal solutions. Section 4.3 proposes power allocation algorithms for the HPWS. In Section 4.4, numerical simulations are provided for realistic power line and wireless data. Finally, concluding remarks are placed in Section 4.5.

4.1 PROBLEM FORMULATION

Let an OFDM scheme with N_S subcarriers be applied over a hybrid communication system as the one described in Chapter 2. In such an OFDM scheme, the cyclic prefix (CP) length is assumed to be $L_{CP} \geq \max_m\{L_m\} - 1$, with L_m denoting the CIR length associated with the m^{th} medium. In addition, the same OFDM symbol is simultaneously transmitted over all channels and the N_C received symbols are later combined. Therefore, $X_{1,k} = X_{2,k} = \ldots = X_{N_C,k}, \forall k$. In addition, the random symbol transmitted over the k^{th} subchannel is $X_k \in \mathcal{M}$, where $\mathcal{M}$ denotes an M-ary constellation. In other words, the same modulation is used over all subcarriers. By applying the MRC at the receiver side, the resulting SNR for the k^{th} subchannel can be again described as

$$\gamma_k = \sum_{m=1}^{N_C} p_{m,k}\overline{\gamma}_{m,k}, \forall k. \tag{4.1}$$

Regardless of the assumed transmission power constraints, i.e, SPC or SPCC, each subcarrier will experience a different SNR, γ_k, therefore a distinct BEP is obtained per subcarrier. The BEP, in its turn, depends on the digital modulation and can be defined as a function of γ_k as $P_{e,k}(\gamma_k)$. If the BEP is averaged over the subchannel indices, then it can be expressed as

$$\overline{P_e} = \frac{1}{N_S}\sum_k P_{e,k}\left(\sum_m p_{m,k}\overline{\gamma}_{m,k}\right). \tag{4.2}$$

Notice that using a combining technique makes the average BEP calculated in (4.2) essentially different from that of non-hybrid systems. Once the transmitter knows the values of $\overline{\gamma}_{m,k}$ (based on a feedback channel, for instance), a power allocation optimization problem related to the minimization of the average BEP in hybrid communication systems can be written as

$$\overline{P}_{e,\min} = \min_{p_{m,k}} \frac{1}{N_S}\sum_k P_{e,k}\left(\sum_m p_{m,k}\overline{\gamma}_{m,k}\right), \tag{4.3}$$

subject to either

$$\text{SPC}\begin{cases}\sum\limits_{m,k} p_{m,k} \leq P_T \\ p_{m,k} \geq 0, \ \forall\ k, m\end{cases} \tag{4.4}$$

or

$$\text{SPCC}\begin{cases}\sum\limits_{k} p_{m,k} \leq P_m, \ \forall m \\ p_{m,k} \geq 0, \ \forall\ k, m.\end{cases} \tag{4.5}$$

Although [25] formulated and solved a similar problem for a SIMO system, its results cannot be applied to a hybrid communication system with parallel channels since the last one has less control over the transmission power. In other words, hybrid transceivers can allocate the available power to distinct subcarriers and media, whereas a SIMO transceiver allocate the total transmission power only to different subcarriers. In this sense, the following research question arises: *"How could the transmission power be allocated in a hybrid communication system*

for minimizing the average bit error probability under the sum power or sum power-channel constraints?" Section 4.2 and Section 4.3 present answers to this research question.

4.2 OPTIMAL POWER ALLOCATION FOR MINIMIZING THE AVERAGE BIT ERROR PROBABILITY

To solve the optimization problem described in Section 4.1, the BEP equation must be properly defined. The BEP is calculated at the demodulator input, which coincides with the output of the maximal-ratio combiner. At this point, the frequency-domain additive noise can be modeled by a Gaussian random variable - see Chapter 2. Hence the BEP equations for Gaussian channels can be used. In this regard, they can be expressed as follows [98]:

$$P_{\mathrm{e},k}(\gamma_k) \approx a_M Q\left(\sqrt{b_M \gamma_k}\right), \tag{4.6}$$

where a_M and b_M are functions of the constellation order, M, and depend on the adopted modulation; $Q(\cdot)$ is the complementary cumulative distribution function (CDF) of the standard Gaussian distribution. Table 2 lists a_M and b_M for some of the most used coherent modulations, such as pulse amplitude modulation (PAM), phase-shift keying (PSK), and quadrature amplitude modulation (QAM).

Once the BEP at the k^{th} subchannel is given by (4.6), the average BEP described by (4.2) can be rewritten as

$$\overline{P_{\mathrm{e}}} = \frac{a_M}{N_{\mathrm{S}}} \sum_k Q\left(\sqrt{b_M \sum_m p_{m,k} \overline{\gamma}_{m,k}}\right). \tag{4.7}$$

In order to investigate the convexity of $\overline{P_{\mathrm{e}}}$, let the derivative of (4.7) with respect to p_{m_1,k_1} be

Table 2 – a_M and b_M as a function of the modulation order, M, for different coherent modulations [98]

Modulation		a_M	b_M
M-PAM		$\frac{2(M-1)}{M\log_2(M)}$	$\frac{3}{M^2-1}$
M-PSK	$M=2$	1	1
	$M>2$	$\frac{2}{\log_2(M)}$	$2\sin^2(\pi/M)$
M-QAM	Rectangular	$\frac{4(\sqrt{M}-1)}{\sqrt{M}\log_2(M)}$	$\frac{3}{M-1}$
	Non-rectangular	$\frac{4}{\log_2(M)}$	$\frac{3}{M-1}$

Source: Personal collection.

given by

$$\frac{\partial \overline{P_{\mathrm{e}}}}{\partial p_{m_1,k_1}} = \frac{a_M}{N_{\mathrm{S}}} \frac{\partial}{\partial p_{m_1,k_1}} \left[Q\left(\sqrt{b_M \sum_m p_{m,k_1} \overline{\gamma}_{m,k_1}} \right) \right] \tag{4.8}$$

$$= \frac{a_M}{N_{\mathrm{S}}} \left[Q'\left(\sqrt{b_M \gamma_{k_1}} \right) \left(\frac{b_M \overline{\gamma}_{m_1,k_1}}{2\sqrt{b_M \gamma_{k_1}}} \right) \right], \tag{4.9}$$

$\forall m_1 \in \{1, 2, \ldots, N_{\mathrm{C}}\}$ and $k_1 \in \{1, 2, \ldots, N_{\mathrm{S}}\}$, where $Q'(x) = -1/\sqrt{2\pi} \exp(-x^2/2)$ represents the derivative of the Q-function; and $\gamma_{k_1} = \sum_m p_{m,k_1} \overline{\gamma}_{m,k_1}$. Hence, the first derivative of $\overline{P_{\mathrm{e}}}$ with respect to p_{m_1,k_1} is given by

$$\frac{\partial \overline{P_{\mathrm{e}}}}{\partial p_{m_1,k_1}} = \frac{-a_M b_M \overline{\gamma}_{m_1,k_1}}{2N_{\mathrm{S}}\sqrt{2\pi}} \left[\exp\left(-\frac{b_M}{2} \gamma_{k_1} \right) \frac{1}{\sqrt{b_M \gamma_{k_1}}} \right], \forall m_1, k_1. \tag{4.10}$$

The second derivative of $\overline{P_{\mathrm{e}}}$ with respect to p_{m_2,k_2} can be then given by

$$\frac{\partial^2 \overline{P_{\mathrm{e}}}}{\partial p_{m_2,k_2} \partial p_{m_1,k_1}} = \frac{-a_M b_M \overline{\gamma}_{m_1,k_1}}{2N_{\mathrm{S}}\sqrt{2\pi}} \frac{\partial}{\partial p_{m_2,k_2}} \left[\exp\left(-\frac{b_M}{2} \gamma_{k_1} \right) \frac{1}{\sqrt{b_M \gamma_{k_1}}} \right]. \tag{4.11}$$

Note that $\partial^2 \overline{P_{\mathrm{e}}} / \partial p_{m_2,k_2} \partial p_{m_1,k_1} = 0$ if $k_1 \neq k_2$. On the other hand, if $k_1 = k_2$, then

$$\frac{\partial^2 \overline{P_{\mathrm{e}}}}{\partial p_{m_2,k_2} \partial p_{m_1,k_1}} = \frac{-a_M b_M \overline{\gamma}_{m_1,k_1}}{2N_{\mathrm{S}}\sqrt{2\pi}} \left[-\exp\left(-\frac{b_M}{2} \gamma_{k_1} \right) \frac{b_M \overline{\gamma}_{m_2,k_1}}{2\sqrt{b_M \gamma_{k_1}}} - \right.$$

$$\left. - \exp\left(-\frac{b_M}{2} \gamma_{k_1} \right) \frac{b_M \overline{\gamma}_{m_2,k_1}}{2(b_M \gamma_{k_1})^{\frac{3}{2}}} \right] \tag{4.12}$$

$$= \underbrace{\frac{a_M b_M^2 \overline{\gamma}_{m_1,k_1} \overline{\gamma}_{m_2,k_1}}{4N_{\mathrm{S}}\sqrt{2\pi}}}_{\in \mathbb{R}^+} \underbrace{\exp\left(-\frac{b_M}{2} \gamma_{k_1} \right)}_{\in \mathbb{R}^+} \underbrace{\left(\frac{1 + \left(b_M \gamma_{k_1} \right)^{-1}}{\sqrt{b_M \gamma_{k_1}}} \right)}_{\in \mathbb{R}^+}. \tag{4.13}$$

All terms of the above equation are real and positive numbers. Therefore, the Hessian matrix of the objective function is positive semi-definite within the considered domain of $p_{m,k}$ and therefore (4.7) is convex [92].

In addition to the objective function being convex, all constraints established in (4.4) and (4.5) are linear (affine) functions and therefore Slater's condition holds [92]. The KKT conditions can be then applied for achieving the optimal solutions. The first step to finding such solutions is to define the derivative of the *Lagrangian* for the optimization problem under both SPC and SPCC. For the SPCC, one has

$$\frac{\partial \mathcal{L}}{\partial p_{q,i}} = \frac{1}{N_{\mathrm{S}}} \frac{\partial P_{\mathrm{e},i}(p_{q,i})}{\partial p_{q,i}} + \lambda_q - \mu_{q,i}, \tag{4.14}$$

$\forall q \in \{1, 2, \ldots, N_{\mathrm{C}}\}$ and $i \in \{1, 2, \ldots, N_{\mathrm{S}}\}$; where $\lambda_q \in \mathbb{R}^+$ and $\mu_{q,i} \in \mathbb{R}^+$ are *Lagrange* multipliers. Whereas $\mu_{q,i}$ is associated with the transmission power being equal to or greater

than zero in every subcarrier and media, λ_q relates to the sum-power channel constraint. For the SPC, one can just omit the subscript q of λ_q in (4.14).

In sequel, the KKT conditions can be used for obtaining the following system of equations:

$$\frac{1}{N_{\mathrm{S}}}\frac{\partial P_{\mathrm{e},i}(p_{q,i})}{\partial p_{q,i}} + \lambda_q - \mu_{q,i} = 0, \forall q, i \tag{4.15}$$

$$\mu_{q,i}(-p_{q,i}) = 0, \forall q, i \tag{4.16}$$

$$\lambda\left(\sum_{q,i} p_{q,i} - P_{\mathrm{T}}\right) = 0, \quad \text{if SPC} \tag{4.17}$$

$$\lambda_q\left(\sum_{i} p_{q,i} - P_q\right) = 0, \forall q \quad \text{if SPCC.} \tag{4.18}$$

Based on (4.10) and (4.15), one can obtain the equation as follows

$$\frac{\lambda_q - \mu_{q,i}}{\overline{\gamma}_{q,i}} = \frac{a_M b_M}{2N_{\mathrm{S}}\sqrt{2\pi}} \exp\left(-\frac{b_M}{2}\gamma_i\right) \frac{1}{\sqrt{b_M \gamma_i}}, \forall q, i, \tag{4.19}$$

in which $\gamma_i = \sum_m p_{m,i}\overline{\gamma}_{m,i}$. Note that the right side of the above equation does not depend on the medium index q and, therefore, for any two media $c \in \{1, 2, \ldots, N_{\mathrm{C}}\}$ and $d \in \{1, 2, \ldots, N_{\mathrm{C}}\}$, one has the following equation:

$$\frac{\overline{\gamma}_{c,i}}{\overline{\gamma}_{d,i}} = \frac{\lambda_c - \mu_{c,i}}{\lambda_d - \mu_{d,i}}, \forall i. \tag{4.20}$$

Such an equation is precisely the same as (3.30) obtained by Chapter 3 for the maximization of the achievable data rate. From now, sum power and sum power-channel constraints are addressed separately hereafter.

4.2.1 Sum Power Constraint

As the SPC is assumed, (4.20) results in

$$\frac{\overline{\gamma}_{c,i}}{\overline{\gamma}_{d,i}} = \frac{\lambda - \mu_{c,i}}{\lambda - \mu_{d,i}}, \forall i. \tag{4.21}$$

From (4.16), for both $p_{c,i} \neq 0$ and $p_{d,i} \neq 0$, the values of $\mu_{c,i}$ and $\mu_{d,i}$ have to be null, which would imply in $\overline{\gamma}_{c,i} = \overline{\gamma}_{d,i}$ from (4.21). On the other hand, in order to have $p_{c,i} \neq 0$ and $p_{d,i} = 0$, it is required that $\mu_{c,i} = 0$ and $\mu_{d,i} \geq 0$, which result in $\overline{\gamma}_{c,i} \geq \overline{\gamma}_{d,i}$. Therefore, only one medium must be used per subchannel index unless two or more media have the greatest and equal nSNRs. Hence, a resulting nSNR in the k^{th} subchannel can be defined as

$$\overline{\gamma}_k \triangleq \max_m \{\overline{\gamma}_{m,k}\}, \forall k. \tag{4.22}$$

This finding indicates that the use of SC or MRC techniques imply in the same performance if power allocation is performed, and it is identical to the result obtained for the maximization of the achievable data rate in Chapter 3.

4.2.2 Sum Power-Channel Constraint

When the SPCC is considered, the analysis of (4.20) for a given subchannel $I \in \{1, 2, \ldots, N_S\}$ is helpful. Similar to Chapter 3, the following remarks can be stated:

- For a given subchannel I for which $\frac{\overline{\gamma}_{c,I}}{\overline{\gamma}_{d,I}} > \frac{\lambda_c}{\lambda_d}$, the value of $\mu_{b,I}$ must be greater than zero in order to decrease the denominator on the right side of (4.20). As a consequence, $p_{d,I} = 0$.
- For a given subchannel I for which $\frac{\overline{\gamma}_{c,I}}{\overline{\gamma}_{d,I}} < \frac{\lambda_c}{\lambda_d}$, the numerator on the right side of (4.20) must decrease. Therefore, $\mu_{c,I}$ must be greater than zero and then $p_{c,I} = 0$.

For a given subchannel I such that $\frac{\overline{\gamma}_{c,I}}{\overline{\gamma}_{d,I}} = \frac{\lambda_c}{\lambda_d}$, it is not possible to affirm whether the transmission powers $p_{c,I}$ and $p_{d,I}$ will be equal to zero or not. In a practical situation, however, the probability of $\frac{\overline{\gamma}_{c,I}}{\overline{\gamma}_{d,I}}$ being exactly equal to $\frac{\lambda_c}{\lambda_d}$ is extremely low due to the frequency selectivity of the associated channels. Thus, its occurrence can be disregarded with negligible performance losses. In particular, there are only two theoretical cases where this equality can hold: c and d have equal nSNRs; or the conditions for data communication in one medium are much better than in the other, i.e., the nSNR values or transmission power of a medium are very high compared to those of the other. Given that c and d can be any combination of N_C taken two at a time, the probability of two or more media being used in the same subcarrier index for minimizing the average BEP is quite low.

4.2.3 Further Comments

The literature has shown that transmitting the same information through different media can benefit data communication if the SNRs are within similar ranges [36]. In contrast, it is here demonstrates that transmitting the same information through different media (i.e., receive diversity) may be equivalent to wasting resources (e.g., transmission power) if the transmitter knows the instantaneous nSNRs of the considered media. Interestingly, it holds even when there are distinct power constraints over the involved media.

Focused on maximizing the achievable data rate, Chapter 3 showed that at most one medium should be used per subchannel if the transmitter has the instantaneous knowledge of the nSNRs. In the current chapter, it is proved that this is also valid for the minimization of the bit error probability and therefore it holds for data communication in general, which is significantly strong. In this context, the following cases deserve attention:

- Case #1: All nSNR values in one medium are higher than their counterparts in the other medium within the hybrid coherence time. For instance, $\overline{\gamma}_{1,k} \geq \overline{\gamma}_{2,k}, \forall k$.
- Case #2: There is no dominance of one medium over the other in terms of nSNR within the hybrid coherence time. Therefore, $\exists k | \overline{\gamma}_{1,k} \leq \overline{\gamma}_{2,k}$ and $\exists k | \overline{\gamma}_{1,k} \geq \overline{\gamma}_{2,k}$.

If the SPC is assumed, the media diversity should not be exploited in Case #1, i.e., HPWSs should only allocate power to the medium with higher nSNR values to achieve the best performance.

On the other hand, Case #2 means that the existing diversity between both channels can be exploited to improve the system performance compared to the non-hybrid mode. Assuming the SPCC, the occurrence of Cases #1 or #2 does not result in using only one medium over the entire frequency band since the total transmission power must be used in all media. However, the theoretical findings suggest using at most one medium per subchannel index for maximizing the available resources.

4.3 POWER ALLOCATION ALGORITHMS FOR HPWSs

In this section, power allocation algorithms are proposed for minimizing the average BEP in HPWSs under SPC and SPCC. Those power allocation algorithms aim to solve the system of equations composed of the KKT conditions (4.15)-(4.19). Nonetheless, dealing with (4.19) is not an easy task due to its shape. A possible solution is to implement a general optimization solver, such as the interior-point algorithm [99]. However, it requires high computational cost to obtain the exact solution (see [99] for further information). An alternative and feasible solution is to use an approximation for $P_{\mathrm{e},k}(\cdot)$ and consequently replace (4.19) by a simpler equation.

In [100], useful bounds for the Q-function are presented. Among them, it is that $Q(x) \leq (1/2)\exp(-x^2/2)$. Following [25], the given upper bound is applied into the objective function so that it can be expressed as

$$\overline{P_{\mathrm{e}}} = \frac{a_M}{2N_{\mathrm{S}}} \sum_k \exp\left(\frac{-b_M}{2} \sum_m p_{m,k}\overline{\gamma}_{m,k}\right). \tag{4.23}$$

Similar to Section 4.2, it can be proved that such an objective function is also convex and therefore a unique and optimal solution solves the system of equations composed of the KKT conditions. Now, (4.19) is replaced by the following equation:

$$\frac{\lambda_q - \mu_{q,i}}{\overline{\gamma}_{q,i}} = \frac{a_M b_M}{4N_{\mathrm{S}}} \exp\left(\frac{-b_M}{2} \sum_m p_{m,i}\overline{\gamma}_{m,i}\right), \forall q, i. \tag{4.24}$$

Again, the medium index q does not affect the right side of the above equation and, for this reason, (4.20) also holds for this objective function. As a consequence, all conclusions for the objective function given by (4.7) are also valid for (4.23). Moreover, Park's algorithm [25] solves a similar system of equations with a focus on non-hybrid system; therefore, it will be helpful hereafter.

4.3.1 Sum Power Constraint

Once the conclusions of the previous section are also valid for the current objective function, the procedure to obtain a power allocation algorithm for the HPWS assuming the SPC is straightforward. First, an equivalent data communication medium composed of only the subchannels with the highest nSNRs among all media is defined based on (4.22). Then the optimization problem subjected to the SPC is reduced to the non-hybrid case and, as a

consequence, running Park's algorithm [25] is sufficient to obtain the power transmission values allocated to all subcarriers. Algorithm #3 is proposed to find the transmission powers that minimize the average BEP in HPWS under the SPC. As a result, the final solution can be achieved at a computational cost of order $O(N)$ (see Chapter 3).

Algorithm #3: Power allocation algorithm for minimizing the average BEP in HPWS under the SPC

Input :

$\overline{\gamma}_{1,k}$ is the nSNR of the 1st medium ($m = 1$) and k^{th} subchannel, $k \in \{1, 2, \ldots, N_{\text{S}}\}$

$\overline{\gamma}_{2,k}$ is the nSNR of the 2nd medium ($m = 2$) and k^{th} subchannel, $k \in \{1, 2, \ldots, N_{\text{S}}\}$

P_{T} is the total transmission power

Mod is the coherent modulation

M is the modulation order

Output :

$p_{1,k}$ is the power allocated to the 1st medium and k^{th} subchannel, $k \in \{1, 2, \ldots, N_{\text{S}}\}$

$p_{2,k}$ is the power allocated to the 2nd medium and k^{th} subchannel, $k \in \{1, 2, \ldots, N_{\text{S}}\}$

begin

$\mathcal{K} = \{1, 2, \ldots, N_{\text{S}}\}$;

$p_{1,k} = 0, \forall k \in \mathcal{K}$;

$p_{2,k} = 0, \forall k \in \mathcal{K}$;

$\{\overline{\gamma}_k\} = \max\{\overline{\gamma}_{1,k}, \overline{\gamma}_{2,k}\}, \forall k \in \mathcal{K}$;

$\{q\} = \arg\max\{\overline{\gamma}_{1,k}, \overline{\gamma}_{2,k}\}, \forall k \in \mathcal{K}$;

$[\{p_k\}, \lambda] = \text{ParkAlgorithm}(\{\overline{\gamma}_k\}, P_{\text{T}}, Mod, M), \forall k \in \mathcal{K}$;

$\{p_{q,k}\} = \{p_k\}$;

end

4.3.2 Sum Power-Channel Constraint

Assuming SPCC, let power line and wireless media be defined by $c = 1$ and $d = 2$. It was previously concluded that nSNR ratio values above and below the λ_1/λ_2 ratio are respectively characterized by $p_{2,i} = 0$ and $p_{1,i} = 0$. By applying such values into (4.24) and based on the fact that $\mu_{q,i} \geq 0$, the following equations can be obtained:

- $p_{1,i} = 0$:

$$\frac{a_M b_M}{4N_{\text{S}}} \exp\left(\frac{-b_M}{2} p_{2,i} \overline{\gamma}_{2,i}\right) = \frac{\lambda_2 - \mu_{2,i}}{\overline{\gamma}_{2,i}} \tag{4.25}$$

and

$$p_{2,i} \geq \frac{-2}{b_M \overline{\gamma}_{2,i}} \ln\left(\frac{4N_{\text{S}}\lambda_1}{a_M b_M \overline{\gamma}_{1,i}}\right). \tag{4.26}$$

- $p_{2,i} = 0$:

$$\frac{a_M b_M}{4N_{\text{S}}} \exp\left(\frac{-b_M}{2} p_{1,i} \overline{\gamma}_{1,i}\right) = \frac{\lambda_1 - \mu_{1,i}}{\overline{\gamma}_{1,i}} \tag{4.27}$$

and

$$p_{1,i} \geq \frac{-2}{b_M \overline{\gamma}_{1,i}} \ln\left(\frac{4N_S\lambda_2}{a_M b_M \overline{\gamma}_{2,i}}\right). \tag{4.28}$$

In Chapter 3, Algorithm #2 was proposed to solve a similar problem aimed at maximizing the achievable data rate. The differences between that problem and the current one are on the structure of (4.25) to (4.28). Whereas in Chapter 3 (4.25) and (4.27) were solved by the waterfilling algorithm, they can here be solved by the Park's algorithm [25]. Therefore, a similar algorithm structure can be used just by changing the parts related to those equations. In this sense, Algorithm #4 is designed to output transmission powers that minimize the average BEP in HPWS under the SPCC. Such an algorithm attains computation cost of order $O(N^2)$, just as presented in Chapter 3, and therefore it is of reasonable implementation. The overall idea is the same, i.e., to sweep the λ_1/λ_2 ratio from $\min_i\{\overline{\gamma}_{1,i}/\overline{\gamma}_{2,i}\}$ up to $\max_i\{\overline{\gamma}_{1,i}/\overline{\gamma}_{2,i}\}$ and, at each iteration, to run a Park's algorithm [25] for the subcarriers above λ_1/λ_2 and another one for subcarriers below it. After finding the powers, the restrictions defined by (4.26) and (4.28) are verified and then the final result is defined by the iteration with the lowest number of violated restrictions, which is zero for the optimal situation.

4.4 NUMERICAL ANALYSES

In this section, the effectiveness of the power allocation algorithms proposed for minimizing the average BEP of the HPWS under sum power and sum power-channel constraints is evaluated. In this regard, the performances of the proposed power allocation algorithms are validated through a comparison with the optimal solutions, which are obtained by the IP method [96, 99]. The IP method provides the optimal solutions because it minimizes (4.7), whereas the proposed power allocation algorithms minimizes (4.23). Furthermore, comparisons with other power allocation algorithms are carried out. In particular, Park's algorithm [25], UA, and the algorithms proposed for maximizing the achievable data rate in Chapter 3 are taken into account.

In order for all power allocation algorithms to be fairly compared, all of them assume complete knowledge of the power line and wireless nSNRs. Furthermore, the average BEP achieved by any of the power allocation algorithms is calculated using the same equation, although the considered algorithms seek to optimize different equations. After obtaining the transmission powers that are given by each of them, the average BEP is computed by (4.7). Moreover, the total number of subchannels is $N_S = 128$ and the number of channels is $N_C = 2$ (i.e., the HPWS). Also, the assumed total transmission power is within the following range $P_T \in [-20, 25]$ dBm. For results associated with the SPCC, $P_1 = \alpha P_T$ and $P_2 = (1-\alpha)P_T$, with $\alpha \in [0, 1]$. Those relations are also applied to obtain numerical results using UA and Park's algorithms, where the power allocation is performed for each medium individually after split the total transmission power between power line and wireless parts.

Algorithm #4: Power allocation algorithm for minimizing the average BEP in HPWS under the SPCC

Input :

$\overline{\gamma}_{1,k}$ is the nSNR of the 1st medium ($m = 1$) and k^{th} subchannel, $k \in \{1, 2, \ldots, N_{\text{S}}\}$

$\overline{\gamma}_{2,k}$ is the nSNR of the 2nd medium ($m = 2$) and k^{th} subchannel, $k \in \{1, 2, \ldots, N_{\text{S}}\}$

P_1 is the maximum transmission power to be distributed in the first medium

P_2 is the maximum transmission power to be distributed in the second medium

Mod is the coherent modulation

M is the modulation order

Output :

$p_{1,k}$ is the power allocated to the 1st medium and k^{th} subchannel, $k \in \{1, 2, \ldots, N_{\text{S}}\}$

$p_{2,k}$ is the power allocated to the 2nd medium and k^{th} subchannel, $k \in \{1, 2, \ldots, N_{\text{S}}\}$

begin

$p_{1,k} = 0, \forall k$;

$p_{2,k} = 0, \forall k$;

Compute a_M and b_M from Mod and M;

$\mathcal{A} = \{1, 2, \ldots, N_{\text{S}}\}$;

$\mathcal{B} = \varnothing$;

$\mathcal{A}_{\text{v}} = \mathcal{A}$;

$\mathcal{B}_{\text{v}} = \mathcal{B}$;

$N_{\text{v}} = N_{\text{S}}$;

while $[(\mathcal{A}_{\text{v}} \cup \mathcal{B}_{\text{v}}) \neq \varnothing]$ & $[\text{Card}\{\mathcal{B}\} \neq N_{\text{S}} - 1]$ **do**

$q = \arg\min_{\mathcal{A}} \{\overline{\gamma}_{1,a}/\overline{\gamma}_{2,a}\}, \forall a \in \mathcal{A}$;

$\mathcal{A} = \mathcal{A} - q$;

$\mathcal{B} = \mathcal{B} \cup q$;

$[\{p_{1,a}\}, \lambda_1] = \text{ParkAlgorithm}(\{\overline{\gamma}_{1,a}\}, P_1, Mod, M), \forall a \in \mathcal{A}$;

$[\{p_{1,b}\}, \lambda_2] = \text{ParkAlgorithm}(\{\overline{\gamma}_{2,b}\}, P_2, Mod, M), \forall b \in \mathcal{B}$;

$\mathcal{A}_{\text{v}} = \left\{a \in \mathcal{A} | \exp\left(\frac{-b_M p_{1,a} \overline{\gamma}_{1,a}}{2}\right) > \frac{4N_{\text{S}}\lambda_2}{a_M b_M \overline{\gamma}_{2,a}}\right\}$;

$\mathcal{B}_{\text{v}} = \left\{b \in \mathcal{B} | \exp\left(\frac{-b_M p_{2,b} \overline{\gamma}_{2,b}}{2}\right) > \frac{4N_{\text{S}}\lambda_1}{a_M b_M \overline{\gamma}_{1,b}}\right\}$;

if $\text{Card}\{\mathcal{A}_{\text{v}} \cup \mathcal{B}_{\text{v}}\} \leq N_{\text{v}}$ **then**

$\mathcal{X} = \mathcal{A}$;

$\mathcal{Y} = \mathcal{B}$;

$p_{1,x} = p_{1,a}, \forall x \in \mathcal{X}$;

$p_{2,y} = p_{2,b}, \forall y \in \mathcal{Y}$;

$N_{\text{v}} = \text{Card}\{\mathcal{A}_{\text{v}} \cup \mathcal{B}_{\text{v}}\}$;

end

end

$p_{1,k} = p_{1,x}, \forall k \in \mathcal{X}$;

$p_{2,k} = p_{2,y}, \forall k \in \mathcal{Y}$;

end

4.4.1 Channel Impulse Response and Additive Noise

In this chapter, numerical results considers the same nSNRs of Chapter 3, which comply with broadband power line [79] and wireless [94] communication standards. The power line nSNRs originate from channel impulse response and additive noise PSD of a measurement campaign for broadband and in-home PLC, reported in [15]. The considered channel is filtered by a rectangular window in the frequency band $1.7 - 81.7$ MHz. The wireless nSNRs, on the other hand, came from the wideband wireless channel model reported in [97] and circularly symmetric complex AWGN model. In addition, the wireless channel considers a total frequency bandwidth equal to 80 MHz centered at 5.8 GHz. Similar to Chapter 3, the noise power on the wireless medium is computed so that $\sum_k |\overline{\gamma}_{1,k}| = \sum_k |\overline{\gamma}_{2,k}|$ in order to only evaluate the existing diversity between power line and wireless channels.

4.4.2 Average Bit Error Probability Analysis

In Figures 13(a) and 13(b), the performances of Algorithms #3 and #4 are compared with the optimal solutions, which are achieved by the interior-point algorithm (denoted by IPA). Figures 13(a) and 13(b) respectively consider PSK and square QAM constellations, with $\alpha = 0.5$ being assumed for the SPCC results. For both QAM and PSK, the performances of Algorithms #3 and #4 match the IPA performances if $P_{\mathrm{T}} \geq 10$ dBm, regardless of the modulation order. As practical situations usually assume $P_{\mathrm{T}} > 10$ dBm, it can be stated that the proposed power allocation algorithms yield imperceptible performance losses compared to the optimal solution in realistic scenarios. For $P_{\mathrm{T}} < 10$ dBm, Algorithms #3 and #4 slightly disagree with the IPA since the upper bound of the Q-function worsens. Nonetheless, the gap between the average BEP of the proposed power allocation algorithms and IP-based algorithms is still quite small. Such a gap is, for example, less than 10^{-1} for 16-PSK and 64-QAM. Notice that the greater is M, the lower is b_M and the argument of the Q-function - see Table 2 and (4.6). For this reason, the impact of low P_{T} values is more evident when M increases.

Similar to Chapter 3, the transmission power constraints, SPC and SPCC, are compared based on the average BEP ratio:

$$\rho^{\beta}(\alpha) \triangleq \frac{\overline{P_{\mathrm{e}}}^{\beta}(\alpha)}{\overline{P_{\mathrm{e}}}^{\mathrm{SPC}}(\alpha)}, \tag{4.29}$$

with $\beta \in \{\mathrm{SPC},\mathrm{SPCC}\}$ and $\overline{P_{\mathrm{e}}}^{\mathrm{SPC}}(\alpha)$ and $\overline{P_{\mathrm{e}}}^{\mathrm{SPCC}}(\alpha)$ being computed based on the outputs of Algorithms #3 and #4. Again, the optimal value of α_{opt} is the one in which $\rho^{\mathrm{SPC}}(\alpha_{\mathrm{opt}}) = \rho^{\mathrm{SPCC}}(\alpha_{\mathrm{opt}})$. In addition, the states $\alpha = 0$ and $\alpha = 1$ can be used to compare the performances of hybrid and non-hybrid system in terms of average BEP. All the available power is allocated to the first medium if $\alpha = 1$ and, as a consequence, only the wireless channel is considered. On the other hand, if $\alpha = 0$, then the total transmission power is allocated only to the power line channel. Also, QAM is adopted henceforth; however, similar conclusions can be drawn for other coherent modulation schemes.

Figure 13 – Average BEP as a function of P_{T} for Algorithms #3 and #4 and IP-based algorithms ($\alpha = 0.5$)

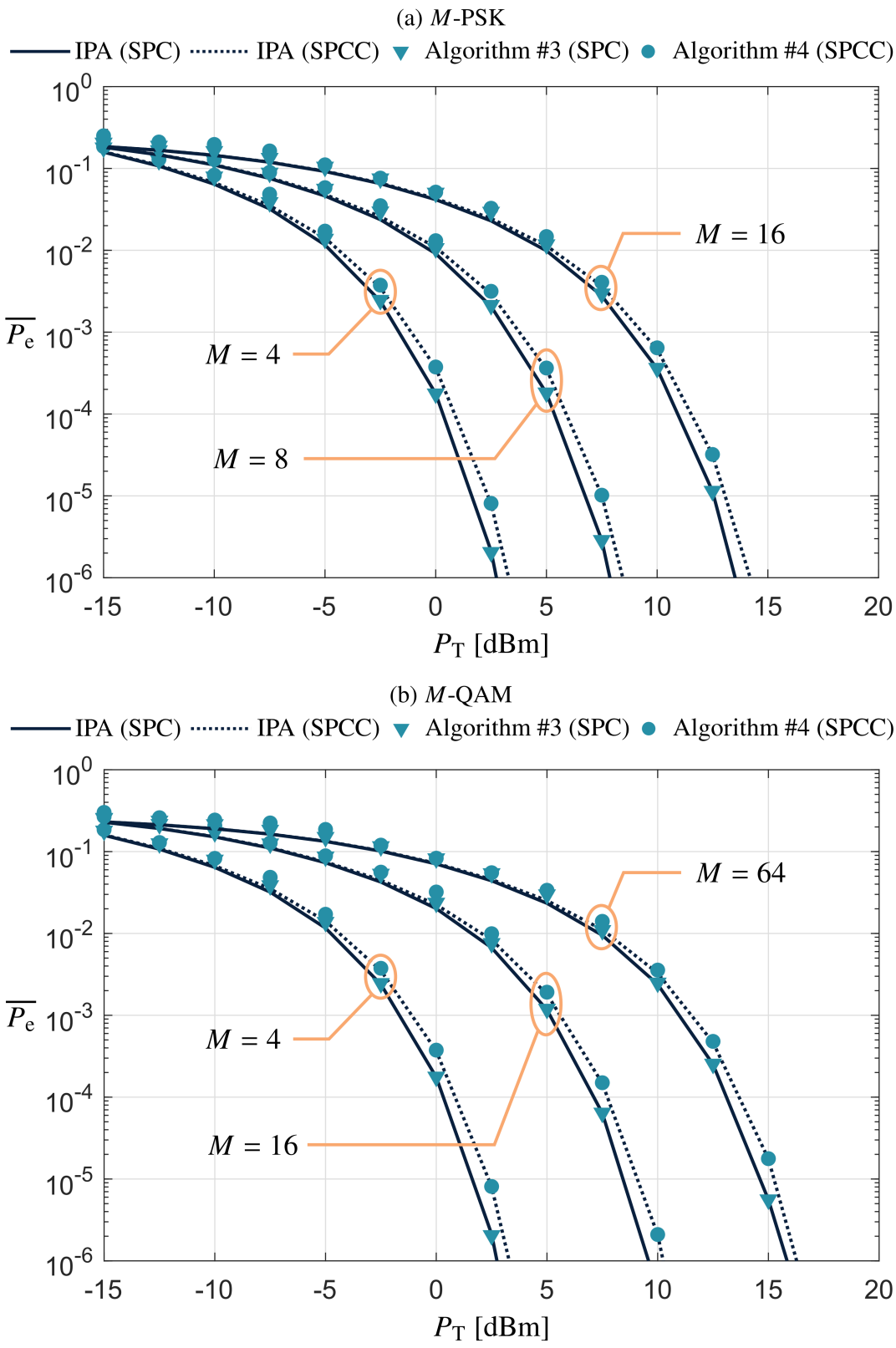

Source: Personal collection.

Figures 14 and 15 respectively show the average BEP ratio for 4-QAM and 16-QAM with zooms inside. Also, total transmission power values equal to -10 dBm and 5 dBm are taken into account. First of all, it is observed that the SPC results define a lower bound for the SPCC results, which is contrary to what was seen for the achievable data rate in Chapter 3. Due to the larger number of constraints of the SPCC (one by channel) compared to the SPC, the best performances are always associated with the SPC, which is visually observed as an upper bound in case of achievable data date analyses and as a lower bound if the average BEP is considered. Furthermore, the value of α_{opt} changes not only with the total transmission power, but also with the modulation order M. To illustrate it, Table 3 lists the optimal α for the cases presented in Figures 14 and 15. This behavior is associated with the different frequency selectivity of power line and wireless channels as well as the nonlinearity of the Q-function. Finally, by comparing non-hybrid (i.e., $\alpha = 0$ and $\alpha = 1$) and hybrid performances, it is shown that the higher the total transmission power, the greater the dominance of hybrid systems over the non-hybrid systems in terms of average BEP. For instance, for $P_{\text{T}} = -10$ dBm, the average BEP ratio between hybrid and non-hybrid performance may range from 1.2 to almost 3.0, whereas it ranges from 5.8 to much more than 10 for 5 dBm. Finally, Figures 16(a) and 16(b) present the average BEP obtained by Algorithm #4 for distinct α values in order to compare hybrid and non-hybrid performances. These figures show that power line and wireless systems are clearly outperformed by the HPWS.

Table 3 – Optimal α for the presented cases

	4-QAM		16-QAM	
	$P_{\text{T}} = -10$ dBm	$P_{\text{T}} = 5$ dBm	$P_{\text{T}} = -10$ dBm	$P_{\text{T}} = 5$ dBm
α_{opt}	0.70	0.85	0.60	0.80

Source: Personal collection.

Figures 17(a) and 17(b) show how the proposed power allocation algorithms outperform the ones already presented in the literature in terms of average BEP. In these figures, $\alpha = 0.70$ is assumed because it allows Algorithms #3 and #4 to provide average BEPs as close as possible in the entire range of simulated P_{T} values. The proposed power allocation algorithms for SPC and SPCC are compared with their respective versions designed to maximize the achievable data rate (i.e, Algorithms #1 and #2) as well as UA and Park's algorithm.

Note that Algorithms #3 and #4 require a total transmission power around 2.5 dB less than that needed by Park's algorithm for a given average BEP. It results in a significant power reduction for achieving the same average BEP. Comparing the performances of Algorithms #3 and #4 and the performance of UA, a larger difference is noticed in terms of required total transmission power. For instance, the proposed power allocation algorithms require a total transmission power around 10 dB less than that needed by uniform power allocation if $\overline{P_{\text{e}}} = 10^{-4}$. Such a difference is approximately 12 dB if $\overline{P_{\text{e}}} = 10^{-6}$. Overall, the dominance of the proposed power allocations

Figure 14 – Average BEP ratio versus α for different total transmission powers (4-QAM)

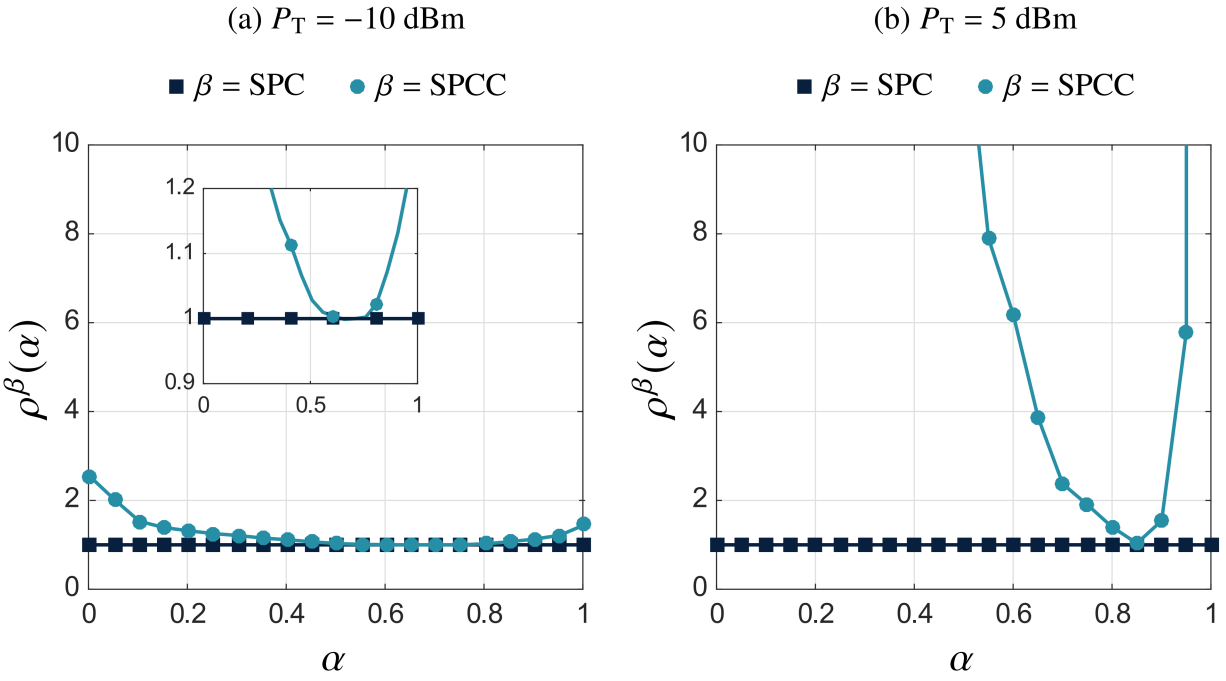

Source: Personal collection.

Figure 15 – Average BEP ratio versus α for different total transmission powers (16-QAM)

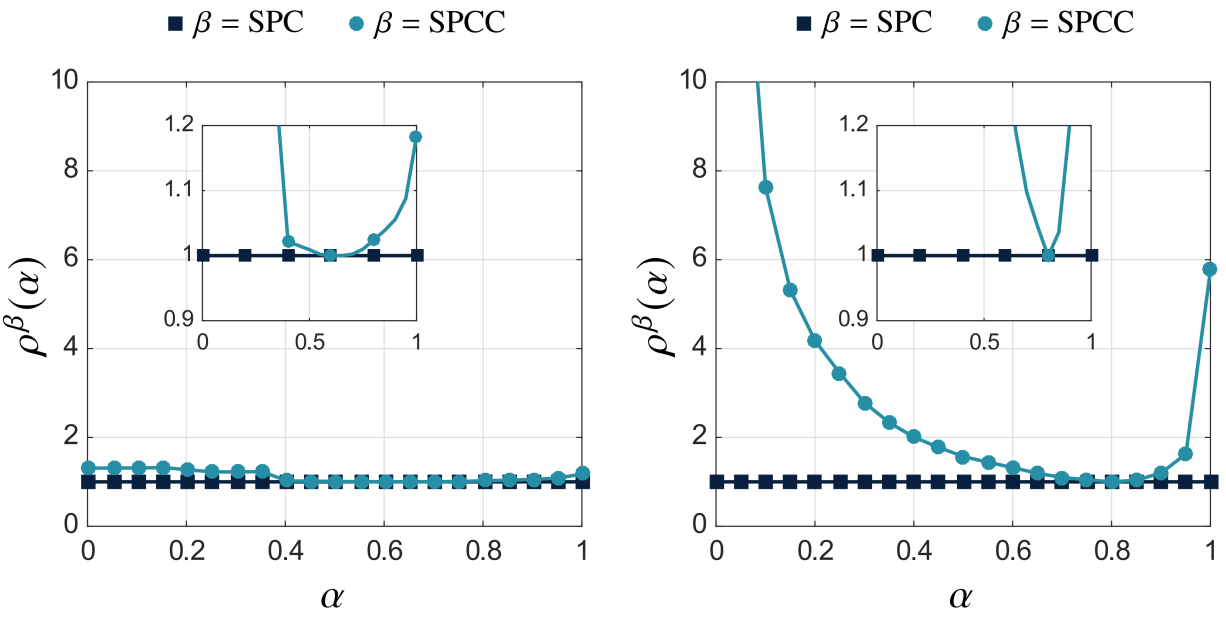

Source: Personal collection.

algorithms over the other options from the literature is clearly stated in terms of average BEP. Finally, it is observed that the power allocation algorithms proposed for maximizing the achievable data rate in Chapter 3 provide average BEP values close to those of UA and, as a consequence, they are consistently outperformed by Algorithms #3 and #4. This result is extremely important

Figure 16 – Average BEP as a function of P_T for Algorithm #4 with different α values

(a) 4-QAM

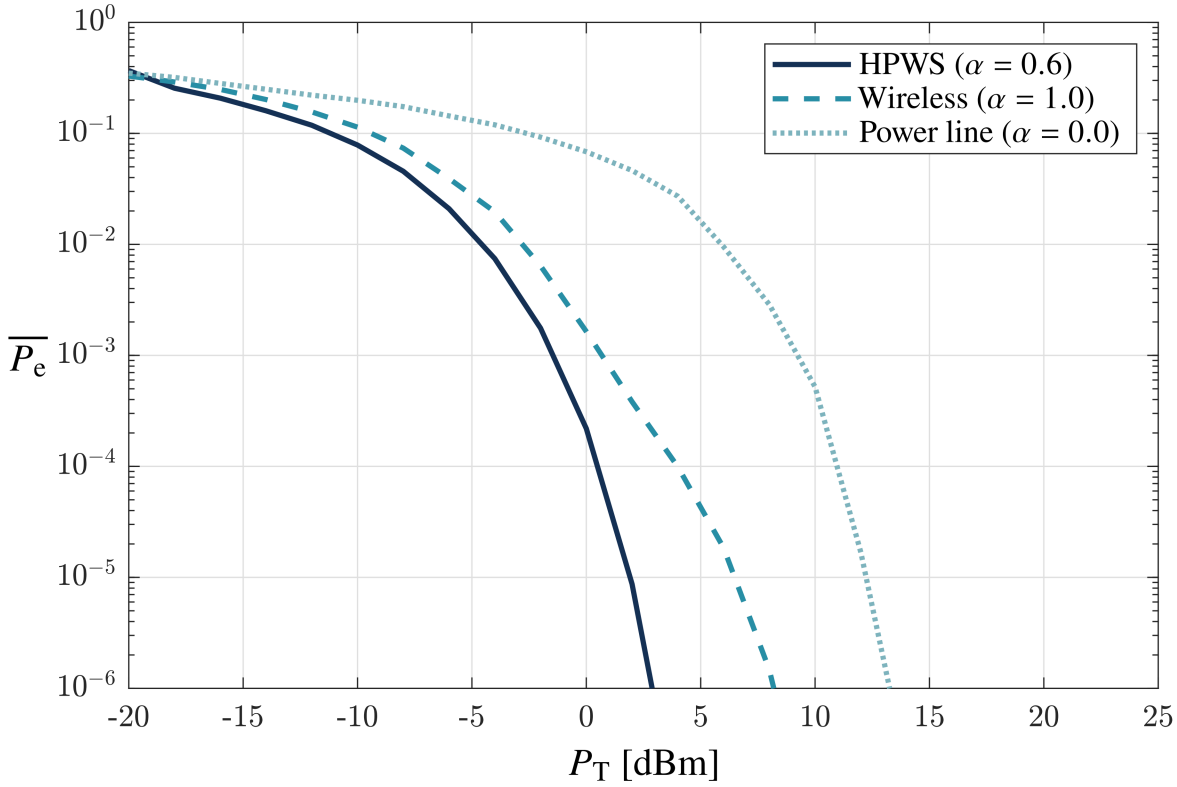

(b) 16-QAM

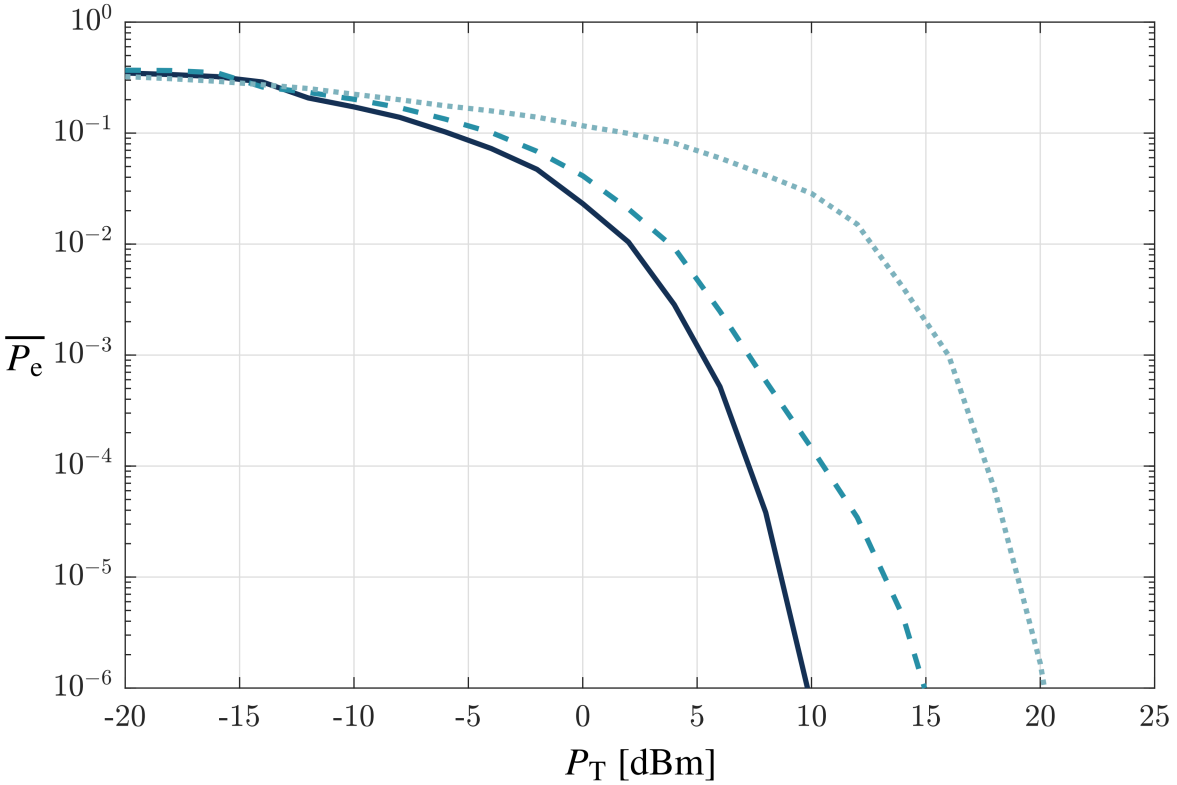

Source: Personal collection.

Figure 17 – Performance comparison among the proposals, Park's algorithm, and uniform power allocation ($\alpha = 0.70$)

(a) 4-QAM

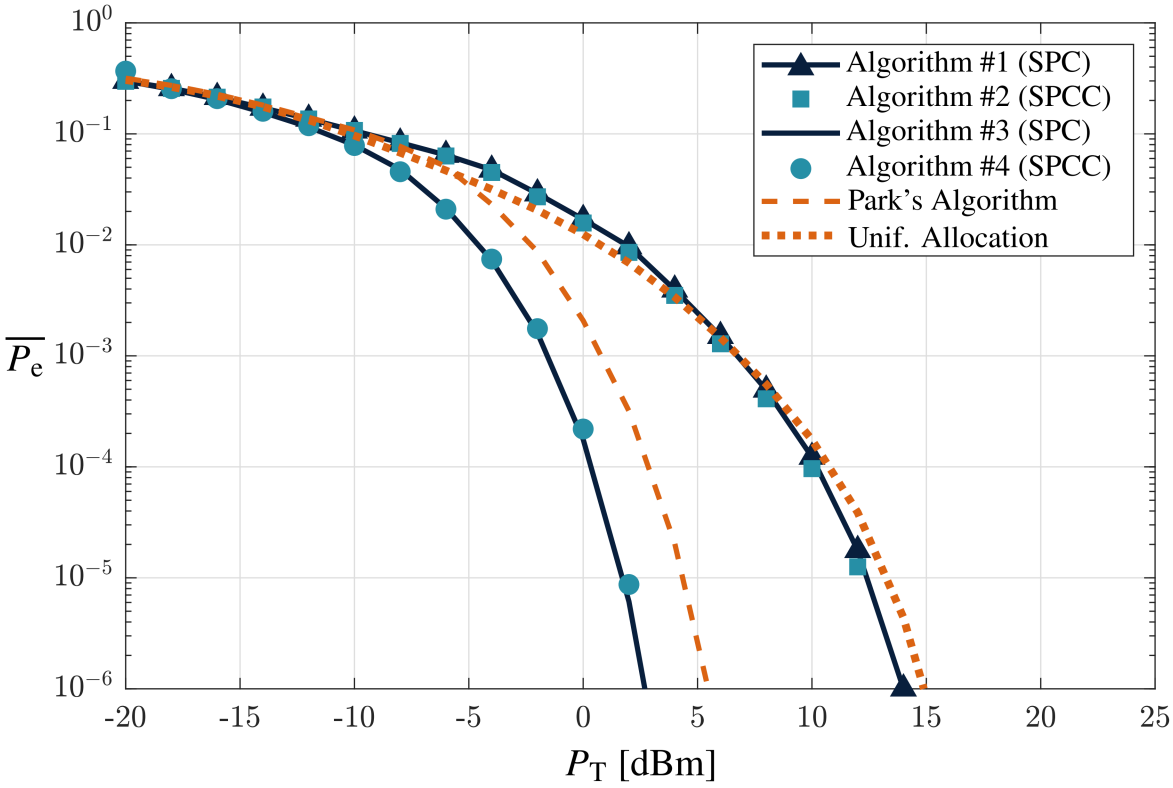

(b) 16-QAM

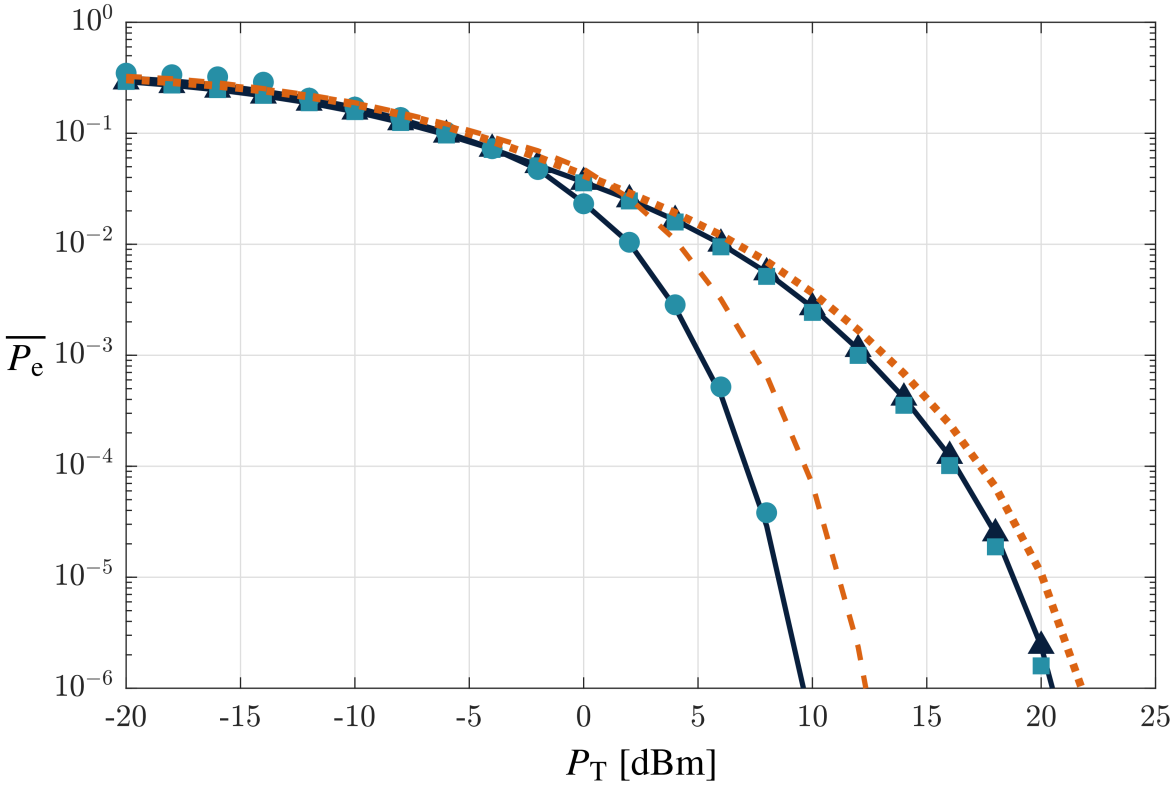

Source: Personal collection.

to show that maximizing the achievable data rate does not imply minimizing the average BEP and vice versa. Therefore, if the main objective is to yield higher achievable data rate, then Algorithms #3 and #4 are clearly outperformed by Algorithms #1 and #2, see Figure 18.

4.4.3 Transmission Power Benchmarks

In order to make Algorithms #3 and #4 reproducible, this subsection gives benchmarks for the transmission powers outputted from them. Similar to Chapter 3, synthetic data are considered so that one can implement Algorithms #3 and #4 and verify the obtained results. For this purpose, the same simulation environment as that of Chapter 3 is assumed. In other words, $\overline{\gamma}_{1,k} = 35$ dB and $\overline{\gamma}_{2,k} = 70 - 4k$ dB, $\forall k \in \{1, 2, \ldots, N_S\}$, with $N_S = 16$. Again, synthetic nSNR values are considered in this section only to make comparisons easier. Also, 4-QAM constellation is assumed. To be fair, $P_1 = 0.5P_T$ and $P_2 = 0.5P_T$.

Table 4 lists the transmission powers for every subcarrier and medium, which are outputted by Algorithms #3 and #4 when $P_T = 10$ dBm. Note that Algorithms #3 and #4 allocate the same power to all subcarriers for the first medium. This is due to the constant nSNR values of such medium. Also, Figure 19 shows the average bit error probability for $P_T \in \{0, 2, \ldots, 30\}$.

Figure 18 – Performance comparison among the proposed power allocation algorithms in terms of achievable data rate ($\alpha = 0.6$ and $M = 4$)

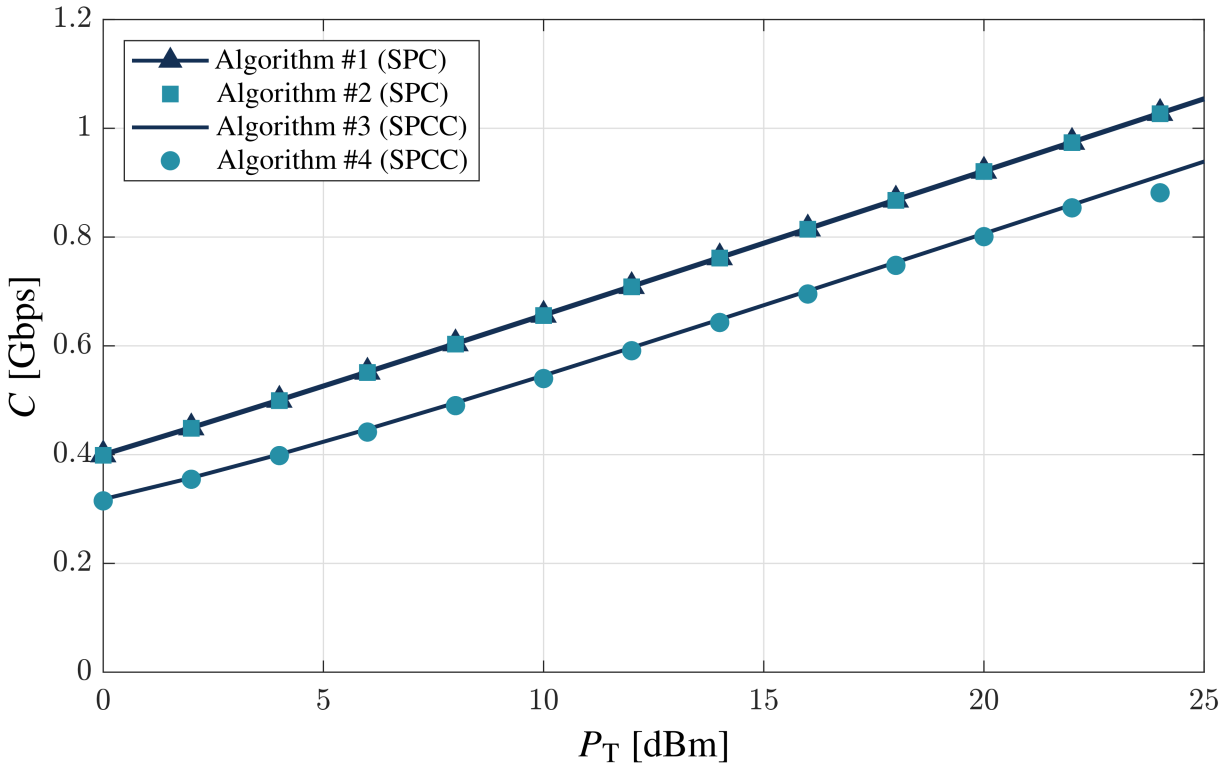

Source: Personal collection.

Table 4 – Transmission powers obtained from Algorithm #3 and #4 (P_T = 10 dBm)

Transmission power (μW)				
k	Algorithm #3		Algorithm #4	
	$p_{1,k}$	$p_{2,k}$	$p_{1,k}$	$p_{2,k}$
1	0.0	4.4	0.0	4.6
2	0.0	10.0	0.0	10.4
3	0.0	22.1	0.0	23.3
4	0.0	48.1	0.0	51.1
5	0.0	102.4	0.0	110.0
6	0.0	211.0	0.0	230.1
7	0.0	413.9	0.0	461.8
8	0.0	747.7	0.0	868.1
9	1055.0	0.0	0.0	1447.2
10	1055.0	0.0	0.0	1793.2
11	1055.0	0.0	833.3	0.0
12	1055.0	0.0	833.3	0.0
13	1055.0	0.0	833.3	0.0
14	1055.0	0.0	833.3	0.0
15	1055.0	0.0	833.3	0.0
16	1055.0	0.0	833.3	0.0

Source: Personal collection.

Figure 19 – Average bit error probability as a function of P_T

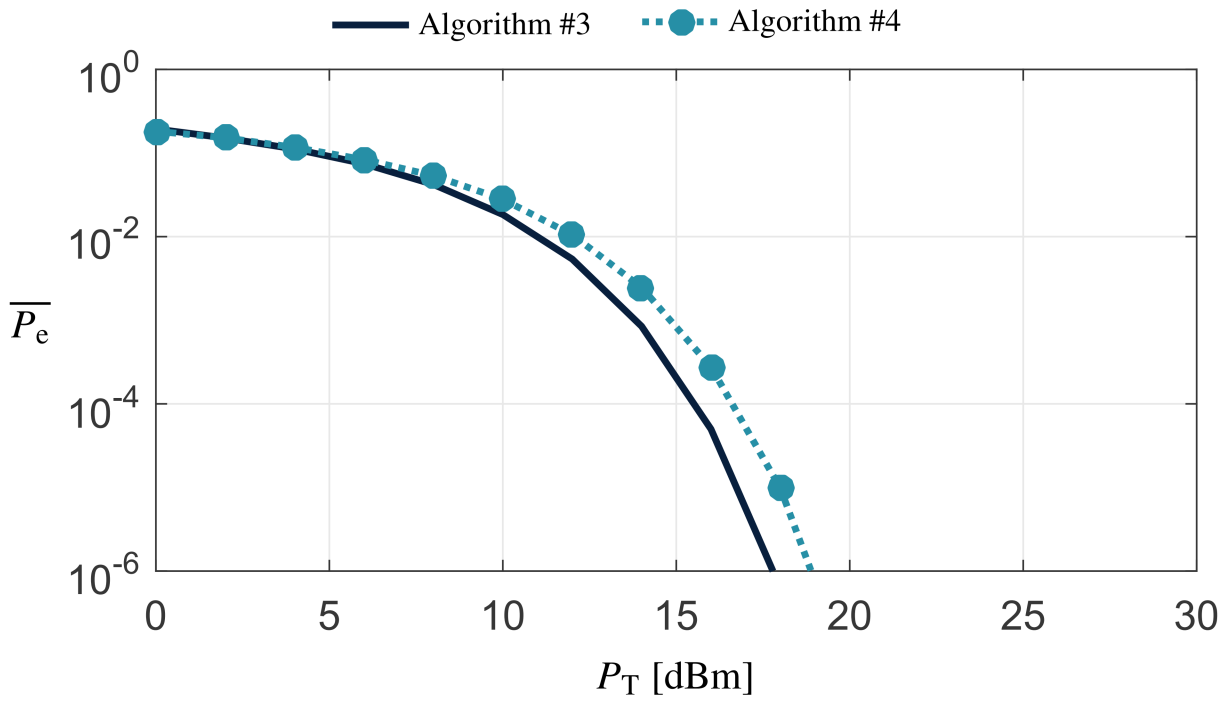

Source: Personal collection.

4.5 SUMMARY

This chapter has investigated power allocation for minimizing the average bit error probability in hybrid communication systems that use OFDM and MRC. Based on [25] and on Chapter 3, optimization problems have been formulated under the sum power and sum power-channel constraints, and solutions to solve both of them have been provided. Moreover, numerical results have validated the proposed solutions and compared them with other power allocation algorithms.

5 SUBCARRIER PERMUTATION FOR PERFORMANCE IMPROVEMENT

In the previous chapters, the frequency-domain representation of the transmitted signals is assumed to be the same in both wireless and power line branches and, at the receiver, an individual OFDM scheme was considered for each medium. Based on these assumptions, the data transmitted through distinct subchannels can be combined to allow symbol detection at a higher SNR and, as a consequence, key parameters of a data communication system, such as achievable data rate and average BEP, can be improved. To better exploit the frequency diversity between wireless and power line media, [46] proposed subcarrier permutation prior to symbol combining in an HPWS. The overall idea is that the information in a given subchannel of the power line medium is combined with the information in a different subchannel associated with the wireless medium. To do so, the only constraint was to perform the reverse permutation at the transmitter previously. By considering uniform power allocation and focusing on the increase of the achievable data rate, [46, 101] showed that the subcarrier indices of a medium should be sorted in descending order of their SNRs and then paired with the subcarrier indices of the other medium sorted in ascending order of their SNRs.

Despite the initial efforts presented by [46, 101], subcarrier permutation can be further investigated to improve the performance of HPWSs. For instance, subcarrier permutation has not been studied to minimize the average BEP under uniform power allocation. Furthermore, the simultaneous optimization of subcarrier permutation and power allocation has not been pursued to either maximize the achievable data rate or minimize the average BEP. In order to fill all the aforementioned gaps, this chapter investigates subcarrier permutation to either maximize the achievable data rate or minimize the average BEP in HPWSs. Based on waterfilling [24] and Park [25] as well as the findings obtained in Chapters 3 and 4, the subcarrier permutation proposed in [101] is scrutinized. In particular, the main contributions of the current chapter are as follows:

- The investigation of subcarrier permutation in HPWSs for either maximizing achievable data rate or minimizing average BEP under uniform or optimal power allocation, considering two different sets of transmission power constraints: SPC and SPCC.
- The demonstration that the optimization of the subcarrier permutation in an HPWS must be performed before power optimization regardless of the set of transmission power constraints and that it must be based on the nSNR instead of SNR.

The rest of this chapter is organized as follows: Section 5.1 formulates the optimization problem associated with subcarrier permutation in HPWSs; Section 5.2 presents the optimal subcarrier permutation in HPWSs for each type of power allocation; Section 5.3 analyzes the subcarrier permutation based on numerical results; finally, the chapter is summarized in Section 5.4.

5.1 PROBLEM FORMULATION

Based on the system model presented in Chapter 2, it was previously considered the use of an OFDM scheme whose frequency-domain transmitted symbols are such that $X_{2,k} = X_{1,k}, \forall k$, in order to combine the received symbols. In this chapter, however, a permutation matrix is used in the frequency domain similar to [101]. Figures 20(a) and 20(b) respectively show the HPWS transmitter and receiver architectures when the subcarrier permutation applies. In these figures, $\mathbf{X}_m = [X_{m,1}\ X_{m,2}\ \ldots\ X_{m,N_S}]^T$, $\mathbf{Y}_m = [Y_{m,1}\ Y_{m,2}\ \ldots\ Y_{m,N_S}]^T$, $\forall m \in \{1, 2\}$, and $\mathbf{P}$ is an N_S-size square permutation matrix which has only one element equal to one per row and per column and zeros elsewhere.

By applying the permutation matrix at the transmitter side, one has $X_{2,\Phi_k} = X_{1,k}, \forall k$. Hence, as the reverse permutation is performed at the receiver side, the symbol received at the k^{th} subchannel by the first medium interface can be combined with the symbol received at the subchannel Φ_k in the second medium. If the MRC is employed, then the resulting SNR at the k^{th} subcarrier is $\gamma_k = p_{1,k}\overline{\gamma}_{1,k} + p_{2,\Phi_k}\overline{\gamma}_{2,\Phi_k}$. As a result, data communication system performance will be driven based on the values of Φ_k and $p_{m,k}, \forall m, k$. For instance, the achievable data rate

Figure 20 – HPWS transmitter and receiver architectures with subcarrier permutation

(a) HPWS transmitter

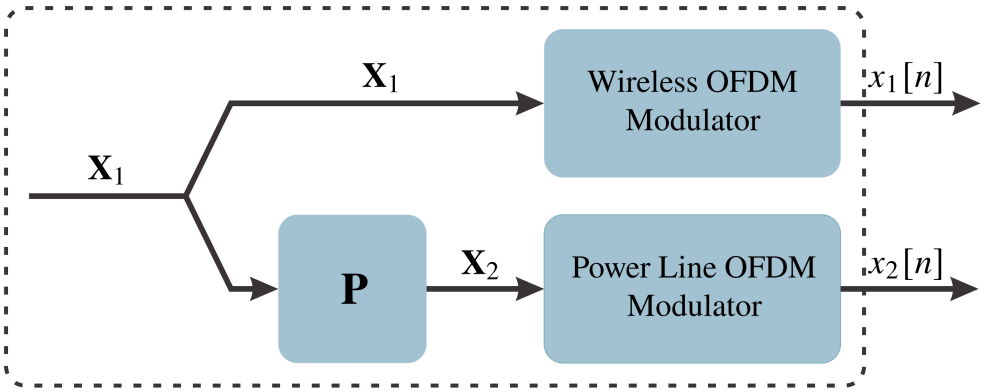

(b) HPWS receiver

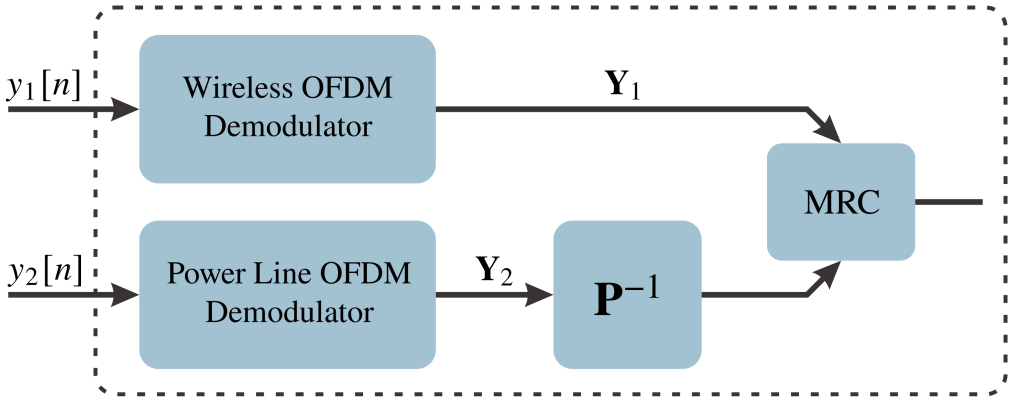

Source: Personal collection.

will be given by

$$R = \frac{B_{\mathrm{w}}}{N_{\mathrm{S}}} \sum_{k} \log_2 (1 + \gamma_k) \tag{5.1}$$

$$= \frac{B_{\mathrm{w}}}{N_{\mathrm{S}}} \sum_{k} \log_2 \left(1 + p_{1,k}\overline{\gamma}_{1,k} + p_{2,\Phi_k}\overline{\gamma}_{2,\Phi_k}\right). \tag{5.2}$$

On the other hand, by considering an OFDM scheme with no intersymbol interference, i.e., a guard interval longer than the delay spread of the channels, the average BEP will be described as

$$\overline{P_{\mathrm{e}}} = \frac{1}{N_{\mathrm{S}}} \sum_{k} P_{\mathrm{e},k} (\gamma_k) \tag{5.3}$$

$$= \frac{1}{N_{\mathrm{S}}} \sum_{k} P_{\mathrm{e},k} \left(p_{1,k}\overline{\gamma}_{1,k} + p_{2,\Phi_k}\overline{\gamma}_{2,\Phi_k}\right), \tag{5.4}$$

where again $P_{\mathrm{e},k}(\cdot)$ is a function of the SNR that defines the bit error probability at the k^{th} subchannel and depends on the assumed modulation.

The impact of the hybridism and subcarrier permutation on the data communication system performance can be noticed by looking at (5.2) and (5.4). On the one hand, the hybridism is based on the MRC technique to allow the SNR to be composed of the sum of individual SNRs and, consequently, to increase the overall SNR. The subcarrier permutation, on the other hand, serves to ensure that the subcarriers of each media are combined in the best order possible. Notice that both the achievable data rate or the average BEP can be improved, or even deteriorated, depending on the Φ_k values. However, once the hybrid transmitter has a certain knowledge of the channel conditions (e.g., nSNR values), such information can be used to improve system performance. In this sense, an optimization problem on Φ_k can be defined as

$$\min_{\Phi_k} \sum_{k=1}^{N_{\mathrm{S}}} f(\Phi_k, p_{m,k}), \tag{5.5}$$

where $f(\cdot)$ is a functional chosen according to the main objective, which can be either maximizing the achievable data rate and then

$$f(\Phi_k, p_{m,k}) = -\frac{B_{\mathrm{w}}}{N_{\mathrm{S}}} \log_2 \left(1 + p_{1,k}\overline{\gamma}_{1,k} + p_{2,\Phi_k}\overline{\gamma}_{2,\Phi_k}\right) \tag{5.6}$$

or minimizing the average BEP and consequently

$$f(\Phi_k, p_{m,k}) = \frac{1}{N_{\mathrm{S}}} P_{\mathrm{e},k} \left(p_{1,k}\overline{\gamma}_{1,k} + p_{2,\Phi_k}\overline{\gamma}_{2,\Phi_k}\right). \tag{5.7}$$

Note that both main objectives define different optimization problems, which in their turn cannot be simultaneously solved; therefore, a choice between them have to be made.

Regardless of the choice, it is possible to also optimize $p_{m,k}$, instead of just optimizing Φ_k. With this in mind, the two constraints on the transmission power can be considered: SPC

and SPCC. Based on these transmission power constraints, the following optimization problem arises:

$$\min_{\Phi_k, p_{m,k}} \sum_{k=1}^{N_S} f(\Phi_k, p_{m,k}), \tag{5.8}$$

subject to either

$$\text{SPC} \begin{cases} \sum\limits_{m,k} p_{m,k} \leq P_T \\ p_{m,k} \geq 0, \ \forall \ k, m \end{cases} \tag{5.9}$$

or

$$\text{SPCC} \begin{cases} \sum\limits_{k} p_{m,k} \leq P_m, \ \forall m \\ p_{m,k} \geq 0, \ \forall \ k, m. \end{cases} \tag{5.10}$$

Note that all optimization problems related to subcarrier permutation can be presumably classified as nondeterministic polynomial-time (NP)-hard problems [102]. This is because the variables to be optimized are indices of elements of the objective function and, therefore, a computer would have to calculate all possible permutations ($N_S!$ in total) to find the optimal solution. Nonetheless, [46] proposed a polynomial-time algorithm to find a global and deterministic solution for the subcarrier permutation problem in HPWSs by considering the achievable data rate and uniform power allocation. In this regard, the following research question arises: *"Could an optimal solution for the subcarrier permutation problem in an HPWS be found in polynomial time considering either achievable data rate or average BEP under uniform or optimal power allocation?"* An answer to this question is presented in Section 5.2, where the solution proposed for maximizing the achievable data rate under uniform power allocation is proven to be optimal for any of the aforementioned optimization problems. In other words, the following statement will be proved:

In order for the achievable data rate or the average BEP to be optimized in an HPWS, the information transmitted through the subchannel with the highest nSNR of a medium must be the same transmitted through the subchannel with the lowest nSNR of the other medium; then the information transmitted through the subchannel with the second highest nSNR of a medium must be equal to that in the subchannel with the second lowest nSNR of the other medium; and so forth.

5.2 OPTIMAL SUBCARRIER PERMUTATION FOR PERFORMANCE IMPROVEMENT IN AN HPWS

In this section, the described subcarrier permutation is proved to be optimal for any of the optimization problems previous formulated when the HPWS transmitter knows all nSNR values, $\overline{\gamma}_{m,k}, \forall m, k$. Furthermore, when the optimization problem is only on Φ_k, the uniform power allocation applies. There are then optimization problems associated with three types of power allocation (uniform and optimal under SPC and SPCC) and two different goals (maximization of the achievable data rate and minimization of the average BEP).

The result of the optimal subcarrier permutation is obtained with simple sorting algorithms and therefore it has computational complexity of order $O(N_{\mathrm{S}} \log_2(N_{\mathrm{S}}))$. Also, observe that the optimal subcarrier permutation is slightly different from that proposed in [46, 101] because the current one is based on the nSNR instead of the SNR. Indeed, [89] showed that nSNR is the right parameter to be considered when power allocation is performed. Last but not least, the attained permutation is the same for all types of power allocation and, for this reason, it can be conclude that the subcarrier permutation and power allocation problems are decoupled in the HPWS, although the subcarrier permutation acts on the transmission powers - see (5.2) and (5.4). The proof of the optimality of the described permutation for each type of power allocation is individually analyzed henceforth.

5.2.1 Uniform Power Allocation

By assuming uniform power allocation and subcarrier permutation, the resulting SNR after applying the MRC can be written as follows:

$$\begin{aligned} \gamma_k &= \frac{P_1}{N_{\mathrm{S}}}\overline{\gamma}_{1,k} + \frac{P_2}{N_{\mathrm{S}}}\overline{\gamma}_{2,\Phi_k} && (5.11)\\ &= \frac{P_2}{N_{\mathrm{S}}}\left(\frac{P_1}{P_2}\overline{\gamma}_{1,k} + \overline{\gamma}_{2,\Phi_k}\right) && (5.12)\\ &= p\beta_k, && (5.13) \end{aligned}$$

where $\beta_k = \frac{P_1}{P_2}\overline{\gamma}_{1,k} + \overline{\gamma}_{2,\Phi_k}$ and $p = \frac{P_2}{N_{\mathrm{S}}}$. Based on that, the achievable data rate of the HPWS can be expressed as

$$R = \frac{B_{\mathrm{w}}}{N_{\mathrm{S}}} \sum_k \log_2\left(1 + p\beta_k\right) \tag{5.14}$$

and the average BEP is given by

$$\overline{P_{\mathrm{e}}} = \frac{1}{N_{\mathrm{S}}} \sum_k P_{\mathrm{e},k}\left(p\beta_k\right). \tag{5.15}$$

Note that the initial objective is to maximize (5.14) or minimize (5.15) on Φ_k; however, the optimization of these equations on β_k is not new in the literature and their results can be helpful now. Whereas the maximization of (5.14) was formerly solved by the well-known waterfilling algorithm [24], the solution that minimizes (5.15) was first obtained by the Park algorithm [25]. Although the use of these algorithms implies in different results, a careful analysis of both shows that β_k must be constant with k to either maximize the achievable data rate or minimize the average BEP, since p is constant.

In order for β_k to be constant, there is a need for total flexibility in the values of $\overline{\gamma}_{1,k}$ and $\overline{\gamma}_{2,k}$. Nonetheless, this level of flexibility is not feasible since CIR and noise characteristics cannot be controlled by the designer at all. In this sense, the best option is to consider the

average value of β_k as

$$\overline{\beta} = \frac{1}{N_S}\sum_k \beta_k \tag{5.16}$$

$$= \frac{1}{N_S}\sum_k \left(\frac{P_1}{P_2}\overline{\gamma}_{1,k} + \overline{\gamma}_{2,k}\right) \tag{5.17}$$

and then minimize the mean squared error (MSE) to this value, which can be expressed as

$$\epsilon = \frac{1}{N_S}\sum_k \left|\overline{\beta} - \beta_k\right|^2 \tag{5.18}$$

$$= \frac{1}{N_S}\sum_k \left|\left(\overline{\beta} - \frac{P_1}{P_2}\overline{\gamma}_{1,k}\right) - \overline{\gamma}_{2,\Phi_k}\right|^2 \tag{5.19}$$

$$= \frac{1}{N_S}\left(\sum_k d_k^2 + \sum_k \overline{\gamma}_{2,\Phi_k}^2 - \sum_k 2d_k\overline{\gamma}_{2,\Phi_k}\right), \tag{5.20}$$

where $d_k = \overline{\beta} - \frac{P_1}{P_2}\overline{\gamma}_{1,k}$.

Observe that the results of the first two summation terms of (5.18) are not impacted by subcarrier permutation, i.e., the values of Φ_k just change the final result of the last summation term. As a consequence, the minimization of the MSE can be further simplified as follows

$$\min_{\Phi_k}\epsilon \equiv \min_{\Phi_k} -\sum_k 2d_k\overline{\gamma}_{2,\Phi_k} \equiv \min_{\Phi_k}\sum_k \overline{\gamma}_{1,k}\overline{\gamma}_{2,\Phi_k}. \tag{5.21}$$

Therefore, the minimization of the MSE can be reduced to the problem of minimizing the sum of the product of two sets where the permutation is allowed. Such a problem is already known and its solution is precisely the subcarrier permutation previously described, see the proof in Appendix C. Note that this finding is equivalent to that obtained by [46] for maximizing the achievable data rate; however, the current manner of achieving it allows to address not only the maximization of the achievable data rate but also the minimization of the average BEP, which is of great value for designing data communication systems.

5.2.2 Optimal Power Allocation - Sum Power Constraint

Regarding optimal power allocation, Chapters 3 and 4 respectively presented how to maximize the achievable data rate and minimize the average BEP in an HPWS without subcarrier permutation. By assuming the SPC, both studies demonstrated that an amount of power should be allocated only to the subcarrier associated with the highest nSNR per subchannel index. In other words, the total transmission power should be distributed only to an equivalent medium with the following nSNRs:

$$\overline{\gamma}_k = \max_m\{\overline{\gamma}_{m,k}\}, \qquad \forall k. \tag{5.22}$$

In other words, the transmitter allocates non-zero power to the subcarriers in the best subchannels per index and null power elsewhere.

Figure 21 – An application of the optimal subcarrier permutation and the equivalent medium obtained by optimal power allocation under SPC

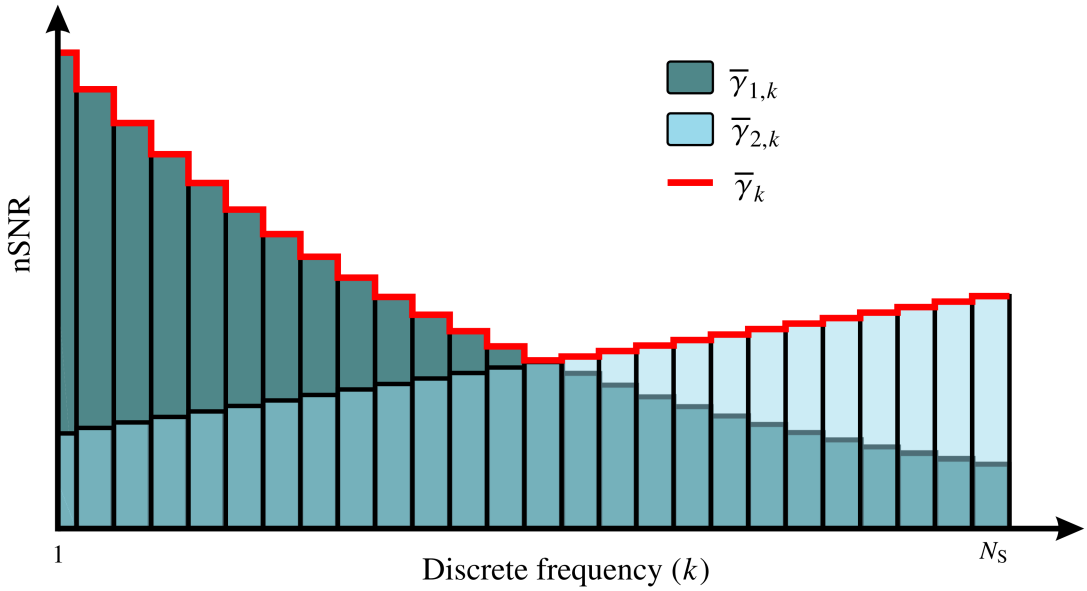

Source: Personal collection.

If subcarrier permutation is performed after optimal power allocation, then it has no impact on the system performance since the subchannels that do not have the highest nSNR per index are disregarded. For this reason, the following proposition can be stated:

Proposition 1*: The optimization of subcarrier permutation has to be accomplished before the optimal power allocation for performance improvement in an HPWS.*

Note that SNR values are only known after defining the transmission power and, as a consequence, there is no information on the SNR at the time the subcarrier permutation is carried out. Therefore, the proposition below can also be written:

Proposition 2*: The optimization of the subcarrier permutation has to be performed based on the nSNR in an HPWS.*

Following, notice that the optimization of the values of Φ_k needs to be carried out so that the equivalent medium considered by power optimization is the best possible, i.e., it has the N_S highest values of nSNR among all possible. As the best subcarriers of one medium are combined with the worst subcarriers of the other and vice versa, a subchannel with nSNR among the N_S highest ones, which could be unused if compared to a slightly better subchannel, will not be disregarded. At the same time, any subchannel with nSNR out of the N_S highest ones, which would be used if compared to a slightly worse subchannel, will not be used. Hence (5.22) yields the highest nSNRs possible as the described permutation is employed. Figure 21 illustrates the arrangement of subchannels made by the optimal subcarrier permutation and the equivalent medium over which the optimal power allocation is carried out. This figure clearly shows that the equivalent medium is composed of the subchannels with the N_S highest nSNR values.

5.2.3 Optimal Power Allocation - Sum Power-Channel Constraint

Taking into account optimal power allocation under the SPCC, only one medium must be used per subchannel as well; therefore, Propositions 1 and 2 also hold for the SPCC. However, the medium to be used is not that with the highest nSNR per subchannel. It was shown in Chapter 3 for the maximization of the achievable data rate, and extended by Chapter 4 for the minimization of the average BEP, that an analysis of the nSNR ratio must be carried out to obtain the information on which medium should be used at each subchannel. The nSNR ratio with subcarrier permutation is given by

$$r_k = \frac{\overline{\gamma}_{1,k}}{\overline{\gamma}_{2,\Phi_k}}, \forall k. \tag{5.23}$$

According to the previous chapters, the power allocation algorithm finds a ratio, λ_1/λ_2, such that subchannels whose nSNR ratio values are above it are used only in the first medium, whereas the others (subchannels whose nSNR ratio values are below λ_1/λ_2) are considered only in the second medium. For sake of simplicity, consider $\lambda' = \lambda_1/\lambda_2$. Figure 22 shows the aforementioned result for the nSNR values of the same media depicted in Figure 21. Notice that the constant λ' split the total subcarriers into two independent sets. The former, composed of subcarriers with the nSNR ratios greater than λ', is used in the first medium. And the latter, formed by subcarriers with the nSNR ratios below λ', is exploited in the second medium. The sets $\mathcal{A} = \{k|r_k \geq \lambda'\}$ and $\mathcal{B} = \{k|r_k < \lambda'\}$ are composed of subchannel indices whose nSNR ratio are respectively above and below λ' and, as a consequence, must be respectively used only in the first and second media. Therefore, the optimization problem related to the SPCC can be written as

$$\min_{\Phi_k, p_{m,k}} \sum_{k\in\mathcal{A}} f(p_{1,k}, p_{2,k} = 0) + \sum_{k\in\mathcal{B}} f(p_{1,k} = 0, p_{2,k}), \tag{5.24}$$

subject to

$$\sum_{k\in\mathcal{A}} p_{1,k} \leq P_1, \quad \sum_{k\in\mathcal{B}} p_{2,k} \leq P_2,$$

and

$$p_{1,k} \geq 0, \ \forall\ k \in \mathcal{A}, \quad p_{2,k} \geq 0, \ \forall\ k \in \mathcal{B}.$$

Observe that (5.8) was divided into two smaller summations so that one of the transmission powers ($p_{1,k}$ or $p_{2,k}$) is equal to zero in each of them and thus it can be assumed that $f(\cdot)$ is no longer affected by Φ_k. Therefore, the impact of Φ_k will be only on the sets $\mathcal{A}$ and $\mathcal{B}$. Once $\mathcal{A}$ and $\mathcal{B}$ are defined, one has two independent power optimization problems that can be solved by either waterfilling or Park algorithms.

Regardless of the value of λ', to optimize the achievable data rate or the average BEP, the subcarrier permutation must guarantee that the highest values of $\overline{\gamma}_{1,k}$ will be given by indices within $\mathcal{A}$, whereas indices within $\mathcal{B}$ must yield the highest values of $\overline{\gamma}_{2,k}$. In this regard, assume, without loss of generality, $\overline{\gamma}_{1,1} \geq \overline{\gamma}_{1,2} \geq \ldots \geq \overline{\gamma}_{1,N_S}$. As the subcarrier permutation described in the end of Section 5.1 is assumed, one has $\overline{\gamma}_{2,\Phi_1} \leq \overline{\gamma}_{2,\Phi_2} \leq \ldots \leq \overline{\gamma}_{2,\Phi_{N_S}}$ and hence

Figure 22 – Illustration of which medium should be used at each subchannel based on the nSNR ratio with optimal subcarrier permutation and SPC

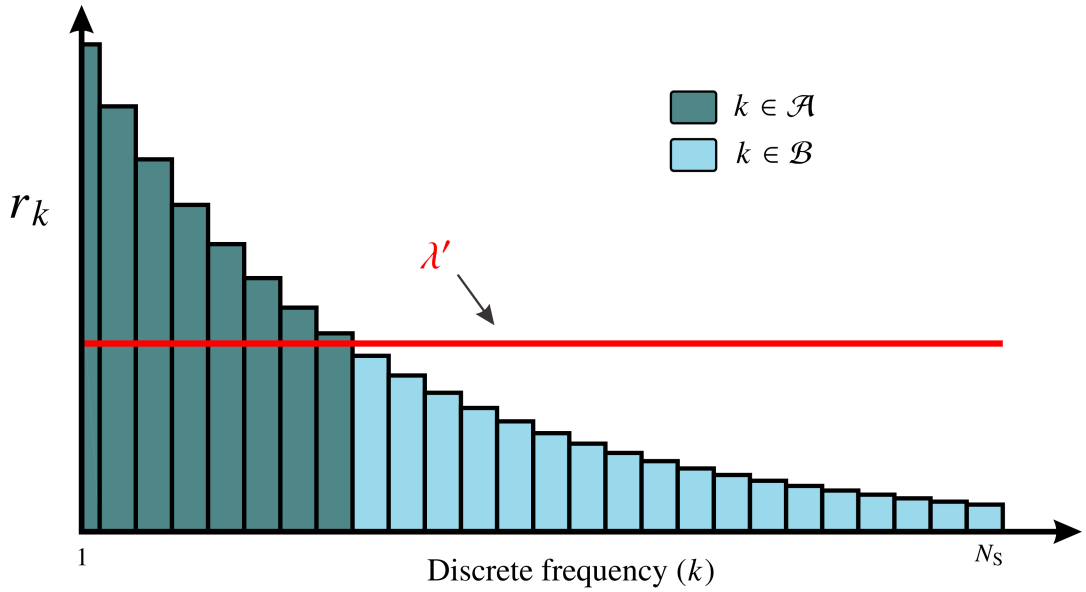

Source: Personal collection.

$r_1 \geq r_2 \geq \ldots \geq r_{N_S}$. In this way, the subchannel indices such that $\overline{\gamma}_{1,k} \geq \lambda' \overline{\gamma}_{2,\Phi_k}$ provide the highest nSNR in the first medium because they are compared to the lowest values of nSNR in the second medium. At the same time, the subchannel indices such that $\overline{\gamma}_{2,\Phi_k} > \overline{\gamma}_{1,k}/\lambda'$ give the highest nSNRs in the second medium since they are compared to the worst nSNRs in the first medium. In summary, when the described subcarrier permutation is considered, subchannels with the highest nSNR ratios are also the subchannels with the highest nSNRs in the first medium and simultaneously subchannels with the lowest nSNR ratios are also the subchannels with the highest nSNRs in the second medium.

5.3 NUMERICAL ANALYSES

In this section, numerical analyses are carried out to evaluate the impact of subcarrier permutation, more specifically the optimal one, on the HPWS performance. In this sense, three different scenarios are considered for comparison purposes. Two of them are the HPWS without subcarrier permutation and the HPWS with optimal subcarrier permutation, which will be respectively represented by WSP and OSP. The third one is the worst case scenario, which is employed to give information on the maximum gain that the optimal subcarrier permutation may reach. This scenario is emulated by matching power line and wireless nSNR values, i.e., the highest nSNR of one medium is combined with the highest nSNR of the other and so on until combining the lowest nSNR of one with the lowest nSNR of the other. The worst case scenario will be henceforth indicated by WCS.

The considered total frequency bandwidth is $B_w = 80$ MHz. Such value is in accordance with the wireless local area network standard IEEE 802.11ac [94] and also with the current power

line studies on broadband communication [79]. The simulations include different CIR samples in order to evaluate the impact of the frequency selectivity of the nSNR curves on the subcarrier permutation results. Moreover, the frequency bandwidth is divided into $N_S = 2048$ subchannels, which meets the nSNR coherence bandwidth criterion for both power line and wireless media [89], and an M-ary QAM constellation is considered.

For performance analysis of SPC and SPCC, it is assumed that $P_1 + P_2 = P_T$ and therefore $P_1 = \alpha P_T$ and $P_2 = (1 - \alpha)P_T$, $\alpha \in [0, 1]$. Only α is enough to establish the amount of the total transmission power that is intended to each medium. Also, the optimal α value is that for which the SPCC equals the SPC performance. Such an optimal value may be different depending on the considered metric performance (achievable data rate or average BEP).

5.3.1 Channel Impulse Response and Additive Noise

The channel impulse responses and additive noise used in the simulations are from power line and wireless broadband residential context, although the system model and the optimal subcarrier permutation can be applied to several contexts. The power line CIR is extracted from the measurement campaign reported in [15], whereas the wireless CIR is obtained from the ultra-wideband channel model (non-line-of-sight residential environment) with the frequency dependence of the antennas being disregarded [97]. To select the frequency bandwidth, B_w, digital bandpass filters in the frequency bands $1.7 - 81.7$ MHz and $5.76 - 5.84$ GHz are used for power line and wireless channels, respectively.

The power line additive noise is also obtained from the measurement campaign reported in [15]. On the other hand, the wireless additive noise is assumed to be circularly symmetric complex AWGN. The wireless noise power is calculated so that the average value of the nSNR is equal in both media, i.e., $\sum_k |\overline{\gamma}_{1,k}| = \sum_k |\overline{\gamma}_{2,k}|$. Based on this, the difference of frequency selectivity offered by each medium can be fairly analyzed. In this regard, two samples of wireless CIRs are used to differ the impact of subcarrier permutation on the data communication system performance depending on the frequency selectivity of the nSNRs. Figure 23 shows the resulting nSNRs for wireless (moderate and high frequency selectivity) and power line media used in this section.

5.3.2 Achievable Data Rate Analysis

First of all, the achievable data rate is here analyzed in terms of the gain ρ_ς, defined by

$$\rho_\varsigma \triangleq \frac{R_\varsigma}{R_{\mathrm{WSP}}}, \tag{5.25}$$

with R_ς denoting the achievable data rate calculated for the scenario $\varsigma \in \{\mathrm{OSP}, \mathrm{WSP}, \mathrm{WCS}\}$. Also, when the optimal power allocation results are evaluated, the value of R_{WSP} for the SPC is taken as reference.

Figures 24(a) and 24(b) show the achievable data rate gains under uniform power allocation for the wireless nSNR with moderate and high frequency selectivity, respectively. By

Figure 23 – nSNR for wireless ($m = 1$) and power line ($m = 2$) media, with moderate and high frequency selectivity for the wireless medium in the considered frequency bandwidth

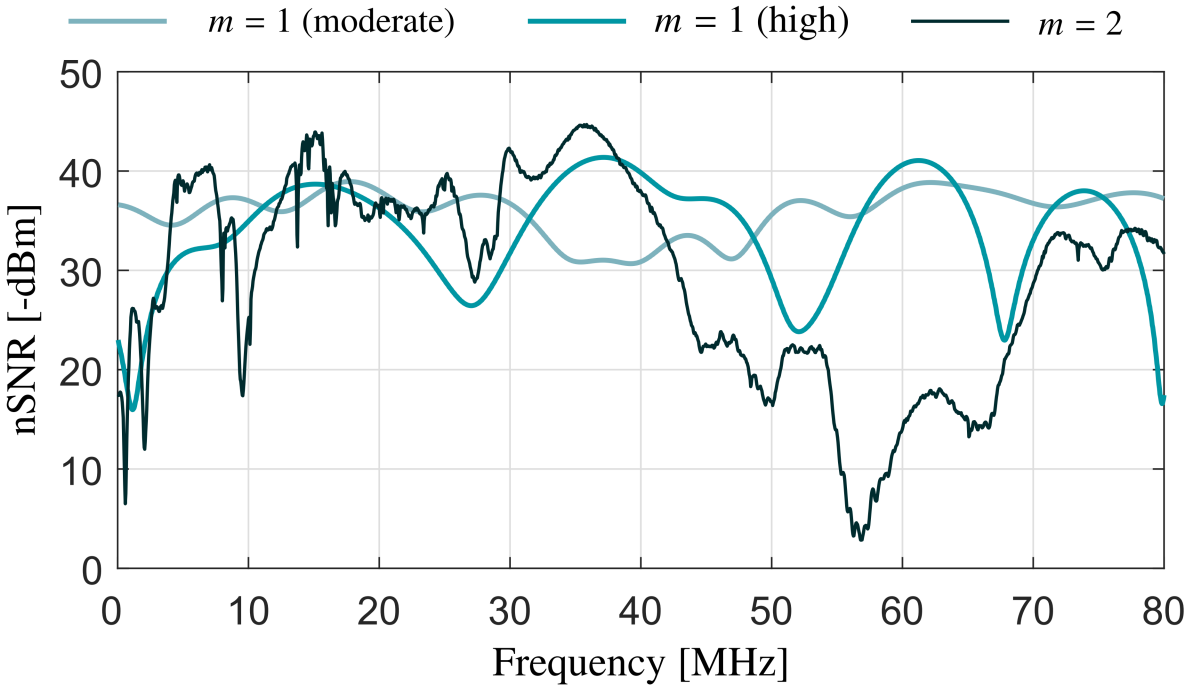

Source: Personal collection.

analyzing these figures, it is quite clear that OSP always outperforms WSP and that the bigger the nSNR frequency selectivity, the greater the achievable data rate gain yielded by OSP. To illustrate it, consider $P_{\mathrm{T}} = 5$ dBm and $P_{\mathrm{T}} = 25$ dBm. In these values, OSP achieves 3% and 2% of gain over WSP for moderate wireless nSNR frequency selectivity, whereas it offers 14% and 7% increase in achievable data rate for high wireless nSNR frequency selectivity. Additionally, such values point out that the greater the total transmission power, the lower the impact of the subcarrier permutation. At last, the maximum gain offered by the OSP (i.e., the difference between OSP and WCS) is bigger than 20% for high and around to 10% for moderate frequency selectivity states.

By considering optimal power allocation, the achievable data rate gains for the wireless nSNR with moderate and high frequency selectivity are respectively depicted in Figures 25(a) and 25(b). Moreover, $\alpha = 0.5$ is assumed for obtaining results under SPCC. Note that the provided gains are similar to those of the uniform power allocation, but for smaller gain variations. Overall, the OSP has always the best performance, greater achievable data rate gains are noticed at nSNR with higher frequency selectivity, and the achievable data rate gains decrease as the total transmission power increases. Also, the achievable data rate gain calculated under SPC is always greater than or equal to that under SPCC assuming the same scenario, which is expected since SPC represents an upper bound for SPCC regarding the achievable data rate - see Chapter 3. However, it is worth observing that, even under SPCC, OSP outperforms WSP under SPC.

Figure 24 – Achievable data rate gain considering uniform power allocation for moderate and high frequency selectivity of the wireless nSNR

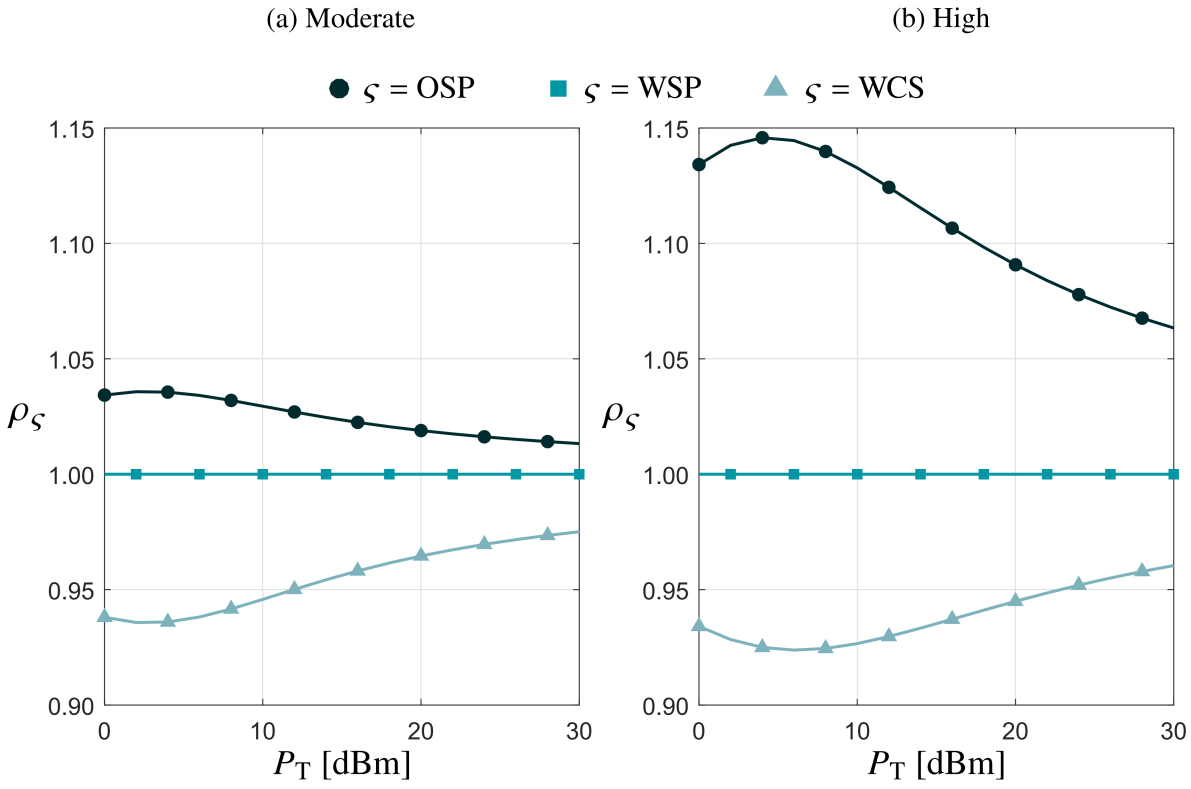

Source: Personal collection.

5.3.3 Average Bit Error Probability Analysis

Now, the average BEP, $\overline{P_{\mathrm{e}}}^{\varsigma}$, is presented as a function of the total transmission power, P_{T}, where ς corresponds to each of the previously mentioned scenarios. To perform the simulations, 4-QAM constellation is applied and therefore $P_{\mathrm{e},k}(\gamma_k) \cong 0.5\, Q\left(\sqrt{\gamma_k}\right)$ [25]. Similar results can be obtained for other modulations since changing $P_{\mathrm{e},k}(\cdot)$ influences all scenarios simultaneously and quantitatively, but the differences in the resulting SNR values are maintained qualitatively.

The average BEP for uniform power allocation can be seen in Figures 26(a) and 26(b) for nSNRs of the wireless medium with moderate and high frequency selectivity, respectively. Note that, regardless of the frequency selectivity of the wireless nSNR, OSP requires the lowest total transmission power for a given value of $\overline{P_{\mathrm{e}}}^{\varsigma}$. In addition, as the frequency selectivity of the wireless nSNR change from moderate to high, the required total transmission power tends to increase significantly for WSP and WCS, but slightly for OSP. Take $\overline{P_{\mathrm{e}}}^{\varsigma} = 10^{-6}$ as reference. For moderate frequency selectivity, WSP and WCS respectively require total transmission power values close to 16 dBm and 17 dBm, whereas OSP requires $P_{\mathrm{T}} \cong 12$ dBm. For high frequency selectivity, the total transmission power values for WSP and WCS are respectively higher than 26 dBm and 30 dBm, whereas it remains close to 12 dBm for OSP. Therefore, the average BEP improvement provided by the optimal subcarrier permutation is significant for any of the two cases of frequency selectivity of the wireless nSNR analyzed, despite being more expressive as

Figure 25 – Achievable data rate gain considering optimal power allocation under SPC (continuous line) and SPCC (dashed line) for moderate and high frequency selectivity of the wireless nSNR

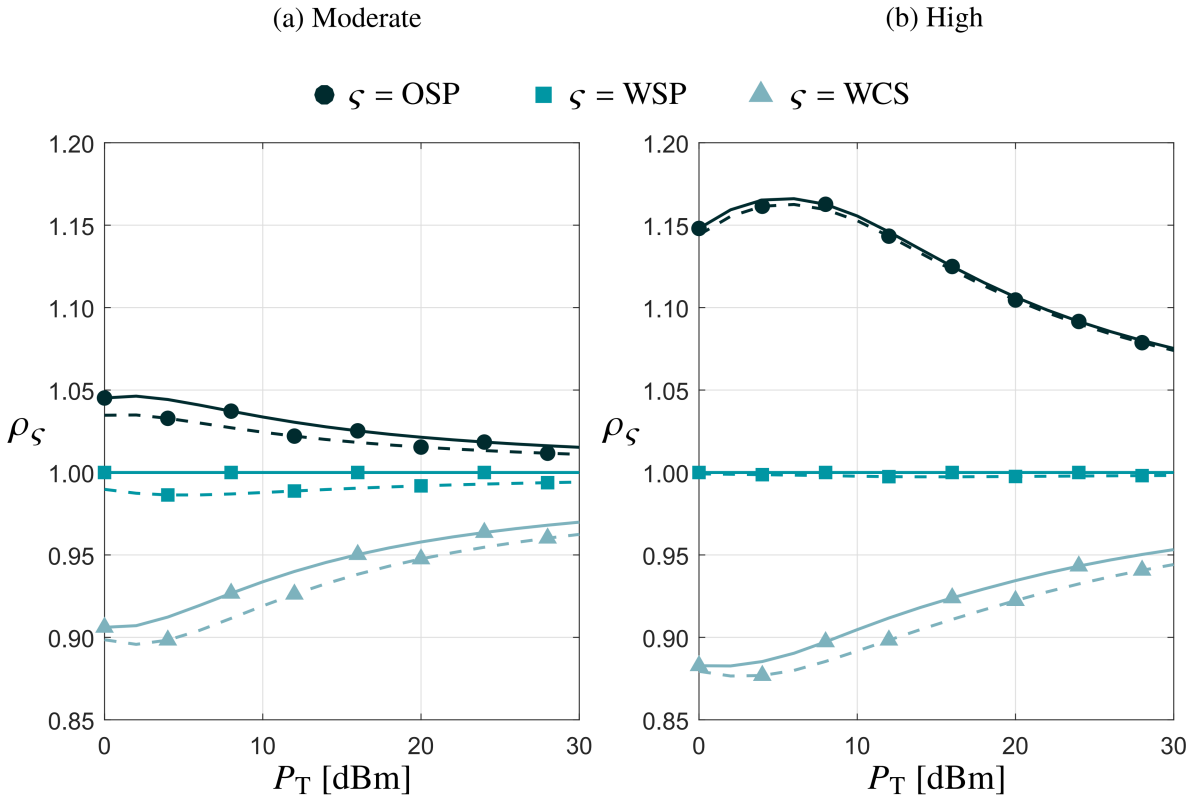

Source: Personal collection.

the nSNR frequency selectivity increases.

Figures 27(a) and 27(b) show the average BEP results for moderate and high frequency selectivity of the wireless nSNR considering optimal power allocation under SPC and SPCC ($\alpha = 0.5$), respectively. Note that the SPCC always requires a total transmission power equal to or greater than that of the SPC for a given average BEP regardless of the frequency selectivity of the considered nSNR curves. Therefore, the SPC is a lower bound for the SPCC with respect to the average BEP, unlike the achievable data rate analysis where the SPC was a upper bound. Moreover, similar to the uniform power allocation results, the OSP always requires the lowest total transmission power given a specific value of $\overline{P_e}^{\varsigma}$. For instance, consider $\overline{P_e}^{\varsigma} = 10^{-6}$ and moderate frequency selectivity of the wireless nSNR. Under SPCC, the required P_T values are around to 9, 10.5, and 12 dBm respectively for OSP, WSP, and WCS, whereas they are higher than 8, 9, and 11 dBm for the same scenarios under SPC. Additionally, as the frequency selectivity of the wireless medium increases, the OSP becomes more dominant since it requires a lower total transmission power compared to those required by WCS and WSP, under SPC or SPCC. Overall, the performance improvement provided by the optimal subcarrier permutation is extremely beneficial when the nSNR of one medium has high frequency selectivity. For moderate frequency selectivity of the nSNR, the OSP is also a good option, but obtaining a more subtle improvement.

Figure 26 – Average BEP considering uniform power allocation for moderate and high frequency selectivity of the wireless nSNR

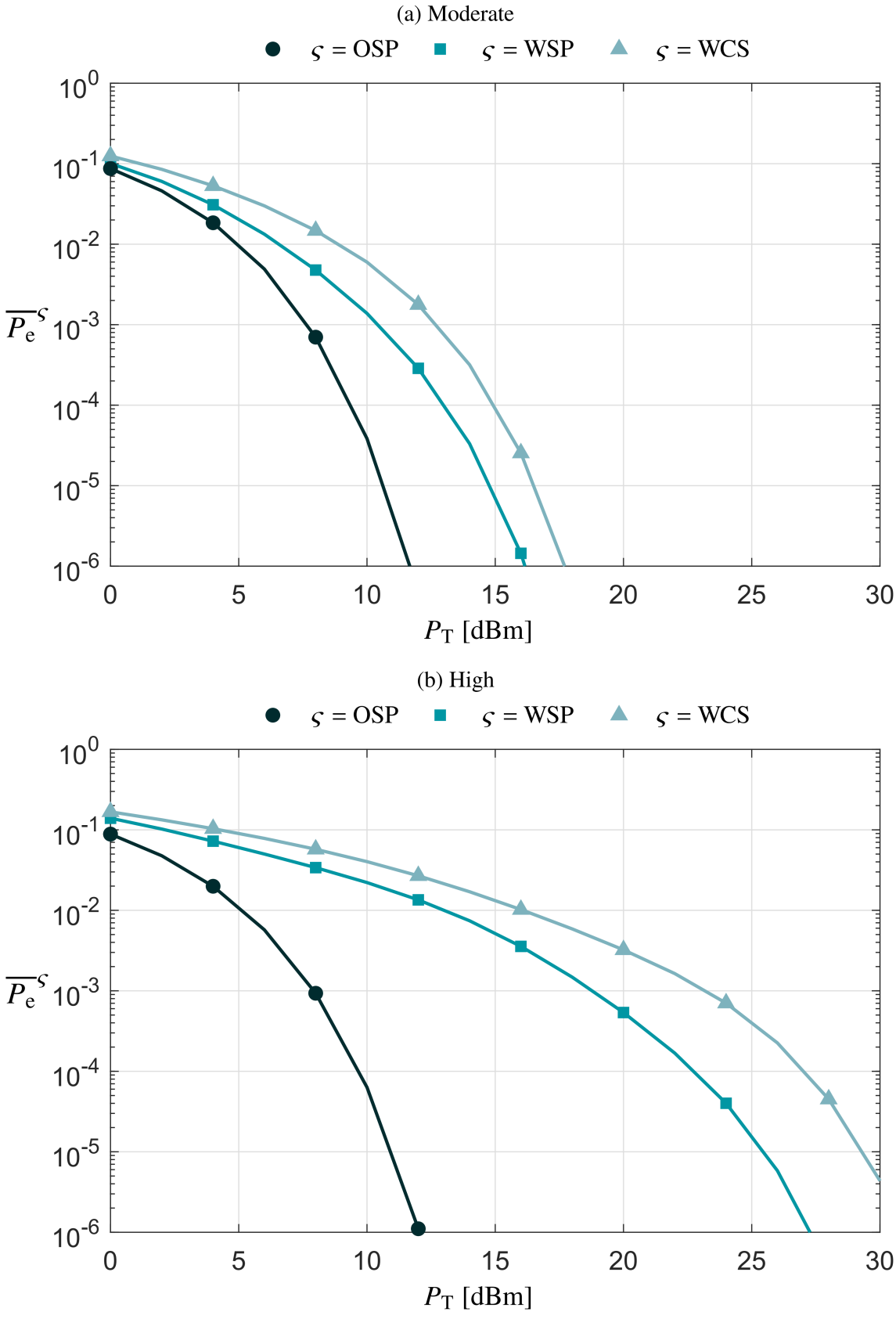

Source: Personal collection.

Figure 27 – Average BEP considering optimal power allocation under SPC (continuous line) and SPCC (dashed line) for moderate and high frequency selectivity of the wireless nSNR

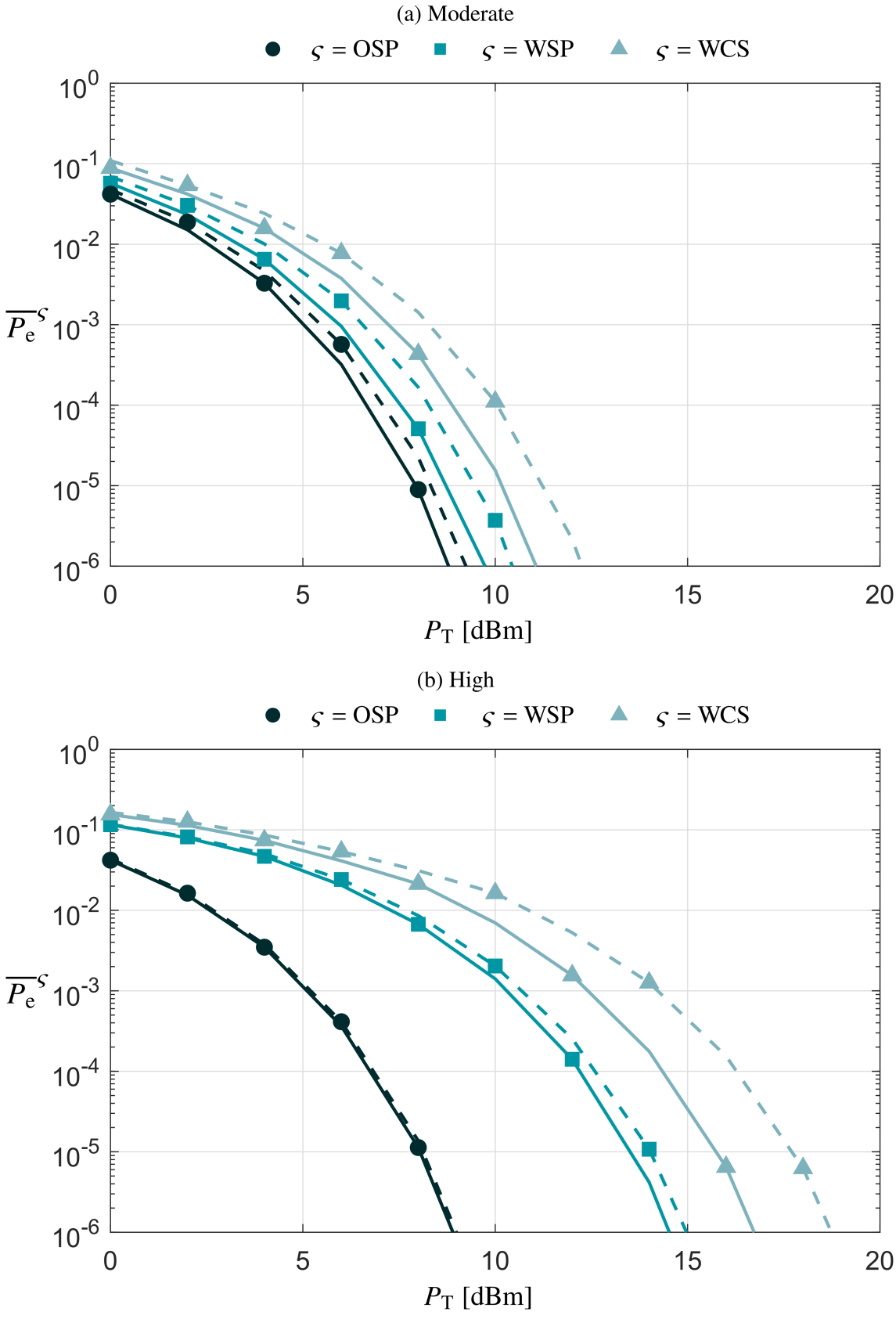

Source: Personal collection.

5.4 SUMMARY

This chapter has studied optimal subcarrier permutation in hybrid power line/wireless systems to better exploit the frequency selectivity of the considered media. By assuming orthogonal frequency-division multiplexing and maximal-ratio combining, subcarrier permutation optimization problems have been formulated for uniform and optimal power allocation under the sum power and sum power-channel constraints. In addition, two objective functions have been considered: achievable data rate and average bit error probability. Previous works, [46,101], have already derived the optimal subcarrier permutation for maximizing the achievable data rate under uniform power allocation, but their findings are here generalized for minimizing the average bit error probability and two other types of power allocation. The major difference is related to use the nSNR instead of SNR. Moreover, since the same subcarrier permutation is optimal for different types of power allocation, it has been demonstrated that subcarrier permutation and power allocation are decoupled from each other.

6 ORTHOGONAL CHIRP-DIVISION MULTIPLEXING IN HPWS

In recent years, the OCDM scheme has been increasingly gaining attention as a promising alternative to multicarrier schemes such as the OFDM scheme assuming uncoded modulations. The data modulation onto orthogonal subchirps [103] based on the DFnT in the OCDM scheme yields higher robustness against, e.g., ISI [104], multipath propagation [21, 105, 106], and narrowband interference [107], besides the well-known robustness to Doppler shifts of chirp spread spectrum-based schemes that is commonly exploited in radar applications [108, 109]. Furthermore, the OCDM scheme has been presented as an excellent solution to improve performance in terms of bit error rate if the CSI is not available at the transmitter side, although it has proved not to be the best option to provide high achievable data rates [110].

Due to the aforementioned reasons, OCDM appears as a potential candidate for satisfying performance and reliability constraints, such as those imposed by beyond 5G and 6G wireless networks [106], as well as IoT and SG applications enabled by power line communication [21]. OCDM-based systems have therefore being considered in a wide range of applications in the power line and wireless communication contexts [20, 21, 106] as well as sensing fields [111–113]. In hybrid communication systems, however, the OCDM scheme has not been investigated yet. In this regard, this chapter aims to fill this gap in the literature and starts the investigation of OCDM scheme in HPWSs. The main contributions of this chapter are as follows:

- The introduction of the OCDM-based HPWS model. It is therefore proposed an HPWS in which the discrete-Fresnel domain representation of the symbols transmitted over wireless and power line media are the same. At the receiver side, MRC technique is applied to combine the symbols in the discrete-Fresnel domain as well.

- The investigation of WSS random processes in the discrete-Fresnel domain. It is demonstrated that a WSS random process in the discrete-time domain is also a WSS random process in the discrete-Fresnel domain with the same mean value and autocorrelation function.

- The extension of the power allocation of the previous chapters to the OCDM-based HPWS. Since the orthogonal subchirps experience the same nSNRs, the power allocation is easily applicable to the OCDM-based HPWS. Besides, the optimal power allocation requires the feedback of only one bit to the transmitter node.

The rest of this chapter is summarized as follows: Section 6.1 addresses the OCDM-based HPWS model; Section 6.2 analyses WSS random processes in the discrete-Fresnel domain; Section 6.3 extends the power allocation of the previous chapters to the OCDM-based HPWS model; Section 6.4 presents numerical results and their analyses, whereas Section 6.5 summarizes the chapter.

6.1 OCDM-BASED HPWS MODEL

This section presents the OCDM-based HPWS model. Similar to Chapter 2, the described HPWS model can be employed to distinct scenarios (e.g. indoor and outdoor) and frequency bands, such as narrowband and broadband ones. A discrete baseband representation of the OCDM-based HPWS model is shown in Figure 28. Following the previous chapters, the subscript "1" indicates the wireless medium, whereas the subscript "2" stand for the power line medium. In addition, the preamble OCDM symbols that are required for channel state acquisition and synchronization are assumed to be individually designed to meet the distinct characteristics of power line and wireless channels. On the other hand, the data symbols transmitted over the two channels are assumed to be equal and they will be the focus of this chapter henceforth.

In OCDM schemes, the Fresnel domain is considered analogously to the frequency domain in OFDM schemes. Throughout the dissertation, capital letters have been usually adopted to denote frequency domain symbols and, thus, a dot over the symbols will be used for indicating Fresnel domain variables hereafter. Therefore, let $\dot{\mathbf{x}} \in \mathbb{C}^{N_S \times 1}$ represent one of the transmitted data symbols in the discrete-Fresnel domain. As the data symbols transmitted over each channel are equal, $\dot{\mathbf{x}}_m = \dot{\mathbf{x}}$ such that $\dot{\mathbf{x}}_m$ represents the discrete-Fresnel domain symbol transmitted over the m^{th} medium, with $m \in \{1, 2, \ldots, N_C\}$ and N_C denoting the number of available channels. The discrete-Fresnel domain transmitted symbols can be still described as $\dot{\mathbf{x}}_m = [\dot{x}_{m,1}\ \dot{x}_{m,2}\ \ldots\ \dot{x}_{m,N_S}]^T$, in which $\dot{x}_{1,k} = \dot{x}_{2,k} = \ldots = \dot{x}_{N_C,k}, \forall k \in \{0, 1, \ldots, N_S - 1\}$, and $\dot{x}_{m,k} \in \mathcal{M}$, with $\mathcal{M}$ indicating an M-ary constellation. In addition, $\mathbb{E}\{\dot{x}_{m,k}\} = 0, \forall\ m,\ k$ and $\mathbb{E}\{|\dot{x}_{m,k}|^2\} = p_{m,k}, \forall\ m,\ k$, with $p_{m,k}$ representing the transmission power in the m^{th} medium and k^{th} subchirp. Also, each medium has an available transmission power equal to $\sum_k p_{m,k} = P_m$ and the total transmission power is $\sum_m P_m = P_T$.

The next step of an OCDM scheme consists of transforming the discrete-Fresnel domain symbols $\dot{\mathbf{x}}_m$ to the discrete-time domain. However, in order to perform baseband data transmission (i.e, power line transmission), the time-domain versions of the transmitted symbols need to be real-valued, whereas passband data transmission can be performed based on complex-valued symbols. In this regard, power line and wireless transmissions consider two distinct Fresnel-to-time transforms. Essentially, the discrete-Fresnel domain symbol transmitted over the wireless

Figure 28 – OCDM-based HPWS model

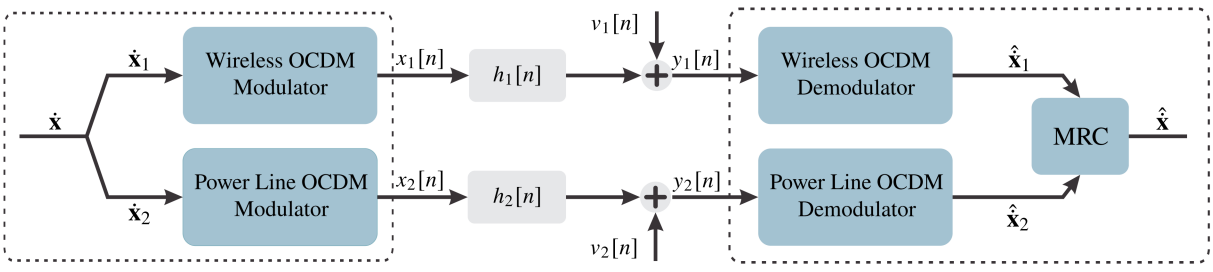

Source: Personal collection.

channel, $\dot{\mathbf{x}}_1$, is directly multiplied by the complex-valued DFnT matrix [20]. On the other hand, the discrete-Fresnel domain symbol transmitted over the power line channel, $\dot{\mathbf{x}}_2$, is mapped into a real-valued symbol, $\dot{\mathbf{x}}_2^{\text{map}}$, and then transformed to discrete-time domain using a real-valued DFnT matrix [21]. Algebraically, the k^{th} element of the mapped transmitted symbol, $\dot{\mathbf{x}}_{m,k}^{\text{map}}$, can be denoted as

$$\dot{x}_{m,k}^{\text{map}} = \dot{x}_{m,k}, \text{for } k = 0, 1, \ldots, N_{\text{S}} - 1, \qquad \text{if } m = 1 \text{ (wireless)} \tag{6.1}$$

and

$$\dot{x}_{m,k}^{\text{map}} = \begin{cases} \sqrt{2}\Re\{\dot{x}_{m,k/2}\}, & \text{for } k = 0, 2, \ldots, 2N_{\text{S}} - 2 \\ \sqrt{2}\Im\{\dot{x}_{m,(k-1)/2}\}, & \text{for } k = 1, 3, \ldots, 2N_{\text{S}} - 1 \end{cases}, \qquad \text{if } m = 2 \text{ (power line)}, \tag{6.2}$$

where $\Re\{\cdot\}$ and $\Im\{\cdot\}$ returns the real and imaginary parts of the input, respectively. Notice that $\dot{\mathbf{x}}_m^{\text{map}} \in \mathbb{C}^{N_{\text{S}} \times 1}$ for $m = 1$ (wireless), whereas $\dot{\mathbf{x}}_m^{\text{map}} \in \mathbb{R}^{2N_{\text{S}} \times 1}$ for $m = 2$ (power line).

Afterwards, the discrete-time domain representation of the symbol transmitted through the m^{th} medium can be expressed as

$$\mathbf{x}_m = \mathbf{\Phi}_m^{\dagger} \dot{\mathbf{x}}_m^{\text{map}}, \tag{6.3}$$

in which $\mathbf{\Phi}_m$ is the DFnT matrix used in the m^{th} medium and $(\cdot)^{\dagger}$ is the Hermitian operator (used for inverse transforms). The DFnT matrix can be decomposed as $\mathbf{\Phi}_m = \mathbf{F}^{\dagger}\mathbf{\Gamma}_m\mathbf{F}$, with $\mathbf{F}$ denoting the normalized version of the DFT matrix and $\mathbf{\Gamma}_m$ being a diagonal matrix composed of the eigenvalues of $\mathbf{\Phi}_m$. The k^{th} eigenvalue of the DFnT matrix for the wireless branch ($m = 1$), with $k \in \{0, 1, \ldots, N_{\text{S}} - 1\}$, is defined by

$$\Gamma_{m,k} \triangleq \mathrm{e}^{-(\mathrm{j}\pi/N_{\text{S}})k^2}, \forall k \in \{0, 1, \ldots, N_{\text{S}} - 1\}. \tag{6.4}$$

And the k^{th} eigenvalue of the DFnT matrix for the power line branch ($m = 2$), with $k \in \{1, 2, \ldots, 2N_{\text{S}}\}$, is given by

$$\Gamma_{m,k} \triangleq \begin{cases} \mathrm{e}^{-(\mathrm{j}\pi/N_{\text{S}})k^2}, & \text{for } k < N_{\text{S}} \\ \mathrm{e}^{(\mathrm{j}\pi/N_{\text{S}})k^2}, & \text{for } k \geq N_{\text{S}}. \end{cases} \tag{6.5}$$

Note that $\mathbf{\Phi}_1 \in \mathbb{C}^{N_{\text{S}} \times N_{\text{S}}}$ (wireless), whereas $\mathbf{\Phi}_2 \in \mathbb{R}^{2N_{\text{S}} \times 2N_{\text{S}}}$ (power line). Moreover, the DFnT and its inverse can be efficiently implemented based on the fast Fourier transform (FFT) and its inverse.

In sequel, a cyclic prefix of length L_{CP} is prepended to the beginning of the discrete-time domain resulting symbol, $\mathbf{x}_m$. To avoid ISI in the OCDM-based HPWS, the CP length has to be $L_{\text{CP}} \geq \max_m\{L_m\} - 1$, with L_m indicating the length of the CIR associated with the m^{th} medium, $\mathbf{h}_m$. After the cyclic prefix insertion, each OCDM symbol is serialized, converted to analog signal, and then transmitted through the communication channel. The transmission of each OCDM symbol occurs during a symbol time interval equal to T_{symb}. Also, $T_{\text{symb}} \ll T_{\text{c}}^{\text{H}}$, with

$T_{\mathrm{c}}^{\mathrm{H}} = \min_{m}\{T_{\mathrm{c}}^{m}\}$ denoting the overall coherence time such that T_{c}^{m} indicates the coherence time of the m^{th} channel. As a consequence, the HPWS can be assumed to be LTI within each symbol time interval. For this reason, it is possible to established a direct relationship between the transmitted and received sequences through the convolution operator. In other words, assuming perfect synchronization, the discrete-time domain signal received in the m^{th} medium can be described as

$$y_m[n] = x_m[n] \star h_m[n] + v_m[n], \tag{6.6}$$

in which $\{x_m[n]\}$ represents the time-domain transmitted sequence composed of successive OCDM symbols; $\{h_m[n]\}_{n=1}^{L_m}$ is an L_m-length sequence that represents the CIR of the m^{th} medium; $\{v_m[n]\}$ is a time-domain sequence that stands for the additive noise in the m^{th} medium, which is modeled as stationary random process; and $\star$ denotes the linear convolution operator.

At the receiver side, after the cyclic prefix removal, each of the received symbols in the discrete-time domain can be expressed as

$$\mathbf{y}_m = \mathbf{C}_{h_m}\mathbf{x}_m + \mathbf{v}_m, \tag{6.7}$$

where $\mathbf{C}_{h_m}$ is the circulant matrix associated with the CIR of the m^{th} medium, and $\mathbf{v}_m$ is a vector that represents the discrete-time domain additive noise in the m^{th} medium. Note that $\mathbf{C}_{h_m} \in \mathbb{C}^{N_{\mathrm{S}}\times N_{\mathrm{S}}}$ and $\mathbf{v}_m \in \mathbb{C}^{N_{\mathrm{S}}\times 1}$ for $m = 1$ (i.e., wireless), whereas $\mathbf{C}_{h_m} \in \mathbb{R}^{2N_{\mathrm{S}}\times 2N_{\mathrm{S}}}$ and $\mathbf{v}_m \in \mathbb{C}^{2N_{\mathrm{S}}\times 1}$ for $m = 2$ (i.e., power line).

Next, channel equalization is performed. This process, however, cannot be easily carried out in either time or Fresnel domains. For the sake of simplicity, zero-forcing channel equalization is considered. According to [20, 21], it can be accomplished in the frequency domain without significantly increasing the computational complexity. Since the DFnT matrix can be decomposed into DFT matrices (direct and reverse forms) and a diagonal matrix of its eigenvalues, the received symbols can be transformed to the discrete-frequency domain to be equalized and then transformed to the discrete-Fresnel domain directly. Therefore, let the discrete-frequency domain representation of the received symbol be as follows:

$$\begin{aligned}
\mathbf{Y}_m &= \mathbf{F}\mathbf{y}_m && (6.8)\\
&= \mathbf{F}\mathbf{C}_{h_m}\mathbf{\Phi}_m^{\dagger}\dot{\mathbf{x}}_m^{\mathrm{map}} + \mathbf{V}_m && (6.9)\\
&= \mathbf{F}\mathbf{C}_{h_m}\mathbf{F}^{\dagger}\mathbf{F}\mathbf{\Phi}_m^{\dagger}\mathbf{F}^{\dagger}\mathbf{F}\dot{\mathbf{x}}_m^{\mathrm{map}} + \mathbf{V}_m && (6.10)\\
&= \mathbf{\Lambda}_{h_m}\mathbf{\Gamma}_m^{\dagger}\mathbf{F}\dot{\mathbf{x}}_m^{\mathrm{map}} + \mathbf{V}_m, && (6.11)
\end{aligned}$$

with $\mathbf{V}_m = \mathbf{F}\mathbf{v}_m$. Following [20,21], the channel effect (i.e., the diagonal matrix $\mathbf{\Lambda}_{h_m}$ of the CFR associated with the m^{th} medium) and the eigenvalues of the DFnT matrix can be jointly removed at the receiver side. As a consequence, an estimate of the transmitted symbol can be obtained as follows:

$$\begin{aligned}
\hat{\mathbf{X}}_m^{\mathrm{map}} &= \mathbf{\Gamma}_m\mathbf{\Lambda}_{h_m}^{-1}\mathbf{Y}_m && (6.12)\\
&= \mathbf{F}\dot{\mathbf{x}}_m^{\mathrm{map}} + \mathbf{\Lambda}_{h_m}^{-1}\mathbf{\Gamma}_m\mathbf{V}_m. && (6.13)
\end{aligned}$$

The inverse DFT can be then applied to obtain an estimate of the discrete-Fresnel domain transmitted signal:

$$\hat{\dot{\mathbf{x}}}_m^{\text{map}} = \mathbf{F}^{\dagger}\hat{\dot{\mathbf{X}}}_m^{\text{map}} \tag{6.14}$$

$$= \dot{\mathbf{x}}_m^{\text{map}} + \dot{\mathbf{v}}_m^{\text{map}}, \tag{6.15}$$

in which $\dot{\mathbf{v}}_m^{\text{map}} = \mathbf{F}^{\dagger}\boldsymbol{\Lambda}_{h_m}^{-1}\boldsymbol{\Gamma}_m\mathbf{V}_m$.

Following, the reverse operation of the mapping carried out at the transmitter side is performed, i.e., an estimate of $\dot{x}_{m,k}$ is obtained. Mathematically, the k^{th} element of the estimate of the discrete-Fresnel domain symbol transmitted through the m^{th} medium is given by

$$\hat{\dot{x}}_{m,k} = \begin{cases} \hat{\dot{x}}_{m,k}^{\text{map}}, & \text{for } k = 0, 1, \ldots, N_{\text{S}} - 1, \quad \text{if } m = 1 \text{ (wireless)} \\ \frac{1}{\sqrt{2}}\left(\hat{\dot{x}}_{m,2k}^{\text{map}} + \text{j}\hat{\dot{x}}_{m,2k+1}^{\text{map}}\right), & \text{for } k = 0, 1, \ldots, N_{\text{S}} - 1, \quad \text{if } m = 2 \text{ (power line)}, \end{cases} \tag{6.16}$$

where $\hat{\dot{x}}_{m,k}^{\text{map}}$ denotes the k^{th} element of $\hat{\dot{\mathbf{x}}}_m^{\text{map}}$. It should be observed that the mapping and its reverse operation are designed so that the SNR experienced at their inputs and outputs is not changed, hence the SNR of $\hat{\dot{x}}_{m,k}$ is the same as the SNR of $\hat{\dot{x}}_m^{\text{map}}$. Moreover, the discrete-Fresnel domain estimated symbols can be represented as a sum of the discrete-Fresnel domain versions of transmitted symbol and noise, i.e., $\hat{\dot{x}}_{m,k} = \dot{x}_{m,k} + \dot{v}_{m,k}$. Hence, the k^{th} element of the combined symbol, $\hat{\dot{\mathbf{x}}}$, can be expressed as

$$\hat{\dot{x}}_k = \sum_m \dot{\alpha}_{m,k}\hat{\dot{x}}_{m,k} = \sum_m \dot{\alpha}_{m,k}\dot{x}_{m,k} + \sum_m \dot{\alpha}_{m,k}\dot{v}_{m,k}. \tag{6.17}$$

6.1.1 MRC Signal-to-Noise Ratio

Given (6.17), the SNR of the symbol estimated at the k^{th} subchirp can be expressed as

$$\dot{\gamma}_k = \frac{\mathbb{E}\left\{\left|\sum_m \dot{\alpha}_{m,k}\dot{x}_{m,k}\right|^2\right\}}{\mathbb{E}\left\{\left|\sum_m \dot{\alpha}_{m,k}\dot{v}_{m,k}\right|^2\right\}} = \frac{\left|\sum_m \dot{\alpha}_{m,k}\sqrt{p_{m,k}}\right|^2}{\sum_m |\dot{\alpha}_{m,k}|^2 p_{\dot{v}_{m,k}}} = \frac{\left|\sum_m \dot{\alpha}_{m,k}\sqrt{p_{\dot{v}_{m,k}}}p_{\dot{v}_{m,k}}^{-1/2}\sqrt{p_{m,k}}\right|^2}{\sum_m |\dot{\alpha}_{m,k}\sqrt{p_{\dot{v}_{m,k}}}|^2}. \tag{6.18}$$

The MRC technique seeks to maximize the SNR of the symbols that result from the combination of symbols received through different media. In order to find the maximum value of $\dot{\gamma}_k$, (6.18) can be rewritten as

$$\dot{\gamma}_k = \frac{\left|\sum_m \dot{A}_k\dot{B}_k\right|^2}{\sum_m |\dot{A}_k|^2}, \tag{6.19}$$

with $\dot{A}_k = \dot{\alpha}_{m,k}\sqrt{p_{\dot{v}_{m,k}}}$ and $\dot{B}_k = p_{\dot{v}_{m,k}}^{-1/2}\sqrt{p_{m,k}}$. By applying the Cauchy-Schwarz inequality, one has

$$\dot{\gamma}_k = \frac{\left|\sum_m \dot{A}_k \dot{B}_k\right|^2}{\sum_m |\dot{A}_k|^2} \leq \frac{\sum_m |\dot{A}_k|^2 \sum_m |\dot{B}_k|^2}{\sum_m |\dot{A}_k|^2} = \sum_m |\dot{B}_k|^2 \tag{6.20}$$

$$\leq \sum_m \dot{\gamma}_{m,k}. \tag{6.21}$$

Consequently, the SNR of the resulting symbol is upper bounded by the sum of the SNRs of the combined ones. The equality holds when $A_k/B_k^* = 1$ and therefore $\alpha_{m,k} = \sqrt{p_{m,k}}/p_{\dot{v}_{m,k}}, \forall m, k$.

6.2 WIDE-SENSE STATIONARY RANDOM PROCESSES IN THE DISCRETE-FRESNEL DOMAIN

The previous section showed that the noise power in every subchirp and medium is required to perform the MRC technique properly in an OCDM-based HPWS. For this purpose, it is necessary to understand the statistics of the additive noise in the Fresnel domain, mainly the mean value and the autocorrelation function (e.g., to derive the noise power) which are enough to deal with random process that are, at least, stationary in the wide sense. This section thus analyzes the behavior of a WSS random process in the discrete-Fresnel domain based on the knowledge of its statistics in the discrete-time domain. For the sake of simplicity, the DFnT used in the passband (i.e., the wireless branch) is assumed.

Let $v_n \in \mathbb{C}$ denote the n^{th} random variable of the noise vector in the discrete-time domain, with $\forall n \in \{0, 1, \ldots, N_S - 1\}$. In the discrete-Fresnel domain, the random variables are denoted by $\dot{v}_k \in \mathbb{C}, \forall\, k \in \{0, 1, \ldots, N_S - 1\}$. Thus, the relationship between v_n and $\dot{v}_k$ is expressed as [20]

$$\dot{v}_k = \frac{e^{-j\frac{\pi}{4}}}{\sqrt{N_S}} \sum_{n=0}^{N_S-1} v_n e^{j\frac{\pi}{N_S}(k-n)^2}. \tag{6.22}$$

Conversely, the inverse form of the DFnT is given by

$$v_n = \frac{e^{j\frac{\pi}{4}}}{\sqrt{N_S}} \sum_{k=0}^{N_S-1} \dot{v}_k e^{-j\frac{\pi}{N_S}(k-n)^2}. \tag{6.23}$$

Since v_n is modeled as a WSS random process and, its mean value is constant over the discrete time index n, i.e., $\mathbb{E}\{v_n\} = \mu, \forall\, n \in \{0, 1, \ldots, N_S - 1\}$. Additionally, its autocorrelation function depends solely on the delay n_d between samples, i.e., $\mathbb{E}\{v_n v_{n+n_d}^*\} = R_v[n_d]$.

Next, Lemmas 3 and 4, Corollary 2, and Theorem 2 are presented to determine the statistics of a WSS random process in the discrete-Fresnel domain.

Lemma 3*: If the mean value of a random process is constant in the discrete-time domain, then the mean value of its discrete-Fresnel domain counterpart assumes the same constant value, i.e.,*

$$\mathbb{E}\{v_n\} = \mathbb{E}\{\dot{v}_k\} = \mu. \tag{6.24}$$

Proof. The mean value of a random process $\dot{v}_k$ in the discrete-Fresnel domain can be expressed as

$$\mathbb{E}\{\dot{v}_k\} = \mathbb{E}\left\{\frac{\mathrm{e}^{-\mathrm{j}\frac{\pi}{4}}}{\sqrt{N_\mathrm{S}}}\sum_{n=0}^{N_\mathrm{S}-1} v_n \mathrm{e}^{\mathrm{j}\frac{\pi}{N_\mathrm{S}}(k-n)^2}\right\} \tag{6.25}$$

$$= \frac{\mathrm{e}^{-\mathrm{j}\frac{\pi}{4}}}{\sqrt{N_\mathrm{S}}}\sum_{n=0}^{N_\mathrm{S}-1} \mathbb{E}\{v_n\}\mathrm{e}^{\mathrm{j}\frac{\pi}{N_\mathrm{S}}(k-n)^2}. \tag{6.26}$$

If mean value of v_n is not a function of the discrete-time domain index n, it can be taken out from the above summation. It therefore holds that

$$\mathbb{E}\{\dot{v}_k\} = \mathbb{E}\{v_n\}\left(\frac{\mathrm{e}^{-\mathrm{j}\frac{\pi}{4}}}{\sqrt{N_\mathrm{S}}}\sum_{n=0}^{N_\mathrm{S}-1} \mathrm{e}^{\mathrm{j}\frac{\pi}{N_\mathrm{S}}(k-n)^2}\right) \tag{6.27}$$

$$= \mu\left(\frac{\mathrm{e}^{-\mathrm{j}\frac{\pi}{4}}}{\sqrt{N_\mathrm{S}}}\sum_{n=0}^{N_\mathrm{S}-1} \mathrm{e}^{\mathrm{j}\frac{\pi}{N_\mathrm{S}}(k-n)^2}\right). \tag{6.28}$$

The mean value of $\dot{v}_k$ can be alternatively expressed as a function of summations of sine and cosine functions and rewritten as

$$\mathbb{E}\{\dot{v}_k\} = \mu\frac{\mathrm{e}^{-\mathrm{j}\frac{\pi}{4}}}{\sqrt{N_\mathrm{S}}}\left[\sum_{n=0}^{N_\mathrm{S}-1}\cos\left(\frac{\pi}{N_\mathrm{S}}(k-n)^2\right) + \mathrm{j}\sum_{n=0}^{N_\mathrm{S}-1}\sin\left(\frac{\pi}{N_\mathrm{S}}(k-n)^2\right)\right]. \tag{6.29}$$

Both the above summations are equal to $\sqrt{N/2}$ [114] since N is even, which is assumed due to the FFT-based implementation of the DFnT and its inverse [20]. Therefore, the mean value of the random process $\dot{v}[k]$ in the discrete-Fresnel domain can be expressed as

$$\mathbb{E}\{\dot{v}_k\} = \mu\frac{\mathrm{e}^{-\mathrm{j}\frac{\pi}{4}}}{\sqrt{N_\mathrm{S}}}\left(\sqrt{\frac{N_\mathrm{S}}{2}} + \mathrm{j}\sqrt{\frac{N_\mathrm{S}}{2}}\right) \tag{6.30}$$

$$= \mu\frac{\mathrm{e}^{-\mathrm{j}\frac{\pi}{4}}}{\sqrt{N_\mathrm{S}}}\left(\mathrm{e}^{\mathrm{j}\frac{\pi}{4}}\sqrt{N_\mathrm{S}}\right) \tag{6.31}$$

$$= \mu. \tag{6.32}$$

□

Based on Lemma 3, Corollary 2 can be stated.

Corollary 2*: A zero-mean additive noise in the discrete-time domain remains a zero-mean additive noise when transformed into the discrete-Fresnel domain.*

Lemma 4*: The autocorrelation function of a wide-sense stationary random process in the discrete-time domain is kept after transformation into the discrete-Fresnel domain.*

Proof. The autocorrelation function of the random process $\dot{v}_k$ in the discrete-Fresnel domain is given by

$$R_{\dot{v}}[k_1, k_2] = \mathbb{E}\{\dot{v}_{k_1}\dot{v}^*_{k_2}\}. \tag{6.33}$$

The above equation can be expanded as follows

$$R_{\dot{v}}[k_1,k_2] = \mathbb{E}\left\{\left(\frac{\mathrm{e}^{-\mathrm{j}\frac{\pi}{4}}}{\sqrt{N_\mathrm{S}}}\sum_{n=0}^{N_\mathrm{S}-1} v_n \mathrm{e}^{\mathrm{j}\frac{\pi}{N_\mathrm{S}}(k_1-n)^2}\right)\left(\frac{\mathrm{e}^{\mathrm{j}\frac{\pi}{4}}}{\sqrt{N_\mathrm{S}}}\sum_{n=0}^{N_\mathrm{S}-1} v_n^* \mathrm{e}^{-\mathrm{j}\frac{\pi}{N_\mathrm{S}}(k_2-n)^2}\right)\right\} \tag{6.34}$$

$$= \frac{1}{N_\mathrm{S}}\mathbb{E}\left\{\sum_{n=0}^{N_\mathrm{S}-1}\sum_{n'=0}^{N_\mathrm{S}-1} v_n v_{n'}^* \mathrm{e}^{\mathrm{j}\frac{\pi}{N_\mathrm{S}}[(k_1-n)^2-(k_2-n')^2]}\right\} \tag{6.35}$$

$$= \frac{1}{N_\mathrm{S}}\sum_{n=0}^{N_\mathrm{S}-1}\sum_{n'=0}^{N_\mathrm{S}-1} \mathbb{E}\{v_n v_{n'}^*\}\mathrm{e}^{\mathrm{j}\frac{\pi}{N_\mathrm{S}}[(k_1-n)^2-(k_2-n')^2]}. \tag{6.36}$$

Since v_n is modeled as a WSS random process, n' can be replaced by $n+n_\mathrm{d}$ and $\mathbb{E}\{v_n v_{n'}^*\}$ can be substituted by $R_v[n_\mathrm{d}]$, yielding

$$R_{\dot{v}}[k_1,k_2] = \frac{1}{N_\mathrm{S}}\sum_{n=0}^{N_\mathrm{S}-1}\sum_{n_\mathrm{d}=-n}^{N_\mathrm{S}-1-n} R_v[n_\mathrm{d}]\mathrm{e}^{\mathrm{j}\frac{\pi}{N_\mathrm{S}}[(k_1-n)^2-(k_2-(n+n_\mathrm{d}))^2]}. \tag{6.37}$$

To adjust the summation indices, (6.37) can be rewritten as a function of $n'' = n + n_\mathrm{d}$, which results in

$$R_{\dot{v}}[k_1,k_2] = \frac{1}{N_\mathrm{S}}\sum_{n''=0}^{N_\mathrm{S}-1}\sum_{n=0}^{N_\mathrm{S}-1} R_v[n''-n]\mathrm{e}^{\mathrm{j}\frac{\pi}{N_\mathrm{S}}[(k_1-n)^2-(k_2-n'')^2]} \tag{6.38}$$

$$= \frac{1}{N_\mathrm{S}}\sum_{n''=0}^{N_\mathrm{S}-1} \mathrm{e}^{-\mathrm{j}\frac{\pi}{N_\mathrm{S}}(k_2-n'')^2}\sum_{n=0}^{N_\mathrm{S}-1} R_v[n''-n]\mathrm{e}^{\mathrm{j}\frac{\pi}{N_\mathrm{S}}(k_1-n)^2} \tag{6.39}$$

$$= \frac{\mathrm{e}^{\mathrm{j}\frac{\pi}{4}}}{\sqrt{N_\mathrm{S}}}\sum_{n''=0}^{N_\mathrm{S}-1} \mathrm{e}^{-\mathrm{j}\frac{\pi}{N_\mathrm{S}}(k_2-n'')^2}\left(\frac{\mathrm{e}^{-\mathrm{j}\frac{\pi}{4}}}{\sqrt{N_\mathrm{S}}}\sum_{n=0}^{N_\mathrm{S}-1} R_v[n''-n]\mathrm{e}^{\mathrm{j}\frac{\pi}{N_\mathrm{S}}(k_1-n)^2}\right). \tag{6.40}$$

Note that the summation over n in (6.40) represents the DFnT of $R_v[n''-n]$. In addition, a circular shift of n'' samples in the discrete-time domain implies a circular shift of n'' samples in the discrete-Fresnel domain since the DFnT corresponds to a multiplication of its the input vector by a circulant matrix [115]. Furthermore, the reversal of discrete-time indices results in the same reversal in the discrete-Fresnel domain. Hence, the autocorrelation function can be further rewritten as

$$R_{\dot{v}}[k_1,k_2] = \frac{\mathrm{e}^{\mathrm{j}\frac{\pi}{4}}}{\sqrt{N_\mathrm{S}}}\sum_{n''=0}^{N_\mathrm{S}-1} \dot{R}_v[n''-k_1]\mathrm{e}^{-\mathrm{j}\frac{\pi}{N_\mathrm{S}}(k_2-n'')^2}, \tag{6.41}$$

in which $\dot{R}_v[\cdot]$ is the discrete-Fresnel version of the autocorrelation function $R_v[\cdot]$. Since the remaining summation represents the inverse DFnT of $\dot{R}_v[n''-k_1]$, (6.41) can be further simplified as

$$R_{\dot{v}}[k_1,k_2] = R_v[k_2-k_1] = R_v[k_\mathrm{d}], \tag{6.42}$$

with $k_\mathrm{d} = k_2 - k_1$. □

Theorem 2*: The wide-sense stationary characteristics of a random process in the discrete-time domain are maintained after transformation into the discrete-Fresnel domain.*

Proof. The proof of Theorem 2 is a consequence of Lemma 3 and Lemma 4. □

Based on Theorem 2, it becomes clear why the OCDM and single carrier with cyclic prefix (SC-CP) schemes perform equally under influence of WSS additive noise, which was only numerically observed for AWGN in [20, 21, 106] but not mathematically proven. This outcome is due to the fact that not only the power associated with v_n remains constant over n, but also the power associated with $\dot{v}_k$ is not a function of the index k. Mathematically, it holds that

$$\mathbb{E}\{|v_n|^2\} = \mathbb{E}\{|\dot{v}_k|^2\} = R_v[0], \tag{6.43}$$

$\forall\, n, k \in \{0, 1, \ldots, N_S - 1\}$. Based on (6.43), it can be noticed that the noise power is constant in the discrete-Fresnel domain regardless of the PSD shape of the WSS random process that describes the noise. In this sense, not only AWGN, which inherently has constant noise power in the discrete-frequency domain, but also other noise types, e.g., colored noise with $1/f^{\alpha}$-shaped PSD will still present constant noise power in the discrete-Fresnel domain. Hence, the MRC weights $\dot{\alpha}_{m,k}$ will also be constant over the subchirps, which considerably reduces the complexity associated with the combining technique compared to its application in the frequency-domain.

Finally, it can be stated that the additive noise power at the k^{th} subchirp and m^{th} medium is as follows:

$$\begin{aligned} p_{\dot{v}_{m,k}} &= \mathbb{E}\{\dot{v}_k \dot{v}_k^*\} && (6.44)\\ &= R_v[0]. && (6.45) \end{aligned}$$

Alternatively,

$$p_{\dot{v}_{m,k}} = \frac{1}{N_S} \sum_{l=0}^{N_S-1} p_{V_{m,l}}, \tag{6.46}$$

in which $p_{V_{m,l}}$ indicates the noise power at the l^{th} subcarrier (frequency domain) and m^{th} medium. Notice that the achieved outcomes make clear why the performances of OCDM and SC-CP schemes are the same under wide-sense stationary additive noise [20, 21, 106].

6.3 POWER ALLOCATION IN THE OCDM-BASED HPWS

Once the noise power has been clearly defined, the SNRs values can be further derived so that power allocation problems can be formulated as in the previous chapters. In this context, the noise power in the discrete-Fresnel domain with the effect of channel equalization has to be defined. As zero-forcing frequency-domain equalization is considered and the noise power in the discrete-Fresnel domain was presented as a function of the noise power in the discrete-frequency domain, the impact of the equalizer gain in each subchannel and medium can be straightforwardly introduced in (6.46). In summary, the SNR of the discrete-Fresnel domain symbol at the k^{th} subchirp and m^{th} medium can be expressed, after the zero forcing equalization,

as

$$\dot{\gamma}_{m,k} = \frac{p_{m,k}}{p_{\dot{v}_{m,k}}} \tag{6.47}$$

$$= p_{m,k}\left(\frac{1}{N_{\mathrm{S}}}\sum_{l=0}^{N_{\mathrm{S}}-1} p_{V_{m,l}}\frac{1}{|H_{m,l}|^2}\right)^{-1} \tag{6.48}$$

$$= p_{m,k}\left(\frac{1}{N_{\mathrm{S}}}\sum_{l=0}^{N_{\mathrm{S}}-1} \overline{\gamma}_{m,l}^{-1}\right)^{-1}, \tag{6.49}$$

where $H_{m,l}$ and $\overline{\gamma}_{m,l}$ again respectively indicates the CFR and nSNR values at the l^{th} subcarrier (frequency domain) and m^{th} medium. In other words, the SNR experienced at the discrete-Fresnel domain after the zero-forcing equalization can be expressed as a function of an harmonic mean of the nSNRs in the discrete-frequency domain, as previously stated in [106, 110].

Since the nSNR is defined as $\dot{\overline{\gamma}}_{m,k} \triangleq \dot{\gamma}_{m,k}/p_{m,k}$, a relationship between the discrete-Fresnel domain and discrete-frequency domain nSNRs can be expressed as

$$\dot{\overline{\gamma}}_{m,k} = \left(\frac{1}{N_{\mathrm{S}}}\sum_{l=0}^{N_{\mathrm{S}}-1} \overline{\gamma}_{m,l}^{-1}\right)^{-1}. \tag{6.50}$$

Note that $\dot{\overline{\gamma}}_{m,k}$ does not depend on the subchirp index k and therefore it is constant over the discrete-Fresnel domain. Based on the given discrete-Fresnel domain nSNR, the functional $f(\cdot)$ can be defined according to the main objective, which can be related to either the achievable data rate

$$f(p_{m,k}) = -\frac{B_{\mathrm{w}}}{N_{\mathrm{S}}}\log_2\left(1 + \sum_{m=1}^{N_{\mathrm{C}}} p_{m,k}\dot{\overline{\gamma}}_{m,k}\right) \tag{6.51}$$

or the average BEP

$$f(p_{m,k}) = \frac{1}{N_{\mathrm{S}}}P_{\mathrm{e},k}\left(\sum_{m} p_{m,k}\dot{\overline{\gamma}}_{m,k}\right). \tag{6.52}$$

In sequel, the power allocation optimization problem on $p_{m,k}$ can be defined as

$$\min_{p_{m,k}} \sum_{k=1}^{N_{\mathrm{S}}} f(p_{m,k}), \tag{6.53}$$

subject to either

$$\mathrm{SPC}\begin{cases} \sum\limits_{m,k} p_{m,k} \leq P_{\mathrm{T}} \\ p_{m,k} \geq 0,\ \forall\, k, m \end{cases} \tag{6.54}$$

or

$$\mathrm{SPCC}\begin{cases} \sum\limits_{k} p_{m,k} \leq P_m,\ \forall m \\ p_{m,k} \geq 0,\ \forall\, k, m \end{cases}. \tag{6.55}$$

The optimization problems above formulated are similar to the power allocation optimization problems presented in Chapters 3 and 4. Although these optimization problems have already

been solved in these chapters by Algorithms #1 to #4, an analytical solution for OCDM-based HPWSs is more useful since the discrete-Fresnel domain nSNRs are constant over the subchirps.

Concerning the SPC, the solutions presented in the previous chapters revealed that only the nSNR with the highest values should be used for maximizing the available resources. Due to the constant value of the nSNRs in each of the subchirps in the discrete-Fresnel domain, the decision process here is significantly simplified. Essentially, only one subchirp comparison is enough to define which media should be used or not. Therefore, the optimization of power allocation in OCDM-based HPWSs assuming the SPC results in using only one medium, which is the best one in terms of nSNRs in the discrete-Fresnel domain. Hence, there is also a reduction in the amount of data transmitted through the feedback channel between receiver and transmitter. In OFDM-based HPWSs, the number of bits associated with one CSI transmission is given by

$$b_{\mathrm{CSI}} = N_{\mathrm{C}} \times N_{\mathrm{S}} \times b_{\mathrm{s}}, \tag{6.56}$$

with b_{s} denoting the number of bits used to quantize each sample of nSNR. On the other hand, only one bit ($b_{\mathrm{CSI}} = 1$) is needed in OCDM-based HPWSs, i.e., the nSNRs do not have to be sent from the receiver to the transmitter. A drastic reduction in the amount of feedback data between receiver and transmitter is therefore experienced when the OCDM scheme is chosen rather than the OFDM scheme in the context of HPWSs. There are several applications, mainly in the IoT and SG fields, in which the feedback channel is constrained by a few bits. For instance, there are power line and wireless standards in which the receiver indicates the quality of the data communication channel through the feedback of a few bits so that the transmitter may switch the adopted modulation. In such cases, the OCDM scheme appears as a solution more appealing to meet data communication reliability demands than the OFDM scheme.

Regarding the SPCC, the solution is even more simple. Basically, the optimal power allocation in OCDM-based HPWSs assuming the SPCC is the uniform power allocation among subchirps and media. This outcome is due to the fact that the nSNR ratios (i.e., $\dot{\overline{\gamma}}_{1,k}/\dot{\overline{\gamma}}_{2,k}$) will be constant over the subchirps indices if the nSNRs in each of the subchirps and media are constant. As a consequence, its minimum, $\min\limits_{k}\left\{\frac{\overline{\gamma}_{1,k}}{\overline{\gamma}_{2,k}}\right\}$, and maximum, $\min\limits_{k}\left\{\frac{\overline{\gamma}_{1,k}}{\overline{\gamma}_{2,k}}\right\}$, values will be equal - see (3.34). In this scenario, one has $\lambda_1/\lambda_2 = \overline{\gamma}_{1,k}/\overline{\gamma}_{2,k}, \forall k$ and therefore all subchirps of all media can be used for data transmission. The power allocation in the OCDM-based HPWS then reduces to the power allocation in non-hybrid systems with constant nSNRs, which is solved by uniform power allocation.

6.4 NUMERICAL ANALYSES

This section numerically evaluates the OCDM-based HPWS through a comparison with the OFDM-based HPWS. Focusing on a power allocation perspective, the maximization of the achievable data rate and the minimization of the average BEP are taken into account under sum power and sum power-channel constraints. Moreover, three different cases are considered in the analyses. The first case assumes that the complete CSI is available at the transmitter node.

The second case regards the transmitter node having partial knowledge of the CSI, e.g., one-bit feedback that indicates the medium with the highest nSNR value in the discrete-Fresnel domain. The third case, on the other hand, considers that no knowledge of the CSI is obtained by the transmitter. The second and third cases are jointly presented.

Throughout this section, uncoded QAM constellation is assumed with modulation order $M = 4$. In addition, the total number of subchannels and media are respectively $N_S = 128$ and $N_C = 2$. The considered total transmission power is within the range $P_T \in [-20, 30]$ dBm. If the SPCC is assumed, then $P_1 = \alpha P_T$ and $P_2 = (1 - \alpha)P_T$, with $\alpha \in [0, 1]$. These relations defined by P_T and α are also applied to the numerical results associated with uniform power allocation. Finally, the considered frequency bandwidth is $B_w = 80$ MHz. Note that α_{opt} (i.e., the value of α that makes the performance under SPCC equal to the performance under SPC) is equal to 0 or 1 regarding OCDM-based HPWSs.

6.4.1 Channel Impulse Response and Additive Noise

The numerical analyses carried out in the current section take into account the same data of Chapters 3 and 4. Therefore, a channel impulse response and an additive noise PSD originated from a measurement campaign for broadband and in-home PLC systems, addressed in [15], are used for obtaining the numerical results. Also, the $1.7 - 81.7$ MHz frequency band is assumed, which is following the broadband power line technology [79]. Regarding the wireless medium, the wideband wireless channel model, described in [97], and circularly symmetric complex AWGN model are assumed. Additionally, in order to consider a total frequency bandwidth equal to $B_w = 80$ MHz, the frequency band ranges from $5,760$ MHz to $5,840$ MHz. The center frequency of 5.8 GHz is chosen since it is within the ISM free band and complies with wireless communication standards, such as the IEEE 802.11ac [94]. Following the previous chapters, the additive noise power associated with the wireless medium is computed so that the average SNRs values in power line and wireless media are equal in the frequency domain. Figure 29 shows the resulting nSNRs for power line and wireless media in both discrete-frequency and discrete-Fresnel domains. Notice that the wireless medium has higher nSNR values than the power line medium in the discrete-Fresnel domain and therefore $\alpha_{opt} = 1$.

6.4.2 Achievable Data Rate Analysis

The achievable data rate analysis starts with the case in which the transmitter node has complete knowledge of the CSI (i.e., all nSNR values of power line and wireless media). In this case, the optimal power allocation can be carried out in OFDM- and OCDM-based HPWSs, whereas the optimal subcarrier permutation can be taken into account for the OFDM-based HPWSs. Regarding OCDM-based HPWSs, subchirp permutation has no impact on the system performance since the same SNR is experienced by all subchirps.

Figure 30 shows the achievable data rate performance of OFDM- and OCDM-based HPWSs under SPC and SPCC assuming complete CSI at the transmitter. In this figure, OSP

indicates the optimal subcarrier permutation and $\alpha = 0.6$ is assumed for results associated with the SPCC. The OFDM with optimal subcarrier permutation and power allocation yields the best performance in terms of achievable data rate regardless of the set of constraints on the transmission power. It is followed by the OFDM scheme without subcarrier permutation and then by the OCDM scheme. Therefore, the OFDM-based HPWSs is better than the OCDM-based HPWSs in terms of achievable data rate when the transmitter has complete knowledge of the CSI, as stated for non-hybrid systems in [110].

Figure 31 illustrates the achievable data rate performance of OFDM- and OCDM-based HPWSs when the transmitter node has partial or no knowledge of the CSI. As previously mentioned, the partial knowledge of the CSI considers that the transmitter has one bit to identify the best medium for data transmission. In this case, all the available power is allocated to the best medium and therefore $\alpha = 1.0$. In case there is no information on the CSI, the transmitter allocates the available power uniformly between power line and wireless medium and then $\alpha = 0.5$. Additionally, uniform power allocation is assumed for OFDM- and OCDM-based HPWSs since there is not enough information to apply another type of power allocation. Figure 31 shows that the achievable data rate performance of the one-bit feedback case matches the optimal performance for both OFDM- and OCDM-based HPWSs. As a consequence, only one bit would be enough to indicate the best medium and then achieve the performance upper bound under uniform power allocation. On the other hand, if the transmitter does not have any

Figure 29 – nSNR for wireless ($m = 1$) and power line ($m = 2$) media in discrete-frequency and discrete-Fresnel domains

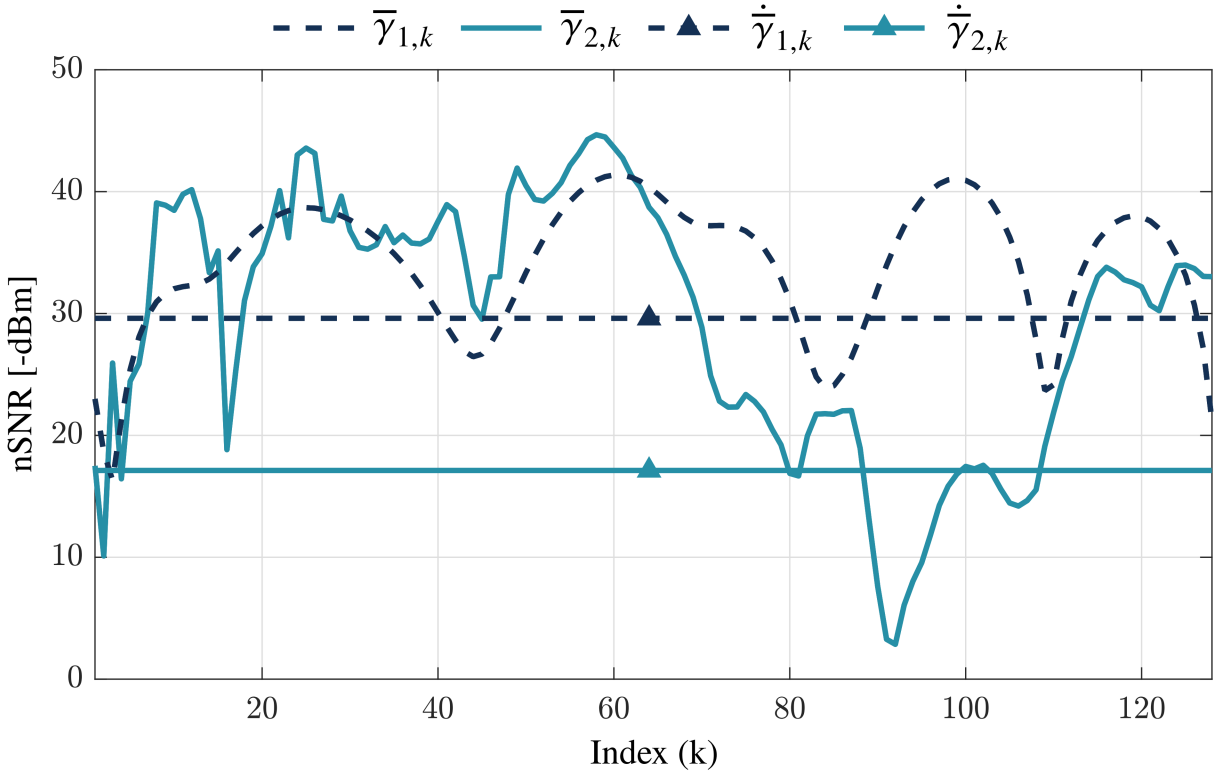

Source: Personal collection.

information on the CSI, the achievable data rate performance worsens, being more detrimental to the OCDM scheme. Overall, if the main objective is to maximize the achievable data rate, then the OCDM-based HPWSs is outperformed by the OFDM-based HPWSs regardless of the level of knowledge on the CSI obtained by the transmitter node.

Figure 30 – Achievable data rate of OFDM- and OCDM-based HPWSs, assuming complete CSI at the transmitter ($\alpha = 0.6$)

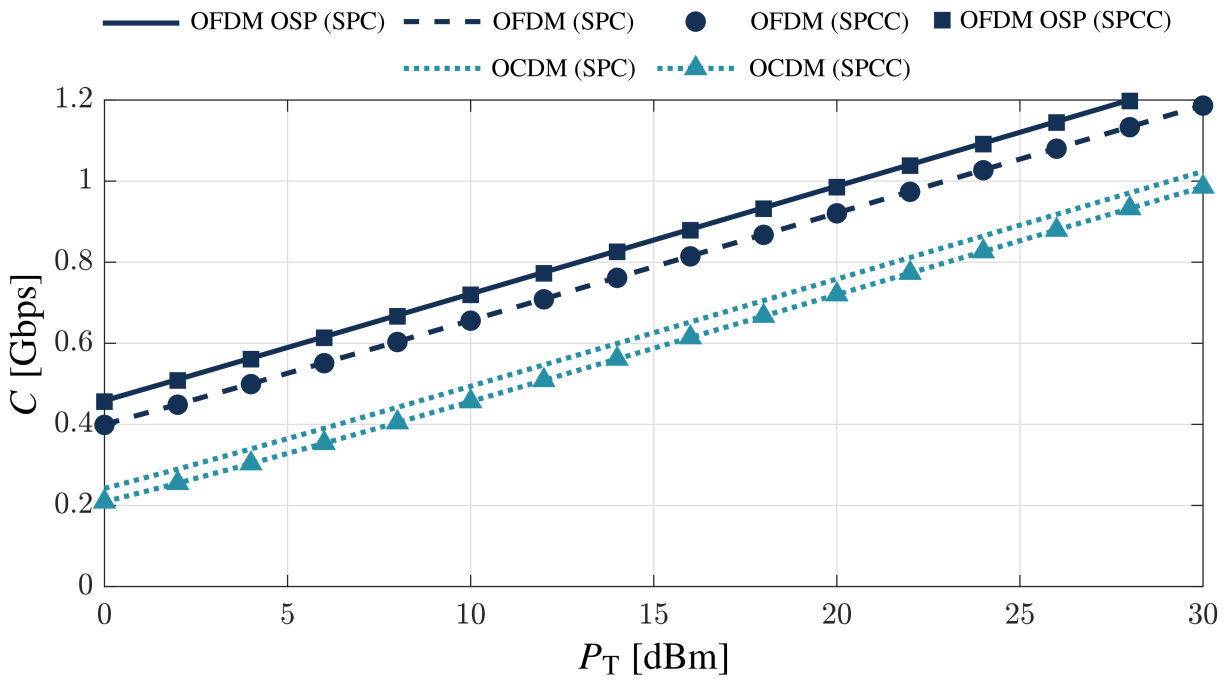

Source: Personal collection.

Figure 31 – Achievable data rate of OFDM- and OCDM-based HPWSs, assuming one-bit feedback and no CSI feedback to the transmitter node

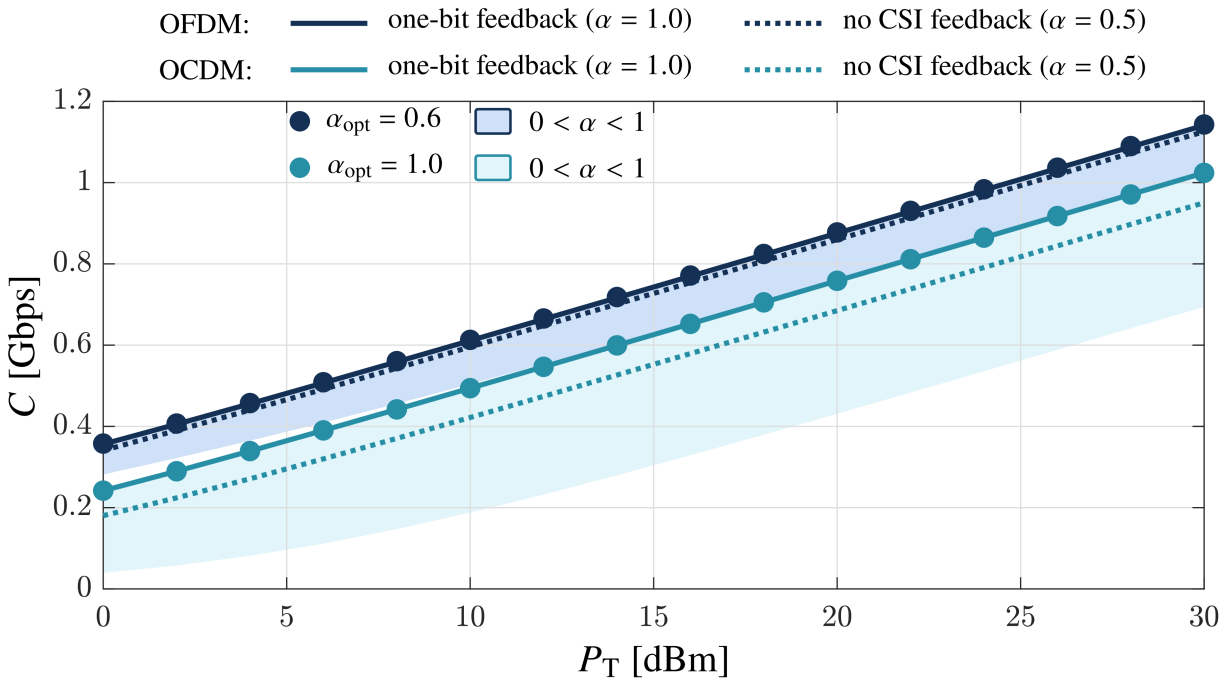

Source: Personal collection.

Figure 32 – Average BEP of OFDM- and OCDM-based HPWSs assuming complete CSI at the transmitter (4-QAM and $\alpha = 0.75$)

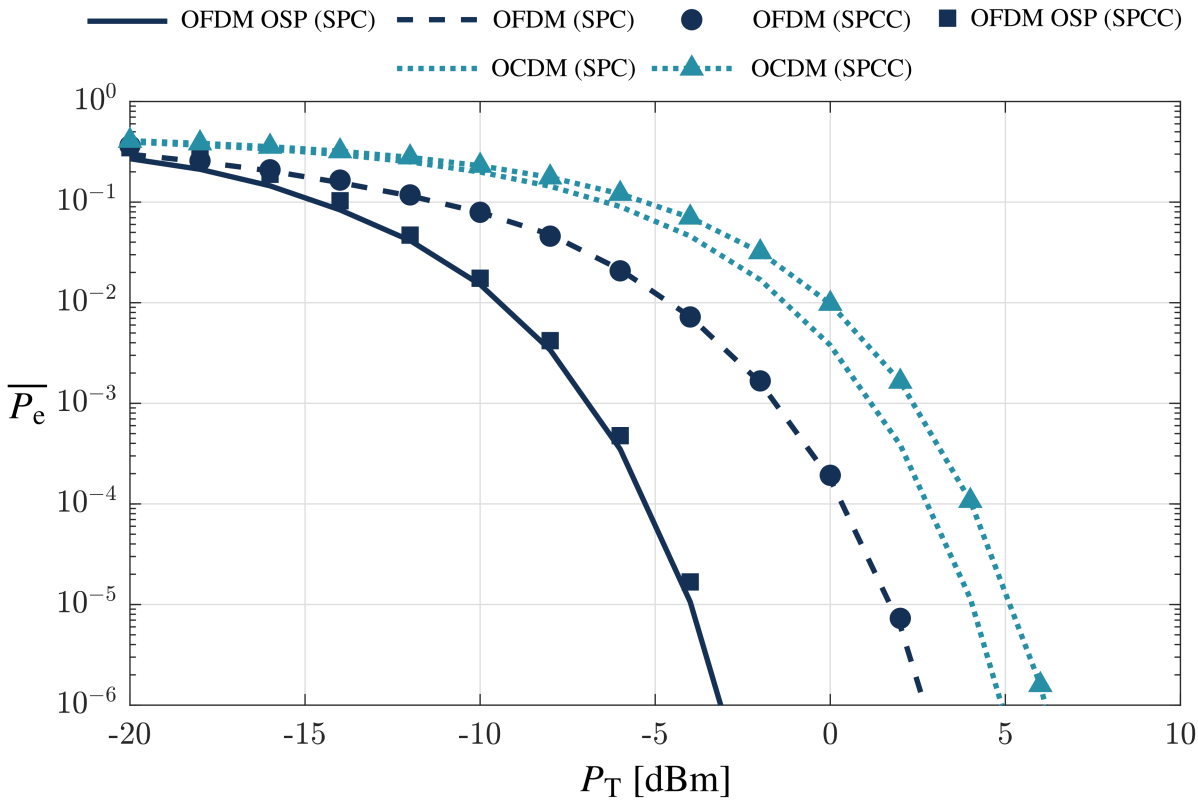

Source: Personal collection.

6.4.3 Average Bit Error Probability Analysis

Figure 32 presents the average BEP performance of OFDM- and OCDM-based HPWSs under SPC and SPCC assuming complete CSI at the transmitter. Note that $\alpha = 0.75$ is assumed for results associated with the SPCC and the optimal subcarrier permutation is again represented by OSP. Similar to the achievable data rate analysis, the best performance in terms of average BEP is achieved by the OFDM-based HPWS with subcarrier permutation, followed by the OFDM-based HPWS without subcarrier permutation and then by the OCDM-based HPWS. As a result, it can be stated that the OFDM scheme is more suitable for HPWSs than the OCDM scheme if the transmitter node has the complete knowledge of the CSI.

Figure 33 shows the average BEP performance of OFDM- and OCDM-based HPWSs for the two remainder cases, i.e., the transmitter node has one bit that indicates the best medium or the transmitter is unaware of the CSI. In this context, uniform power allocation is adopted. Notice that, different from Subsection 6.4.2, the OCDM scheme now provides a better performance compared to the OFDM scheme in terms of average BEP if the transmitter knows the best medium and the total transmission power is greater than -2 dBm. If the transmitter does not have any knowledge of the CSI, the OCDM scheme also provides a better performance; however, it occurs for total transmission power values greater than 2 dBm. Furthermore, the OCDM-based HPWS achieves its best performance at the cost of one-bit feedback, whereas the OFDM-based

Figure 33 – Average bit error probability of OFDM- and OCDM-based HPWSs, assuming one-bit feedback and no CSI feedback to the transmitter node (4-QAM)

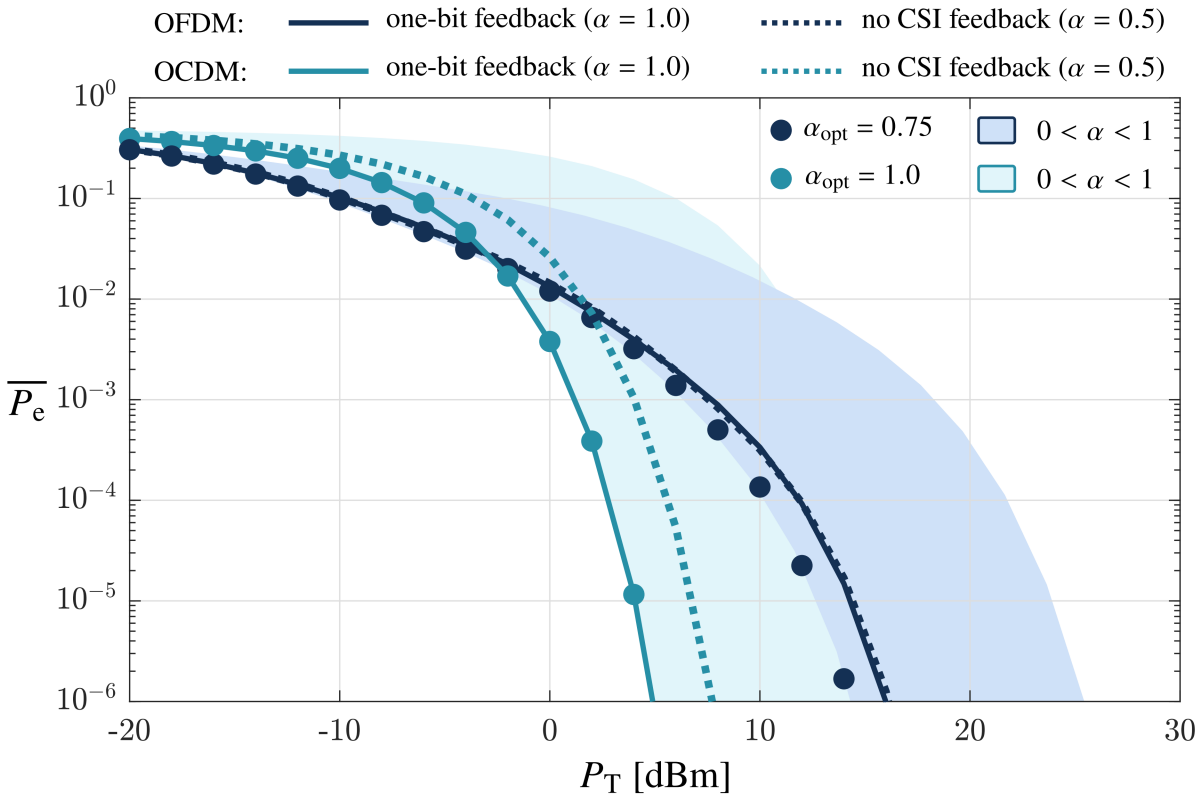

Source: Personal collection.

HPWS does not yield its best using only one medium. Therefore, the OCDM-based HPWS can be considered a more suitable choice within realistic and practical ranges of total transmission power if the aim is to minimize the average BEP under partial or no knowledge of the CSI at the transmitter node.

6.5 SUMMARY

This chapter has introduced the OCDM-based HPWSs for data communication purposes. In this kind of HPWS, the transmission of equal symbols in the discrete-Fresnel domain has been assumed and afterwards the MRC technique has been applied in the same domain. Also, the behavior of WSS random processes in the discrete-time domain has been studied in the discrete-Fresnel domain. It has been demonstrated that the discrete Fresnel transform does not change the mean value and the autocorrelation function, therefore preserving the WSS characteristic of random processes. Finally, power allocation has been analyzed in OCDM-based HPWSs under sum power and sum power-channel constraints. The optimal power allocation is derived from the previous chapters and it is shown to be considerably simple.

7 JOINT CHANNEL ESTIMATION AND SCHMIDL & COX SYNCHRONIZATION FOR OCDM-BASED SYSTEMS

Chapter 6 showed that the OCDM scheme may be an attractive option not only for non-hybrid systems but also for the HPWS. Aiming for practical implementation of these systems, however, there are open issues that require further investigation still in non-hybrid contexts. In this regard, initial efforts to address aspects such as spectrum design under the constraint of the spread spectrum nature of the subchirps that compose OCDM signals have been reported in [116]. Moreover, inspired by the typical pulse compression of chirp-based radar signals, the OCDM scheme has been investigated for performing unbiased or optimal channel estimation in the contexts of coherent optical communication [117, 118] and sensing of power lines [112].

In spite of these recent advances, the estimation and correction of symbol timing and CFO have to be carried out. Whereas the former is related to the identification of the beginning of an OCDM symbol, the latter is associated with the compensation of existing mismatches between transmitter and receiver oscillators. In the OCDM context, however, the CFO estimation was solely investigated in [119]. The authors focused on rapidly time-varying channels and proposed an OCDM symbol structure with reserved subchirps to estimate the CIR and a CFO computation based on the redundancy of the CP samples. The proposed symbol structure, however, may require a long CP length to accurately estimate the CFO. Also, the reserved subchirps for CIR estimation may significantly reduce the spectral efficiency. Hence, the data rate can be significantly impaired if slowly time-varying channels are taken into account. To deal with this class of channels, a single OCDM pilot symbol seems to be more suitable.

In the OFDM context, Schmidl & Cox proposed a technique to estimate both symbol timing and CFO based on the transmission of a single OFDM pilot symbol with two identical halves in the time domain [47]. A straightforward approach to designing such an OFDM symbol is obtained by deactivating alternated subcarriers in the discrete-frequency domain [47]. However, the same approach to pilot design cannot be directly adopted in OCDM-based systems, since symbols are rather designed in the discrete-Fresnel domain [20]. In this context, the main contributions of this chapter are as follows:

- The introduction of a OCDM pilot symbol in the discrete-Fresnel domain whose discrete-time domain representation is composed of two identical halves, therefore enabling the use of the Schmidl & Cox synchronization technique in OCDM schemes. As a result, it is shown that a discrete-Fresnel domain symbol with two identical halves also has two identical halves in the discrete-time domain.

- The demonstration that the aforementioned OCDM pilot symbol can be designed to simultaneously enable Schmidl & Cox synchronization and channel estimation, which results in overhead reduction and hence higher spectral efficiency. This symbol has to be composed of two equal halves in the discrete-Fresnel domain and have an even number of active subchirps for performing channel estimation.

The remainder of this chapter is summarized as follows: Section 7.1 addresses a non-hybrid OCDM-based system model and the Schmidl & Cox synchronization; Section 7.2 presents the discrete-Fresnel domain pilot symbol requirement for performing Schmidl & Cox synchronization, whereas Section 7.3 shows the joint channel estimation and Schmidl & Cox synchronization for OCDM-based systems; Section 7.4 carries out numerical analyses; and Section 7.5 summarizes the chapter.

7.1 OCDM-BASED SYSTEM MODEL

Let an OCDM-based system transmit a frame consisting of $I \in \mathbb{Z}^+$ OCDM symbols. The i^{th} of those symbols, $i \in \{0, 1, \ldots, I-1\}$, is represented in the discrete-Fresnel domain by the vector $\dot{\mathbf{x}}_i$, whose elements are obtained from a digital modulator such that $\dot{\mathbf{x}}_i \in \mathbb{C}^{N_\text{S}\times 1}$ for passband systems (e.g., wireless systems) and $\dot{\mathbf{x}}_i \in \mathbb{R}^{N_\text{S}\times 1}$ for baseband ones (e.g., power line systems). In the discrete-time domain, it holds that

$$\mathbf{x}_i = \mathbf{\Phi}^\dagger \dot{\mathbf{x}}_i, \tag{7.1}$$

where $\mathbf{\Phi}$ represents any DFnT matrix of size $N_\text{S} \in \mathbb{Z}^+$ and $(\cdot)^\dagger$ is the Hermitian operator. For the sake of simplicity, it is henceforth assumed that N_S is even.

According to [20,21], the DFnT matrix can be expressed as $\mathbf{\Phi} = \mathbf{F}^\dagger \mathbf{\Gamma} \mathbf{F}$, in which $\mathbf{F}$ is the normalized version of the N_S-size DFT matrix and $\mathbf{\Gamma} = \text{diag}\{\Gamma_0, \Gamma_1, \ldots, \Gamma_{N_\text{S}-1}\}$ is a diagonal matrix of the eigenvalues of $\mathbf{\Phi}$. Those eigenvalues are defined for OCDM-based systems operating in the passband as

$$\Gamma_k \triangleq \mathrm{e}^{-(\mathrm{j}\pi/N_\text{S})k^2}, \forall k \in \{0, 1, \ldots, N_\text{S}-1\}. \tag{7.2}$$

Conversely, the DFnT matrix in OCDM-based systems operating in the baseband has eigenvalues given by

$$\Gamma_k \triangleq \begin{cases} \mathrm{e}^{-(\mathrm{j}\pi/N_\text{S})k^2}, & \text{for } k < N_\text{S}/2 \\ \mathrm{e}^{(\mathrm{j}\pi/N_\text{S})k^2}, & \text{for } k \geq N_\text{S}/2. \end{cases} \tag{7.3}$$

Notice that $\mathbf{\Phi} \in \mathbb{C}^{N_\text{S}\times N_\text{S}}$ when $\mathbf{\Gamma}$ originates from (7.2), whereas $\mathbf{\Phi} \in \mathbb{R}^{N_\text{S}\times N_\text{S}}$ when $\mathbf{\Gamma}$ derives from (7.3).

Further, the discrete-time domain symbol $\mathbf{x}_i$ has an L_CP-length cyclic prefix prepended to its beginning, $L_\text{CP} \in \mathbb{Z}^+$, and undergoes a parallel-to-serial conversion, originating the sequence $\{x[n]\}_{n=0}^{I(N_\text{S}+L_\text{CP})-1}$ that finally undergoes digital-to-analog conversion and further analog conditioning. In case of passband data transmission, the analog version of $\{x[n]\}_{n=0}^{I(N_\text{S}+L_\text{CP})-1}$ is up-converted to the carrier frequency f_tx.

It is assumed that the resulting signal is transmitted through an LTI communication channel which has a CIR of finite length $L_\text{h} \in \mathbb{Z}^+$ in the discrete-time domain, such that $L_\text{CP} \geq L_\text{h} - 1$. If perfect synchronization can be assumed, the baseband representation of the received signal

can be described in the discrete-time domain as

$$y[n] = \sum_{m=0}^{I(N_S+L_{CP})+L_h-2} x[m]h[n-m] + v[n], \tag{7.4}$$

where $\{h[n]\}_{n=0}^{L_h-1}$ denotes the LTI CIR, and $\{v[n]\}_{n=0}^{I(N_S+L_{CP})+L_h-2}$ denotes the additive noise.

In practice, however, the aforementioned perfect synchronization condition is not realizable. Consequently, a time delay τ_d between the beginning of the received signal and the receiver reference time is experienced. Furthermore, the down conversion of the analog received signal via mixing with a local oscillator signal of frequency f_{rx}, which only takes place in case of passband systems and is followed by low-pass filtering, yields CFO. The existing difference between transmit and receive local oscillator frequencies defines the CFO, which is therefore expressed as $\epsilon = f_{tx} - f_{rx}$. Afterwards, the resulting signal is sampled, originating the sequence $\{r[n]\}$, which is the baseband representation of the time-domain received signal. For the sake of simplicity, sample limits are not assigned to $\{r[n]\}$. Taking the non-perfect symbol timing and carrier frequency synchronization, as well as assuming a sampling period equal to T_s, one can write

$$r[n] = y[n - n_d]e^{j2\pi\epsilon(n-n_d)T_s}, \tag{7.5}$$

where $n_d = \tau_d/T_s$. In practice, the division of τ_d by T_s does not result in an integer and, consequently, the transmitter and receiver references are always changed within a sampling period T_s. For simplicity, it is henceforth assumed that $n_d \in \mathbb{Z}^+$. In order for the received symbols to be processed correctly, $\{y[n]\}_{n=0}^{I(N_S+L_{CP})+L_h-2}$ needs to be extracted from $\{r[n]\}$. In this regard, it is required to estimate the beginning of the received signal and the CFO of passband systems. In summary, n_d and ϵ are unknown by the receiver.

7.1.1 Schmidl & Cox Synchronization

The Schmidl & Cox synchronization is known for being a robust technique that allows the estimation of both the beginning of the received signal and the CFO [47]. Previously proposed for OFDM schemes, this technique is based on the existing redundancy in two equal halves of a pilot symbol in the discrete-time domain and can be divided into symbol timing and CFO estimations, as described below.

7.1.1.1 Symbol Timing Estimation

In order to estimate the beginning of the received symbols, the considered technique exploits the correlation between two consecutive vectors of length $L = N_S/2$. To do so, let them be $\mathbf{r}_n$ and $\mathbf{r}_{n+L}$, such that $\mathbf{r}_n = [r[n]\ r[n+1]\ \ldots\ r[n+L-1]]^T$ and then $\mathbf{r}_{n+L} = [r[n+L]\ r[n+L+1]\ \ldots\ r[n+N-1]]^T$. These vectors represent two windows that slide along the received sequence. Their normalized correlation by the energy of the second

Figure 34 – Normalized correlation, $\{M[n]\}$, for one synchronization pilot symbol

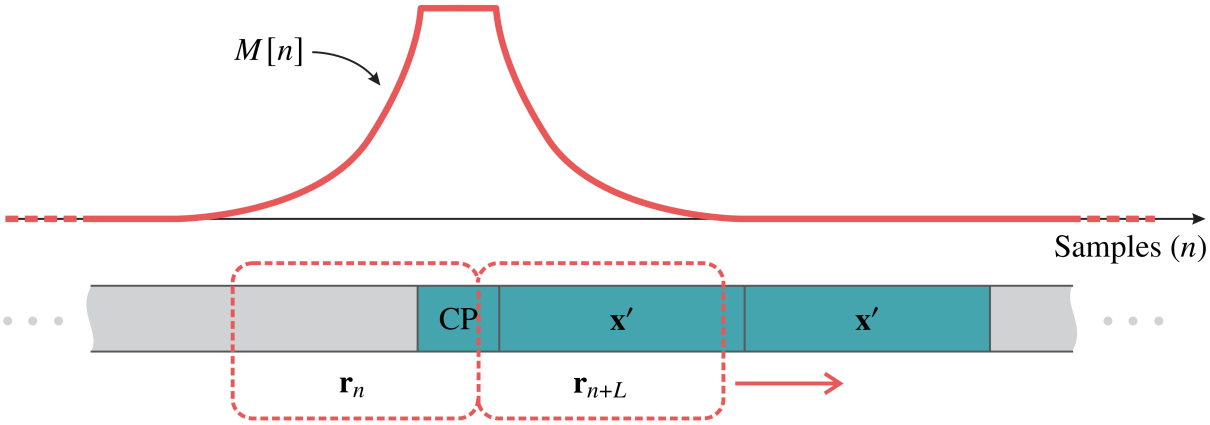

Source: Personal collection.

vector can be expressed as

$$M[n] = \frac{|\mathbf{r}_n^{\dagger}\,\mathbf{r}_{n+L}|^2}{(\mathbf{r}_{n+L}^{\dagger}\,\mathbf{r}_{n+L})^2}. \tag{7.6}$$

Note that $M[n]$ equals one if $\mathbf{r}_n$ and $\mathbf{r}_{n+L}$ are equal and zero if $\mathbf{r}_n$ and $\mathbf{r}_{n+L}$ are orthogonal. Therefore, if a pilot symbol is designed to have two identical halves in the time domain, i.e., $\mathbf{x} = [\mathbf{x}'^T\ \mathbf{x}'^T]^T$, then the correlation is maximized at the beginning of the symbol, as illustrated in Figure 34. In addition, a plateau is produced due to the cyclic prefix and the fact that the pilot symbol is assumed to be different from its anterior and posterior symbols (see Figure 34). As channel and additive noise effects may shift the plateau forward, a suitable estimate of the beginning of the pilot symbol $\widehat{n_{\mathrm{d}}}$ that avoids ISI is the midpoint of the plateau minus L_{CP} [47]. In case of multiple pilot symbols, the average estimate from all plateaus is effective to mitigate the additive noise effect.

According to [47], the correlation function values within the plateaus follow a Gaussian distribution whose mean value is given by

$$\mu_{\mathrm{in}} \approx \frac{1}{(1+1/\gamma)^2}, \tag{7.7}$$

where γ denotes the SNR of the received signal $y[n]$. In addition, the variance can be expressed as

$$\sigma^2_{\mathrm{in,\,pb}} \approx \frac{2\gamma^2[(1+\mu_{\mathrm{in}})\gamma + 2\mu_{\mathrm{in}} + 1]}{L(1+\gamma)^4} \tag{7.8}$$

for passband systems. In case of baseband systems, only one dimension is considered and therefore $\sigma^2_{\mathrm{in,bb}} = 2\sigma^2_{\mathrm{in,pb}}$.

Moreover, the correlation function values outside the plateau obey a chi-square distribution with two degrees of freedom whose mean and variance values are, respectively, given by

$$\mu_{\mathrm{out}} \approx \frac{1}{L} \tag{7.9}$$

and

$$\sigma^2_{\mathrm{out,pb}} \approx \frac{1}{L^2}. \tag{7.10}$$

Regarding baseband systems, the chi-square distribution has one degree of freedom with the same mean value and variance equal to $\sigma^2_{\text{out, bb}} = 2\sigma^2_{\text{out,pb}}$.

Note that based on the probability distribution functions of the regions within and outside the plateaus, the probabilities of either false alarm or not detecting a received symbol can be determined (see [47] for further details).

7.1.1.2 Carrier Frequency Offset Estimation

Once the beginning of the received symbol has been defined, small CFOs (i.e., values within a subcarrier frequency spacing) can be estimated by multiplying the conjugate of every sample in the first pilot symbol half by its counterpart in the second half. Since the two samples are similar, both signal and channel phases will be canceled and only a phase component proportional to CFO and noise will remain. Therefore, a reasonable estimate of the CFO can be obtained from the numerator of (7.6) at the beginning of the pilot symbol plus L_{CP}. In other words, the estimate of the CFO can be obtained using

$$\hat{\epsilon} = \frac{\arg\left\{\mathbf{r}^{\dagger}_{\widehat{n}_{\text{d}}+L_{\text{CP}}}\,\mathbf{r}_{\widehat{n}_{\text{d}}+L_{\text{CP}}+L}\right\}}{\pi N T_{\text{s}}}, \tag{7.11}$$

where $\arg\{\cdot\}$ returns the phase component of a complex number. The variance of the error in the normalized CFO estimate (i.e., $\hat{\epsilon}NT_{\text{s}}$), assuming AWGN channel, is a function of the window length L and the SNR γ, being expressed as [47]

$$\sigma^2_{\epsilon} = \frac{1}{\pi^2 L\gamma}. \tag{7.12}$$

7.2 FRESNEL-DOMAIN PILOT SYMBOL FOR SCHMIDL & COX SYNCHRONIZATION

The synchronization technique proposed by Schmidl & Cox [47], briefly detailed in the previous section, can be used in any scheme if the pilot symbol has two identical halves in the time domain. For OCDM schemes, a possible alternative is to use DFnT matrices of size N_{S} (for data symbols) and $N_{\text{S}}/2$ (for pilot symbols) and then replicate the pilot symbols in the discrete-time domain. In this section, however, a discrete-Fresnel domain symbol whose discrete-time domain version has two identical halves is presented; thus, the use of two DFnT matrices of different sizes is not required. This new approach relies on a specific property of the DFnT and is detailed as follows.

Let $\mathbf{x} = [\mathbf{x}'^T\ \mathbf{x}'^T]^T$ be the discrete-time domain symbol composed of two identical halves, $\mathbf{x}'$, used for synchronization. In the discrete-Fresnel domain, it is given by

$$\dot{\mathbf{x}} = \mathbf{\Phi}\mathbf{x} = \mathbf{\Phi}[\mathbf{x}'^T\ \mathbf{x}'^T]^T. \tag{7.13}$$

Note that the DFnT matrices are square with even size; therefore, $\mathbf{\Phi}$ can be divided into $(N_{\text{S}}/2 \times N_{\text{S}}/2)$-size block matrices and then expressed as

$$\mathbf{\Phi} = \begin{bmatrix} \mathbf{\Phi}_{11} & \mathbf{\Phi}_{12} \\ \mathbf{\Phi}_{21} & \mathbf{\Phi}_{22} \end{bmatrix}. \tag{7.14}$$

Since $\mathbf{\Phi}$ can be decomposed into a diagonal matrix pre and post multiplied by the inverse and direct matrices of the DFT, $\mathbf{\Phi}$ is a circulant matrix [115]. As a consequence, $\mathbf{\Phi}_{11} = \mathbf{\Phi}_{22}$ and $\mathbf{\Phi}_{12} = \mathbf{\Phi}_{21}$. Hence (7.13) can be rewritten as follows

$$\dot{\mathbf{x}} = \begin{bmatrix} \mathbf{\Phi}_{11} & \mathbf{\Phi}_{12} \\ \mathbf{\Phi}_{12} & \mathbf{\Phi}_{11} \end{bmatrix} \begin{bmatrix} \mathbf{x}' \\ \mathbf{x}' \end{bmatrix} = \begin{bmatrix} \mathbf{\Phi}_{11}\mathbf{x}' + \mathbf{\Phi}_{12}\mathbf{x}' \\ \mathbf{\Phi}_{11}\mathbf{x}' + \mathbf{\Phi}_{12}\mathbf{x}' \end{bmatrix} = \begin{bmatrix} \dot{\mathbf{x}}' \\ \dot{\mathbf{x}}' \end{bmatrix}, \tag{7.15}$$

with $\dot{\mathbf{x}}' = \mathbf{\Phi}_{11}\mathbf{x}' + \mathbf{\Phi}_{12}\mathbf{x}'$. It is therefore concluded that, for a discrete-time domain symbol to have two identical halves, its discrete-Fresnel domain representation must also have two identical halves.

If the aforementioned requirement is met, the analytical performance of the symbol time and CFO estimations described in [47] will also hold for OCDM schemes. Since these estimation processes are carried out in the discrete-time domain, the influences of CIR and additive noise on the received signal can be modeled in the same way in both OFDM and OCDM schemes. Consequently, their expected performances are also equal.

7.3 JOINT CHANNEL ESTIMATION AND SCHMIDL & COX SYNCHRONIZATION

Previous works introduced a particular OCDM pilot symbol that enables the channel estimation in the discrete-Fresnel domain [112, 117, 118]. According to them, the k^{th} element of such a symbol in the discrete-Fresnel domain is defined by

$$\dot{x}_k \triangleq \begin{cases} \sqrt{N_\text{S}/N_\text{e}}, & \text{if } k \bmod N_\text{S}/N_\text{e} = 0 \\ 0, & \text{if } k \bmod N_\text{S}/N_\text{e} \neq 0, \end{cases} \tag{7.16}$$

$\forall k \in \{0, 1, \ldots, N_\text{S} - 1\}$; in which $N_\text{e} \in \mathbb{Z}^+$ is the number of CIR estimates within the OCDM pilot symbol and $a \bmod b$ returns the remainder of the division of a by b. The amplitude $\sqrt{N_\text{S}/N_\text{e}}$ is assumed to make the energy of the estimation symbol equal to that of data symbols. Also, the spacing between the beginning of consecutive estimates, i.e., N_S/N_e, must be an integer greater than or equal to L_h so that there is no interference between the CIR estimates [112], which limits the maximum number of estimates within an OCDM symbol. Fig. 35 illustrates the discrete-Fresnel domain symbol used for channel estimation purposes when $N_\text{e} = 4$.

Observe that the symbol described in (7.16) can be formed of two identical halves, enabling the joint channel estimation and Schmidl & Cox synchronization. In this regard, it must hold that

$$\dot{x}_k = \dot{x}_{k+N_\text{S}/2}, \qquad \forall k \in \{0, 1, \ldots, N_\text{S}/2 - 1\}. \tag{7.17}$$

Based on (7.16) and (7.17), it is straightforward that

$$\frac{N_\text{S}}{2} \bmod \frac{N_\text{S}}{N_\text{e}} = 0 \Rightarrow N_\text{e} \bmod 2 = 0 \tag{7.18}$$

for even N_S. Therefore, it is only required that the number of CIR estimates N_e is even for a single OCDM pilot symbol to be used for Schmidl & Cox synchronization as well as channel

Figure 35 – Discrete-Fresnel domain symbol used for channel estimation purposes ($N_e = 4$)

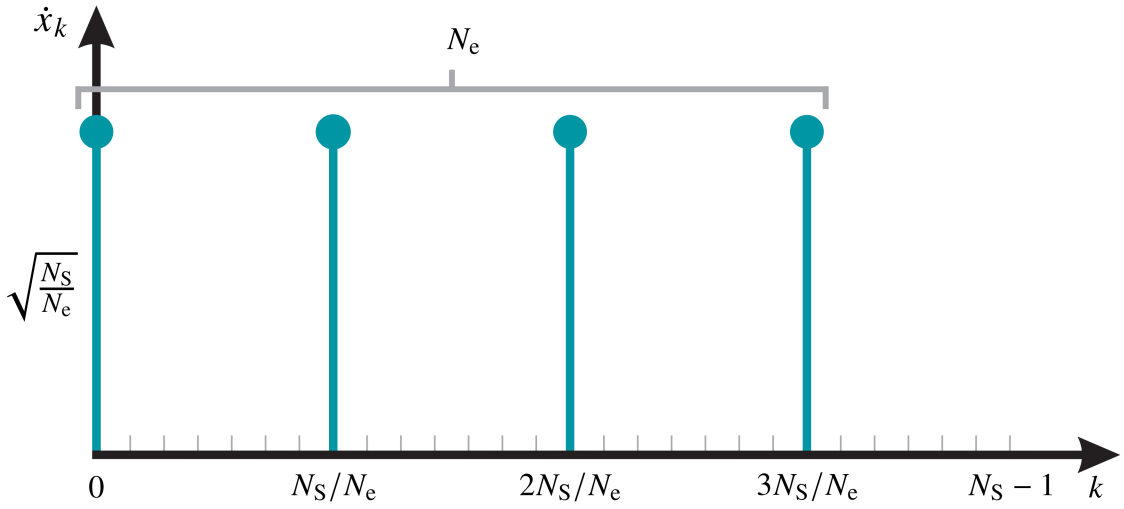

Source: Personal collection.

estimation purposes. Note that it is common to use $N_S \gg L_h$ and therefore the assumption of $N_e \geq 2$ is more than reasonable. In addition, the error variance of the channel estimate is a function of the symbol length N and the SNR γ that can be expressed as [117]

$$\sigma_c^2 = \frac{1}{N\gamma}. \tag{7.19}$$

7.4 NUMERICAL ANALYSES

In this section, the proposed joint channel estimation and Schmidl & Cox synchronization is evaluated. In this regard, Monte Carlo-based simulation and measurements results are presented. The former aims to evaluate the analytical performance of the joint channel estimation and Schmidl & Cox synchronization under distinct SNR values for AWGN channel, whereas the latter have the purpose of validating the practical application of the Schmidl & Cox technique in OCDM-based systems. The assumed parameters were $N = 1024$, $L_{CP} = 128$, and $N_e = 2$. In addition, a stream of $N_B = 256$ blocks was transmitted, each of them formed by two OCDM symbols. While the first OCDM symbol in each block was used to perform the joint channel estimation and Schmidl & Cox synchronization, the second one was composed of quadrature phase-shift keying (QPSK) data symbols. To obtain a real-valued OCDM symbol for baseband transmission, the real and imaginary components of each QPSK symbol are placed alternately into the transmitted symbol [21].

The measurements were performed using the Zynq UltraScale+ RFSoC ZCU111 from Xilinx, Inc. (presented in Figure 36) on which a transmitter, a receiver, and a channel emulator were implemented assuming $f_s = 1/T_s = 50$ MHz. The digital-to-analog converters (DACs) of the transmitter and the analog-to-digital converters (ADCs) of the receiver were directly and respectively connected to the ADCs and DACs of the channel emulator [120]. The considered channel emulator, which was originally proposed for radar target simulation purposes [120], was used for adding delays and frequency shifts to the transmit signal and therefore introduce known

Figure 36 – Measurement setup consisting of transmitter, channel emulator, and receiver implemented on the same Zynq UltraScale+ RFSoC ZCU111 from Xilinx, Inc

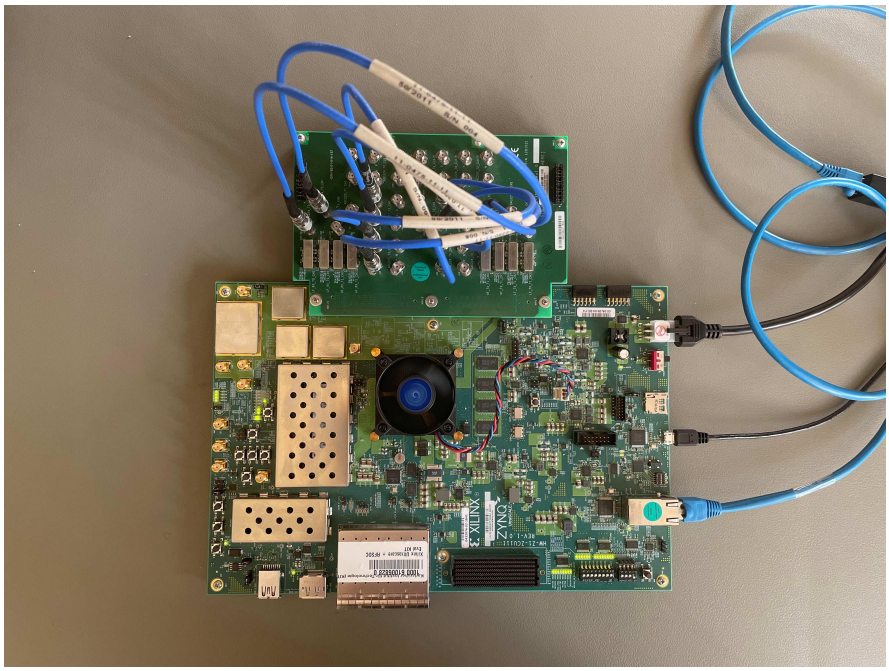

Source: Personal collection.

synchronization errors in it before its reception as

$$y(t) = \sum_{p=0}^{P-1} \alpha_p x(t - \tau_p) \mathrm{e}^{j2\pi f_{\Delta,p} t} + v(t), \tag{7.20}$$

where $y(t)$ and $x(t)$ are the baseband continuous-time domain receive and transmit signals, respectively, and $v(t)$ is the continuous-time domain version of the additive noise $v[n]$. Additionally, P channel taps are considered, with attenuation α_p, delay τ_p, and frequency shift $f_{\Delta,p}$ for the p^{th} tap, $p \in \{0, 1, \ldots, P-1\}$. For the results in this chapter, $P = 1$ was assumed, τ_p was chosen respecting the $L_{\text{CP}} \geq L_{\text{h}} - 1$, α_p was chosen so that an SNR of approximately 22 dB was experienced, and $f_{\Delta,p}$ was used to introduce the desired CFO.

7.4.1 Simulation results

The statistical parameters of the normalized correlation function within and outside the plateaus are presented in Figure. 37. In the figures associated with mean values, namely Figure 37(a) and Figure 37(c), the left y-axis is the same for both passband and baseband results. As for the variance plots, Figure 37(b) and Figure 37(d), the left and right y-axes are considered for passband and baseband results, respectively. Overall, the closed-form expressions based on (7.7) to (7.10) agree with the simulation results, indicating that the performance of the normalized correlation functions of OCDM schemes is the same as for their OFDM counterparts. The simulation results slightly disagree with the theoretical results only in Figure 37(d), which presents the variance of the normalized correlation function outside the plateaus. This outcome

Figure 37 – Mean and variance of the normalized correlation function, within and outside the plateaus, as a function of the SNR

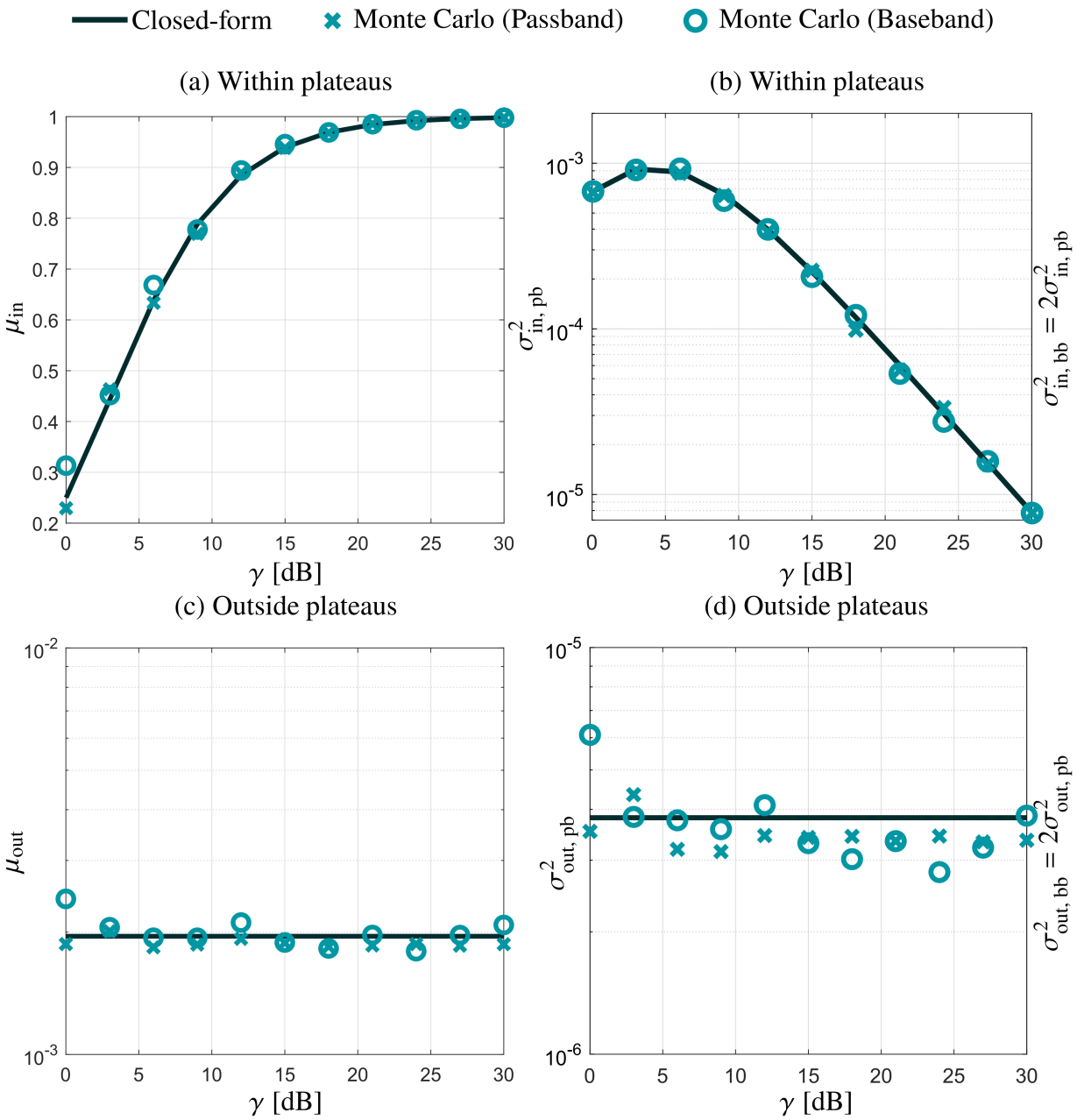

Source: Personal collection.

is related to the approximations assumed for the theoretical computation and is also observed for OFDM schemes in [47].

Figure 38(a) and Figure 38(b) show the theoretical and simulation results for error variances associated with the CFO and CIR estimates, respectively. In addition, simulation results for the proposed technique in [119] under distinct L_{CP} values are displayed for comparison. The CP length was assumed as the CIR length in [119], which influences the number of pilots symbols reserved for CIR estimation. First, theoretical and simulation results of the error variance match for both CFO and CIR. Hence, the CFO estimation in the OCDM scheme achieves the same performance as reported in [47], whereas the performance of the CIR

Figure 38 – Error variance of the normalized CFO and CIR estimates as a function of the SNR

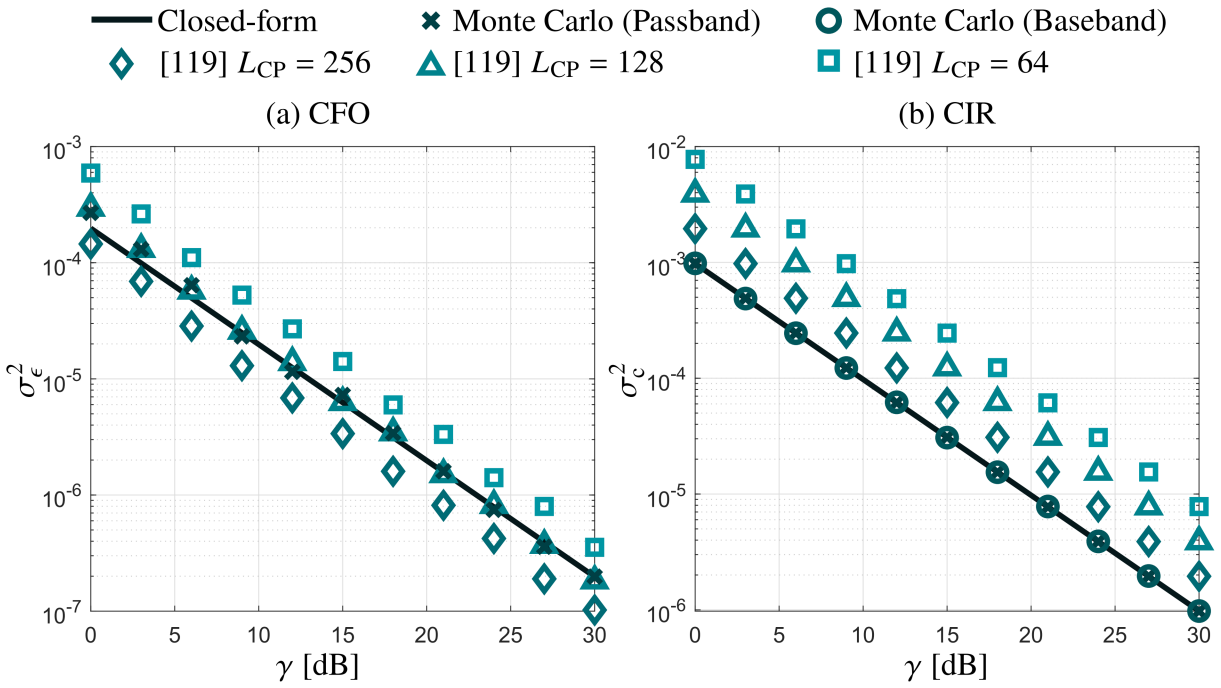

Source: Personal collection.

estimation equals the results of [117]. Note that the technique from [119] requires a long CP to achieve a good performance, whereas such parameter is not relevant to the performance of the proposed technique in this chapter as long as ISI can be avoided. As a consequence, the current contribution arises as a better choice to estimate CFO and CIR with higher spectral efficiency for slowly time-varying channels. Furthermore, the proposed technique in [119] and the one in this chapter could be used together to achieve very accurate CFO and CIR estimates, e.g., following a similar frame structure to the one in [121].

7.4.2 Measurement results

Regarding the measurements results, the symbol timing estimation is firstly analyzed. Figures 39(a) and 39(b) show the beginning of the normalized correlation functions $M[n]$ for passband and baseband systems, respectively. For better comparison with its baseband counterpart, a measurement without CFO, i.e., with ($\epsilon = 0$), is considered for the passband system. In addition to the considered OCDM schemes, the normalized correlation of OFDM schemes under the same conditions are presented for comparison purposes. In the OFDM case, a random data symbol was chosen as a reference to the considered synchronization technique. Note that the correlation functions of OCDM and OFDM schemes match perfectly for both passband and baseband systems, which validates the use of the proposed OCDM pilot symbol for symbol timing estimation. In Figures 39(a) and 39(b), the first sample ($n = 0$) indicates the real beginning of the first block of symbols, whereas the midpoint of the first plateaus is around $n = 68$. This difference, however, does not result in any loss regarding symbols detection since the plateau is free of ISI [47].

Figure 39 – Normalized correlation functions for OCDM and OFDM schemes

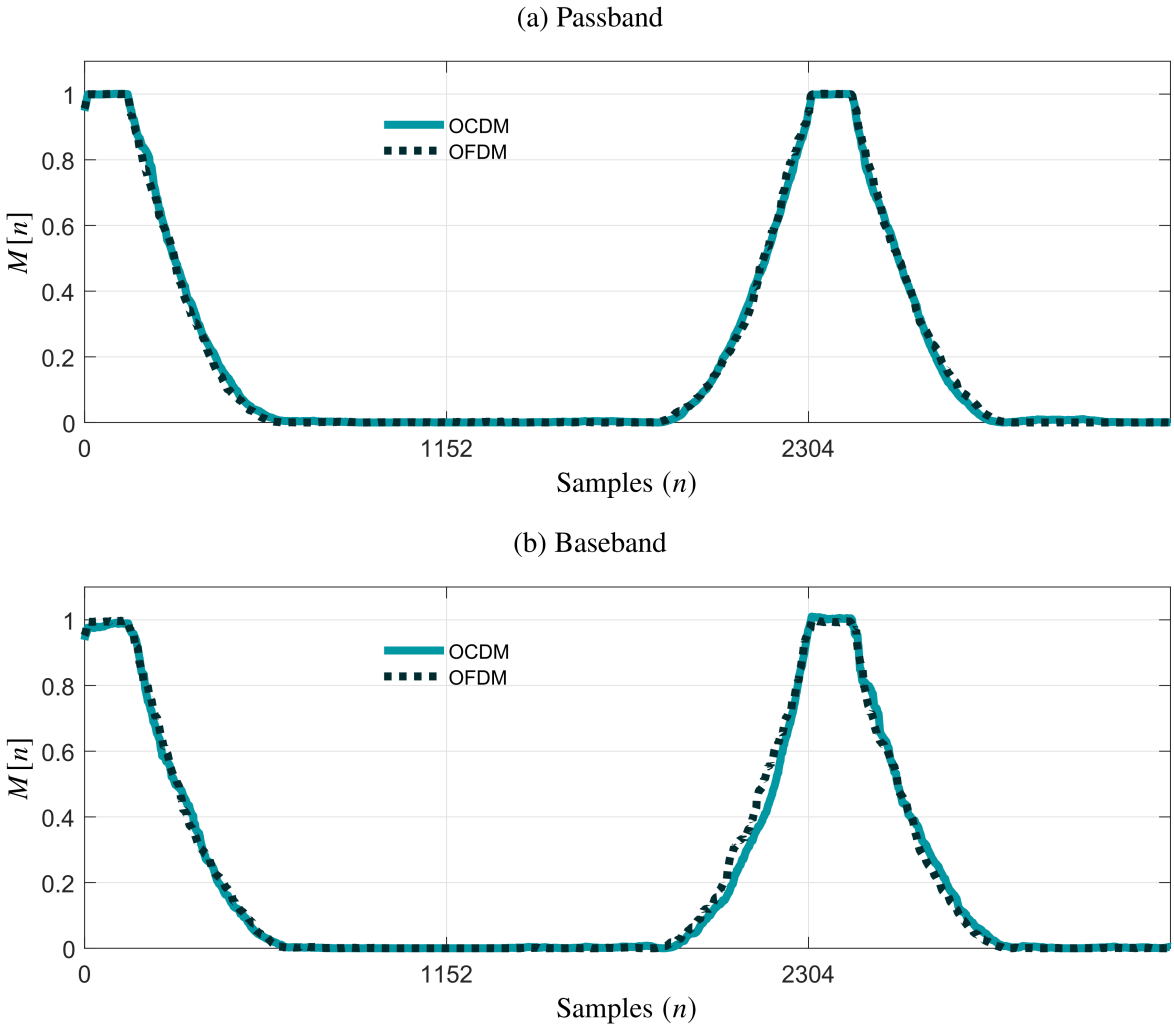

Source: Personal collection.

Next, Figures 40(a) and 40(b) present the CFO estimations for each of the N_{B} transmitted blocks and therefore only passband systems are analyzed. Also, $\widehat{n_{\mathrm{d}}}$ is assumed as initial sample of the OCDM symbol. In these figures, measurements with introduced CFOs by the channel emulator ranging from 0.0 to $0.1\Delta_f$ with a step of $0.02\Delta_f$ were labeled as Measurement #1 to #6, respectively. The aforementioned parameter Δ_f is the frequency resolution of the considered OCDM systems, which is similarly defined to the subcarrier spacing in OFDM systems [122] and assumes value $\Delta_f = f_{\mathrm{s}}/N_{\mathrm{S}} = 48.83$ kHz for both passband and baseband OCDM systems. Again, OFDM results generated under the same conditions of the OCDM results are presented for comparison purposes. Observe that the CFO estimates are close to the actual values introduced by the channel emulator for all measurements. There is a variation around the optimal value, which is solely due to noise effect. The same behavior can be noticed in the CFO estimates in OFDM schemes, indicating that such a variation is expected. In this regard, averaging the CFO estimates accumulated over time is sufficient to yield an accurate CFO estimate.

Figures 41(a), 41(b), and 41(c) show the QPSK data symbols estimates having mean

Figure 40 – CFO estimates in OCDM and OFDM schemes

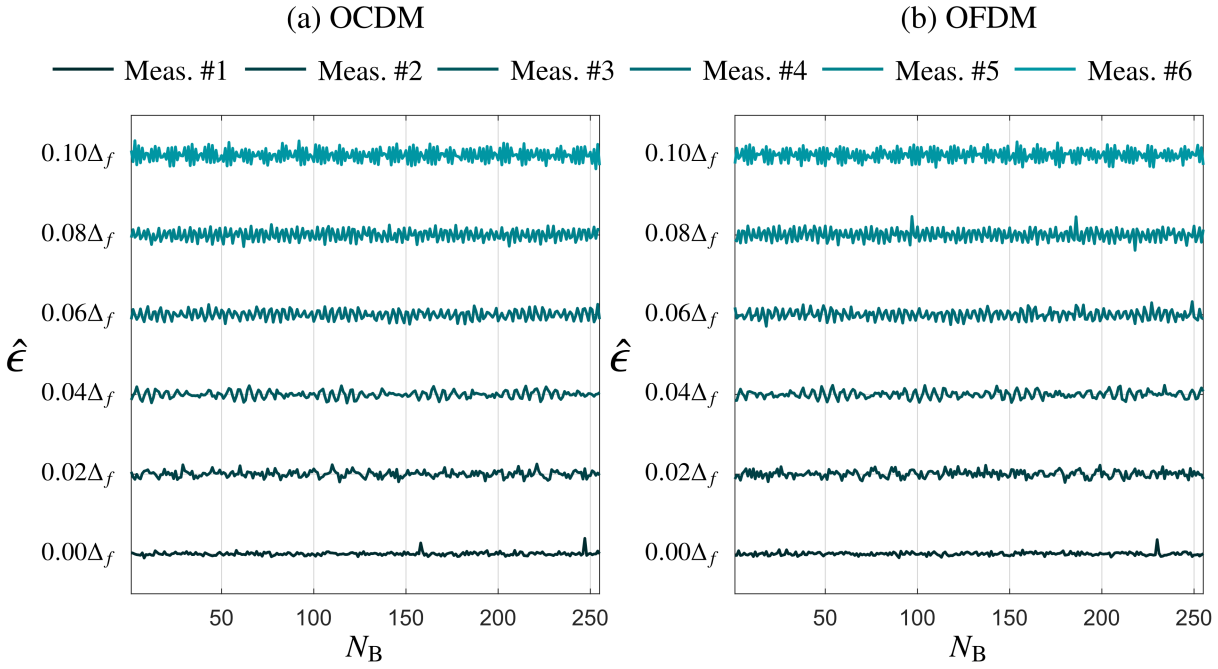

Source: Personal collection.

constellation energy normalized to unity in passband and baseband systems. For obtaining the aforementioned estimates, the midpoint of the plateaus minus L_{CP} was considered as the initial sample of each block, while the CFO estimates were used to compensate the effect of the introduced CFO. Moreover, to recover the transmitted data symbols, zero-forcing equalization was employed as explained in [20, 21]. The channel equalization was performed based on the average of the $N_e = 2$ CIR estimates. In this context, Figures 41(a) and 41(b) present the results for the minimum and maximum of the considered CFO values (Measurements #1 and #6, respectively). It is revealed that the proposed joint channel estimation and Schmidl & Cox synchronization can be effectively applied in passband OCDM schemes since the transmitted symbols can be easily recovered from the received ones. Furthermore, the same conclusion can be draw for baseband OCDM schemes, which is supported by Figure 41(c).

7.5 SUMMARY

This chapter has investigated the symbol timing and carrier frequency synchronization proposed by Schmidl & Cox [47] in combination with channel estimation for an OCDM scheme. It has been proved in the current dissertation that a symbol with two equal halves in the discrete-Fresnel domain results in a symbol with two equal halves in the discrete-time domain, which is the unique requirement to apply the assumed synchronization technique. It has been also presented that the OCDM pilot symbol previously proposed for channel estimation purposes can be composed of two equal halves if the number of channel estimates within the symbol is even. A single OCDM pilot symbol can be therefore used for symbol timing and carrier frequency synchronization as well as channel estimation, significantly shortening the overhead

Figure 41 – QPSK data symbols estimates in passband and baseband systems

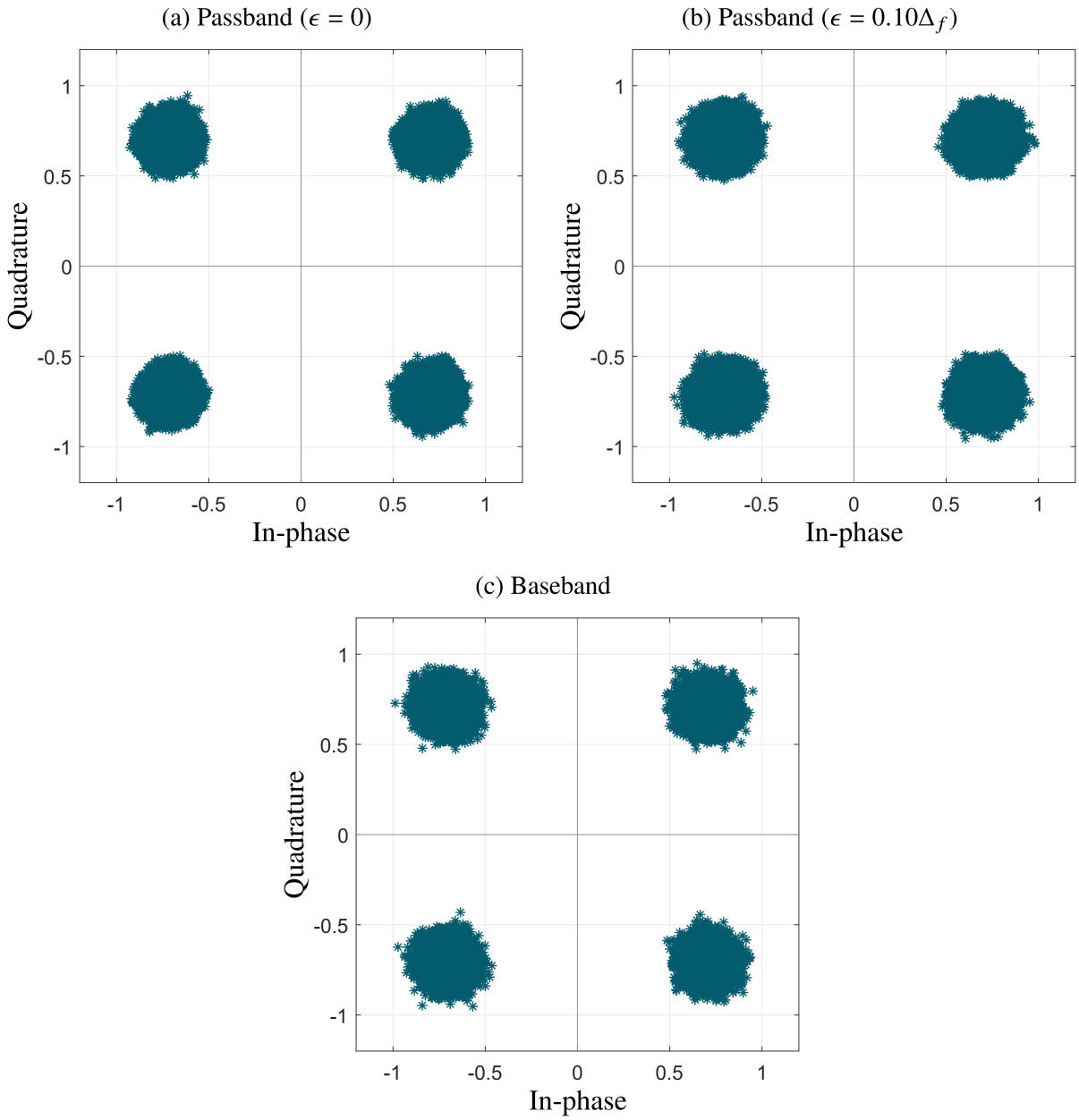

Source: Personal collection.

length in slowly time-varying channels and eventually leading to an increase in data rate. Finally, simulation and measurement results have been discussed and used to validate the proposed joint channel estimation and Schmidl & Cox synchronization.

8 CONCLUSIONS

In this dissertation, the hybrid power line/wireless system, which is characterized by using power line and wireless media in parallel, has been investigated. The current study has focused on different topics to exploit the diversity obtained by using power line and wireless media jointly. Power allocation for maximizing achievable data rate or minimizing the average bit error probability as well as subcarrier permutation are the topics that have been analyzed based on the OFDM scheme. Furthermore, the recently proposed OCDM scheme has been investigated as an alternative to the OFDM scheme in the considered hybrid system.

The optimal power allocation for maximizing the achievable data rate or minimizing the average bit error probability has been analyzed for the first time regarding hybrid power line/wireless systems. Based on the transmission of similar OFDM symbols over power line and wireless channels, and the application of the MRC at the receiver, it has been shown that at most one medium should be used in the same subchannel index to either maximize the achievable data rate or minimize the average bit error probability. The literature states that the same information can be transmitted through different channels to benefit data communication if the SNRs are within similar ranges. This dissertation, however, has demonstrated that transmitting the same information through different channels is equivalent to wasting resources if the instantaneous normalized SNRs of the considered media is known at the transmitter. In particular, this result holds for two distinct sets of transmission power constraints, sum power and sum power-channel constraints. The former limits only the total transmission power, whereas the latter considers a maximum transmission power per channel. For both transmission power constraints, the obtained findings enabled the proposal of power allocation algorithms based on well-known power allocation algorithms for maximizing the achievable data rate and minimizing the average bit error probability in non-hybrid contexts, i.e., waterfilling and Park's algorithms. As a consequence, power allocation algorithms that require a low computational and cost have been designed. Numerical analyses have validated them, proving their optimality and showing their dominance over the options available in the literature.

Regarding subcarrier permutation, its optimality has been investigated for either maximizing the achievable data rate or minimizing the average bit error probability in hybrid power line/wireless system. Although previous works have already presented the optimal subcarrier permutation for maximizing the achievable data rate under uniform power allocation, their achievements have been here extended for minimizing the average bit error probability and other types of power allocation as well. Moreover, this dissertation has shown that subcarrier permutation has to be performed based on the normalized SNR instead of the SNR as previously reported. Therefore, the optimal subcarrier permutation occurs when the subcarrier indices of a medium are sorted in ascending order of their normalized nSNRs and the subcarrier indices of the other medium are sorted in descending order of their normalized SNRs. Numerical results have shown that the higher the frequency selectivity of the normalized SNRs, the better the gains offered by the subcarrier permutation and that subcarrier permutation can be significantly helpful to

improve data communication in terms of achievable data rate or average bit error probability.

Furthermore, this dissertation has proposed the OCDM-based hybrid power line/wireless system model. This type of hybrid communication system assumes that the discrete-Fresnel domain representation of the transmitted symbols are the same in power line and wireless media. MRC technique is then applied to combine the symbols in the discrete-Fresnel domain at the receiver. To find the combining weights of the MRC technique, the additive noise has been thoroughly investigated in the discrete-Fresnel domain. It has been here proved that a wide-sense stationary random process in the discrete-time domain is also a wide-sense stationary random process in the discrete-Fresnel domain so that the mean value and autocorrelation function are equal in both domains. Moreover, the optimal power allocation has been analyzed for OCDM-based hybrid power line/wireless system and it has been demonstrated to be easily carried out since the SNRs values are constant over the subchirps. Numerical analyses have shown that OCDM-based hybrid power line/wireless system may be more appropriate than OFDM-based HPWSs if the transmitter has partial or no knowledge of the channel state information and the major aim is to minimize the average bit error probability.

Finally, a joint channel estimation and Schmidl & Cox synchronization has been proposed for power line and wireless OCDM schemes. Since the Schmidl & Cox synchronization requires a pilot symbol with two identical halves in the discrete-time domain, it has been proved in the current dissertation that the discrete-Fresnel domain representation of such a symbol is composed of two identical halves as well. Hence, a pilot symbol that enables joint channel estimation and synchronization has been derived under the constraint that the number of channel estimates per symbol is even. As a result, a significant reduction in overhead length can be achieved when dealing with slowly time-varying channels, eventually leading to an increase in spectral efficiency. Measurement and simulation results validate the obtained findings for both power line and wireless OCDM schemes.

Overall, this dissertation has investigated different manners and opportunities to benefit data communication based on the existing diversity between power line and wireless media. Achievable data rate and bit error probability gains have been achieved, assuming the use of well-known algorithms and techniques, which in its turn present low computational and economical costs. Hence, the hybrid power line/wireless system can be regarded as a low-cost and reliable data communication system for future generations of communication technologies. Based on the research questions that have been studied in this dissertation, the following topics deserve attention in future works:

- A comparison between the power allocation for minimizing the average bit error probability and the conventional margin adaptive power allocation in hybrid power line/wireless systems.

- A statistical analysis of the benefits of power allocation and subcarrier permutation to the hybrid power line/wireless system performance.

- An investigation of the influence of channel codes and interleavers on power allocation, subcarrier permutation, and modulation schemes regarding hybrid power line/wireless systems.
- A study of the impact that quantization of normalized SNR and transmission power values have on the power allocation in hybrid power line/wireless systems, assuming OFDM and OCDM schemes.
- A further investigation of the advantages and disadvantages of using the OCDM-based hybrid power line/wireless system, e.g., comparing it with other data communication schemes, such as the SC-CP and the OTFDM.

REFERENCES

[1] S. Galli, A. Scaglione, and Z. Wang, "For the grid and through the grid: The role of power line communications in the smart grid," *Proceedings of the IEEE*, vol. 99, no. 6, pp. 998–1027, June 2011.

[2] R. Morello, S. C. Mukhopadhyay, Z. Liu, D. Slomovitz, and S. R. Samantaray, "Advances on sensing technologies for smart cities and power grids: A review," *IEEE Sensors Journal*, vol. 17, no. 23, pp. 7596–7610, Dec. 2017.

[3] R. Ma, H.-H. Chen, Y.-R. Huang, and W. Meng, "Smart grid communication: Its challenges and opportunities," *IEEE Transactions on Smart Grid*, vol. 4, no. 1, pp. 36–46, Mar. 2013.

[4] L. de M. B. A. Dib, V. Fernandes, M. de L. Filomeno, and M. V. Ribeiro, "Hybrid PLC/wireless communication for smart grids and internet of things applications," *IEEE Internet of Things Journal*, vol. 5, no. 2, pp. 655–667, Apr. 2018.

[5] F. Griffiths and M. Ooi, "The fourth industrial revolution - Industry 4.0 and IoT [Trends in Future I&M]," *IEEE Instrumentation & Measurement Magazine*, vol. 21, no. 6, pp. 2–43, Dec. 2018.

[6] M. Wollschlaeger, T. Sauter, and J. Jasperneite, "The future of industrial communication: Automation networks in the era of the internet of things and industry 4.0," *IEEE Industrial Electronics Magazine*, vol. 11, no. 1, pp. 17–27, Mar. 2017.

[7] Cisco Systems, "Cisco annual internet report (2018-2023) white paper," Tech. Rep., 2020. [Online]. Available: https://www.cisco.com/c/en/us/solutions/collateral/executive-perspectives/annual-internet-report/white-paper-c11-741490.pdf

[8] T. Rappaport, *Wireless Communications: Principles and Practice*, 2nd ed. Upper Saddle River, NJ, USA: Prentice-Hall, 2001.

[9] D. Tse and P. Viswanath, *Fundamentals of Wireless Communication*. New York, NY, USA: Cambridge University Press, 2005.

[10] A. Nosratinia, T. E. Hunter, and A. Hedayat, "Cooperative communication in wireless networks," *IEEE Communications Magazine*, vol. 42, no. 10, pp. 74–80, Oct. 2004.

[11] H. Hrasnica, A. Haidine, and R. Lehnert, *Broadband Powerline Communications: Network Design*. New York: John Wiley & Sons, 2005.

[12] J. Song, W. Ding, F. Yang, H. Yang, B. Yu, and H. Zhang, "An indoor broadband broadcasting system based on PLC and VLC," *IEEE Transactions on Broadcasting*, vol. 61, no. 2, pp. 299–308, June 2015.

[13] W. Ding, F. Yang, H. Yang, J. Wang, X. Wang, X. Zhang, and J. Song, "A hybrid power line and visible light communication system for indoor hospital applications," *Computers in Industry*, vol. 68, pp. 170–178, Apr. 2015.

[14] Y. Qian, J. Li, Y. Zhang, and D. N. K. Jayakody, "Performance analysis of an opportunistic relaying power line communication systems," *IEEE Systems Journal*, vol. 12, no. 4, pp. 3865–3868, Dec. 2018.

[15] M. S. P. Facina, H. A. Latchman, H. V. Poor, and M. V. Ribeiro, "Cooperative in-home power line communication: Analyses based on a measurement campaign," *IEEE Transactions on Communications*, vol. 64, no. 2, pp. 778–789, Feb. 2016.

[16] M. L. Filomeno, G. R. Colen, L. G. de Oliveira, and M. V. Ribeiro, "Two-stage single-relay channel model for in-home broadband PLC systems," *IEEE Systems Journal*, vol. 13, no. 1, pp. 204–214, Mar. 2019.

[17] F. H. Juwono, Q. Guo, D. Huang, and K. P. Wong, "Deep clipping for impulsive noise mitigation in OFDM-based power-line communications," *IEEE Transactions on Power Delivery*, vol. 29, no. 3, pp. 1335–1343, June 2014.

[18] S. Zhidkov, "Analysis and comparison of several simple impulsive noise mitigation schemes for OFDM receivers," *IEEE Transactions on Communications*, vol. 56, no. 1, pp. 5–9, Jan. 2008.

[19] G. R. Colen and M. V. Ribeiro, "A flexible multicarrier scheme based on the discrete orthogonal stockwell transform," *IEEE Systems Journal*, vol. 14, no. 4, pp. 5284–5295, Dec. 2020.

[20] X. Ouyang and J. Zhao, "Orthogonal chirp division multiplexing," *IEEE Transactions on Communications*, vol. 64, no. 9, pp. 3946–3957, Sept. 2016.

[21] L. de M. B. A. Dib, G. R. Colen, M. de L. Filomeno, and M. V. Ribeiro, "Orthogonal chirp division multiplexing for baseband data communication systems," *IEEE Systems Journal*, vol. 14, no. 2, pp. 2164–2174, June 2020.

[22] L. G. de Oliveira, M. L. Filomeno, H. V. Poor, and M. V. Ribeiro, "Orthogonal chirp-division multiplexing for power line sensing via time-domain reflectometry," *IEEE Sensors Journal*, vol. 21, no. 2, pp. 955–964, Jan. 2021.

[23] L. G. de Oliveira, M. L. Filomeno, A. J. Han Vinck, and M. V. Ribeiro, "Resource allocation in HS-OFDM-based PLC systems: A tutorial," *Journal of Communication and Information Systems*, vol. 33, no. 1, pp. 308–321, 2018.

[24] J. M. Cioffi, *Chapter 4: Multi-channel modulation*, acessed in Oct. 2021. [Online]. Available: https://cioffi-group.stanford.edu/doc/book/chap4.pdf

[25] C. S. Park and K. B. Lee, "Transmit power allocation for BER performance improvement in multicarrier systems," *IEEE Transactions on Communications*, vol. 52, no. 10, pp. 1658–1663, Oct. 2004.

[26] G. R. Colen, L. G. de Oliveira, A. J. H. Vinck, and M. V. Ribeiro, "A spectral compressive resource allocation technique for PLC systems," *IEEE Transactions on Communications*, vol. 65, no. 2, pp. 816–826, Feb. 2017.

[27] T. M. Cover and J. A. Thomas, *Elements of Information Theory*. John Wiley & Sons, Nov. 2012.

[28] A. M. Sarafi, G. I. Tsiropoulos, and P. G. Cottis, "Hybrid wireless-broadband over power lines: A promising broadband solution in rural areas," *IEEE Communications Magazine*, vol. 47, no. 11, pp. 140–147, Nov. 2009.

[29] W. Gheth, K. M. Rabie, B. Adebisi, M. Ijaz, G. Harris, and A. Alfitouri, "Hybrid power-line/wireless communication systems for indoor applications," in *11th International Symposium on Communication Systems, Networks Digital Signal Processing*, July 2018, pp. 1–6.

[30] M. Kuhn, S. Berger, I. Hammerstrom, and A. Wittneben, "Power line enhanced cooperative wireless communications," *IEEE Journal on Selected Areas in Communications*, vol. 24, no. 7, pp. 1401–1410, July 2006.

[31] T. R. Oliveira, F. J. A. Andrade, A. M. Picorone, H. A. Latchman, S. L. Netto, and M. V. Ribeiro, "Characterization of hybrid communication channel in indoor scenario," *Journal of Communication and Information Systems*, vol. 31, no. 1, pp. 224–235, Dec. 2016.

[32] A. Camponogara, H. V. Poor, and M. V. Ribeiro, "PLC systems under the presence of a malicious wireless communication device: Physical layer security analyses," *IEEE Systems Journal*, vol. 14, no. 4, pp. 4901–4910, Dec. 2020.

[33] V. Fernandes, H. V. Poor, and M. V. Ribeiro, "Dedicated energy harvesting in concatenated hybrid PLC-wireless systems," *IEEE Transactions on Wireless Communications*, vol. 19, no. 6, pp. 3839–3853, June 2020.

[34] A. Camponogara and M. V. Ribeiro, "The effective secrecy throughput for the hybrid PLC/WLC wiretap channel: Analysis based on a measurement campaign," *Journal of Communication and Information Systems*, vol. 36, no. 1, pp. 44–51, Feb. 2021.

[35] V. Fernandes, W. A. Finamore, H. V. Poor, and M. V. Ribeiro, "The low-bit-rate hybrid power line/wireless single-relay channel," *IEEE Systems Journal*, vol. 13, no. 1, pp. 98–109, Mar. 2019.

[36] S. W. Lai and G. G. Messier, "Using the wireless and PLC channels for diversity," *IEEE Transactions on Communications*, vol. 60, no. 12, pp. 3865–3875, Dec. 2012.

[37] M. Sayed and N. Al-Dhahir, "Narrowband-PLC/wireless diversity for smart grid communications," in *IEEE Global Communications Conference*, Dec. 2014, pp. 2966–2971.

[38] S. W. Lai and G. G. Messier, "The wireless/power-line diversity channel," in *IEEE International Conference on Communications*, May 2010, pp. 1–5.

[39] R. M. Oliveira, L. G. de Oliveira, A. B. Vieira, and M. V. Ribeiro, "An enhanced cooperative MAC protocol for hybrid PLC/wireless systems," *Computer Networks*, vol. 163, pp. 145–154, Nov. 2019.

[40] *IEEE Standard for a Convergent Digital Home Network for Heterogeneous Technologies*, IEEE Std. 1905.1, 2013.

[41] M. Heggo, X. Zhu, Y. Huang, and S. Sun, "A hybrid power line and TV white space MIMO system for indoor broadband communications," in *IEEE 84th Vehicular Technology Conference*, Sept. 2016, pp. 1–5.

[42] M. Heggo, X. Zhu, S. Sumei, and Y. Huang, "White broadband power line communication: Exploiting the TVWS for indoor multimedia smart grid applications," *International Journal of Communication Systems*, vol. 30, no. 16, pp. 1–9, May 2017.

[43] M. Heggo, X. Zhu, S. Sun, and Y. Huang, "A cognitive TV white space-broadband power line MIMO system for indoor communication networks," *Journal of the Franklin Institute*, vol. 355, no. 11, pp. 4755–4770, July 2018.

[44] M. Heggo, S. Sun, X. Zhu, and Y. Huang, "TV white space regulated broadband power line communication for point-to-multipoint downlink IoT networks: A standard perspective," *IEEE Internet of Things Journal*, vol. 6, no. 4, pp. 6226–6236, Aug. 2019.

[45] M. Alaa, A. A. Zaidan, B. B. Zaidan, M. Talal, and M. L. M. Kiah, "A review of smart home applications based on internet of things," *Journal of Network and Computer Applications*, vol. 97, pp. 48–65, Nov. 2017.

[46] Y.-S. Sung, Y.-H. Kim, I. Sohn, S.-C. Kim, and J.-H. Lee, "Optimal subcarrier pairing for MRC in powerline/wireless diversity OFDM systems," *Electric Power Systems Research*, vol. 121, pp. 200–206, Apr. 2015.

[47] T. Schmidl and D. Cox, "Robust frequency and timing synchronization for OFDM," *IEEE Transactions on Communications*, vol. 45, no. 12, pp. 1613–1621, Dec. 1997.

[48] Y. Chen, J. K. Hwang, and S. M. Wu, "A reliable power line carrier and wireless data concentrator for broadband energy information network," *IEEE Transactions on Consumer Electronics*, vol. 49, no. 4, pp. 1054–1060, Nov. 2003.

[49] Y. Chen, J. K. Hwang, and W. L. Tseng, "A reliable power line carrier and wireless data concentrator for broadband energy information network," in *IEEE International Conference on Consumer Electronics*, June 2003, pp. 138–139.

[50] L. de M. B. A. Dib, V. Fernandes, and M. V. Ribeiro, "A discussion about hybrid PLC-wireless communication for smart grids," in *34th Brazilian Symposium on Telecommunications and Signal Processing*, Sept. 2016, pp. 848–852.

[51] S. W. Lai, N. Shabehpour, G. G. Messier, and L. Lampe, "Performance of wireless/power line media diversity in the office environment," in *IEEE Global Communications Conference*, Dec. 2014, pp. 2972–2976.

[52] J. Mafra, M. Hosami, L. Freitas, M. Martinelli, and A. Almeida, "Hybrid communication module - motivations, requirements, challenges and implementations," in *IEEE PES Innovative Smart Grid Technologies Latin America*, Oct. 2015, pp. 25–29.

[53] V. L. R. da Costa, V. Fernandes, and M. V. Ribeiro, "Narrowband hybrid PLC/wireless: Transceiver prototype, hardware resource usage and energy consumption," *Ad Hoc Networks*, vol. 94, p. 101945, Nov. 2019.

[54] P. Kiedrowski, B. Boryna, and T. Marciniak, "Last-mile smart grid communications based on hybrid technology as a reliable method of data acquisition and distribution," *Rynek Energii*, no. 104, pp. 127–132, Jan. 2013.

[55] J. Lee and Y. Kim, "Diversity relaying for parallel use of power-line and wireless communication networks," *IEEE Transactions on Power Delivery*, vol. 29, no. 3, pp. 1301–1310, June 2014.

[56] M. Sayed, A. E. Shafie, M. Elgenedy, R. C. Chabaan, and N. Al-Dhahir, "Enhancing the reliability of two-way vehicle-to-grid communications," in *IEEE Intelligent Vehicles Symposium*, June 2017, pp. 1922–1927.

[57] F. N. Igboamalu, A. R. Ndjiongue, and H. C. Ferreira, "PLC-RF diversity: Channel outage analysis," *Telecommunication Systems*, vol. 73, pp. 521–530, 2020.

[58] S. Guzelgo, H. B. Celebi, and H. Arsian, "Analysis of a multi-channel receiver: Wireless and PLC reception," in *European Signal Processing Conference*, Aug. 2010, pp. 1106–1110.

[59] G. Sebaali and B. L. Evans, "Design tradeoffs in joint powerline and wireless transmission for smart grid communications," in *IEEE International Symposium on Power Line Communications and Its Applications*, Mar. 2015, pp. 83–88.

[60] V. Fernandes, M. L. Filomeno, W. A. Finamore, and M. V. Ribeiro, "An investigation on narrow band PLC-wireless parallel channel capacity," in *34th Brazilian Symposium on Telecommunications and Signal Processing*, Sept. 2016, pp. 834–838.

[61] N. Agrawal and P. K. Sharma, "Outage analysis of selection combining based hybrid wireless PLC system," in *9th International Conference on Computing, Communication and Networking Technologies*, July 2018, pp. 1–5.

[62] M. Sayed, T. A. Tsiftsis, and N. Al-Dhahir, "On the diversity of hybrid narrowband-PLC/wireless communications for smart grids," *IEEE Transactions on Wireless Communications*, vol. 16, no. 7, pp. 4344–4360, July 2017.

[63] M. Sayed, G. Sebaali, B. L. Evans, and N. Al-Dhahir, "Efficient diversity technique for hybrid narrowband-powerline/wireless smart grid communications," in *IEEE International Conference on Smart Grid Communications*, Nov. 2015, pp. 1–6.

[64] M. Sayed and N. Al-Dhahir, "Differential modulation diversity combining for hybrid narrowband-powerline/wireless smart grid communications," in *IEEE Global Conference on Signal and Information Processing*, 2016, pp. 876–880.

[65] D. Middleton, "Statistical-physical models of electromagnetic interference," *IEEE Transactions on Electromagnetic Compatibility*, vol. EMC-19, no. 3, pp. 106–127, Aug. 1977.

[66] M. Mokhtar, W. U. Bajwa, and N. Al-Dhahir, "Sparsity-aware joint narrowband interference and impulse noise mitigation for hybrid powerline-wireless transmission," in *IEEE Wireless Communications and Networking Conference*, Mar. 2015, pp. 615–620.

[67] M. Mokhtar, W. U. Bajwa, M. Elgenedy, and N. Al-Dhahir, "Exploiting block sparsity for joint mitigation of asynchronous NBI and IN in hybrid powerline-wireless communications," in *IEEE International Conference on Smart Grid Communications*, Nov. 2015, pp. 362–367.

[68] M. Elgenedy, M. M. Awadin, R. Hamila, W. U. Bajwa, A. S. Ibrahim, and N. Al-Dhahir, "Sparsity-based joint NBI and impulse noise mitigation in hybrid PLC-wireless transmissions," *IEEE Access*, vol. 6, pp. 30 280–30 295, May 2018.

[69] T. Sung and A. Bojanczyk, "Optimal power control and relay capacity for PLC-embedded cooperative systems," in *IEEE Consumer Communications and Networking Conference*, Jan. 2010, pp. 1–5.

[70] Y. Qian, J. Yan, H. Guan, J. Li, X. Zhou, S. Guo, and D. N. K. Jayakody, "Design of hybrid wireless and power line sensor networks with dual-interface relay in IoT," *IEEE Internet of Things Journal*, vol. 6, no. 1, pp. 239–249, Feb. 2019.

[71] V. Fernandes, H. V. Poor, and M. V. Ribeiro, "Analyses of the incomplete low-bit-rate hybrid PLC-wireless single-relay channel," *IEEE Internet of Things Journal*, vol. 5, no. 2, pp. 917–929, Apr. 2018.

[72] S. P. Dash and S. Joshi, "Cooperative device-to-device relaying network with power line communications," in *IEEE Vehicular Technology Conference*, Sept. 2019, pp. 1–5.

[73] Z. Li, Q. Liang, J. Mu, W. Wang, and B. Zhang, "The hybrid architecture of wireless and power line communications in HANs for smart grid security," *Security and Communication Networks*, vol. 8, no. 14, pp. 2404–2410, Mar. 2015.

[74] A. Camponogara, H. V. Poor, and M. V. Ribeiro, "The complete and incomplete low-bit-rate hybrid PLC/wireless channel models: Physical layer security analyses," *IEEE Internet of Things Journal*, vol. 6, no. 2, pp. 2760–2769, Apr. 2019.

[75] A. Salem, K. A. Hamdi, and E. Alsusa, "Physical layer security over correlated log-normal cooperative power line communication channels," *IEEE Access*, vol. 5, pp. 13 909–13 921, 2017.

[76] A. El Shafie, M. F. Marzban, R. Chabaan, and N. Al-Dhahir, "An artificial-noise-aided secure scheme for hybrid parallel PLC/wireless OFDM systems," in *IEEE International Conference on Communications*, May 2018, pp. 1–6.

[77] V. Fernandes, H. V. Poor, and M. V. Ribeiro, "A hybrid power line/wireless dual-hop system with energy harvesting relay," *IEEE Internet of Things Journal*, vol. 5, no. 5, pp. 4201–4211, Oct. 2018.

[78] M. Zimmermann and K. Dostert, "A multipath model for the powerline channel," *IEEE Transactions on Communications*, vol. 50, no. 4, pp. 553–559, Apr. 2002.

[79] L. Yonge, J. Abad, K. Afkhamie, L. Guerrieri, S. Katar, H. Lioe, P. Pagani, R. Riva, D. M. Schneider, and A. Schwager, "An overview of the HomePlug AV2 technology," *Journal of Electrical and Computer Engineering*, pp. 1–20, 2013.

[80] F. J. C. Corripio, J. A. C. Arrabal, L. D. del Rio, and J. T. E. Munoz, "Analysis of the cyclic short-term variation of indoor power line channels," *IEEE Journal on Selected Areas in Communications*, vol. 24, no. 7, pp. 1327–1338, July 2006.

[81] G. R. Colen, H. Schettino, D. Fernandes, L. M. Sirimarco, F. P. V. de Campos, W. A. Finamore, H. A. Latchman, and M. V. Ribeiro, "A temporal compressive resource allocation technique for complexity reduction in PLC transceivers," *Transactions on Emerging Telecommunications Technologies*, vol. 28, no. 2, pp. 1–12, 2017.

[82] Anonymous, "Minutes of the philadelphia meeting december 28, 29, 30, 1926," *Physical Review*, vol. 29, pp. 350–373, Feb. 1927.

[83] J. B. Johnson, *Physical Review*, vol. 32, pp. 97–109, July 1928.

[84] H. Nyquist, "Thermal agitation of electric charge in conductors," *Physical Review*, vol. 32, pp. 110–113, Jul 1928.

[85] M. Zimmermann and K. Dostert, "Analysis and modeling of impulsive noise in broadband powerline communications," *IEEE Transactions on Electromagnetic Compatibility*, vol. 44, no. 1, pp. 249–258, Feb. 2002.

[86] T. Bai, H. Zhang, J. Wang, C. Xu, M. Elkashlan, A. Nallanathan, and L. Hanzo, "Fifty years of noise modeling and mitigation in power-line communications," *IEEE Communications Surveys & Tutorials*, vol. 23, no. 1, pp. 41–69, Firstquarter 2021.

[87] H. Meng, Y. L. Guan, and S. Chen, "Modeling and analysis of noise effects on broadband power-line communications," *IEEE Transactions on Power Delivery*, vol. 20, no. 2, pp. 630–637, Apr. 2005.

[88] A. ElSamadouny, A. El Shafie, M. Abdallah, and N. Al-Dhahir, "Secure sum-rate-optimal MIMO multicasting over medium-voltage NB-PLC networks," *IEEE Transactions on Smart Grid*, vol. 9, no. 4, pp. 2954–2963, July 2018.

[89] G. R. Colen, L. G. de Oliveira, C. B. Zeller, A. J. Han Vinck, and M. V. Ribeiro, "Statistical analysis and modeling of a novel parameter for resource allocation in multicarrier PLC systems," *Transactions on Emerging Telecommunications Technologies*, vol. 28, no. 11, pp. 1–12, 2017.

[90] S. K. Mitra, *Digital Signal Processing: A Computer Based Approach*, 4th ed. USA: McGraw-Hill, Inc., 2010.

[91] R. D. Yates and D. J. Goodman, *Probability and stochastic processes: A friendly introduction for electrical and computer engineers*. John Wiley & Sons, 2014.

[92] S. Boyd and L. Vandenberghe, *Convex Optimization*. New York, NY, USA: Cambridge University Press, 2004.

[93] J. Campello, "Practical bit loading for DMT," in *IEEE International Conference on Communications*, vol. 2, June 1999, pp. 801–805.

[94] *Wireless LAN Medium Access Control (MAC) and Physical Layer (PHY) Specifications*, IEEE Std. 802.11ac, 2013.

[95] T. R. Oliveira, A. A. M. Picorone, S. L. Netto, and M. V. Ribeiro, "Characterization of brazilian in-home power line channels for data communication," *Electric Power Systems Research*, vol. 150, pp. 188–197, Sept. 2017.

[96] R. H. Byrd, J. C. Gilbert, and J. Nocedal, "A trust region method based on interior point techniques for nonlinear programming," *Mathematical Programming*, vol. 89, no. 1, pp. 149–185, Nov. 2000.

[97] A. F. Molisch *et al.*, "IEEE 802.15.4a channel model - final report," IEEE 802.15 WPAN Low Rate Alternative PHY Task Group, Tech. Rep., Nov. 2004.

[98] A. Goldsmith, *Wireless Communications*. Cambridge University Press, 2005.

[99] F. A. Potra and S. J. Wright, "Interior-point methods," *Journal of Computational and Applied Mathematics*, vol. 124, no. 1, pp. 281–302, Dec. 2000.

[100] J. Proakis and M. Salehi, *Digital Communications*, 5th ed. New York, USA: McGraw-Hill, 2008.

[101] Y.-S. Sung, J.-H. Lee, Y.-H. Kim, and S.-C. Kim, "Optimal subcarrier pairing scheme for maximal ratio combining in OFDM power line communications," *International Journal of Electronics and Communications*, vol. 68, no. 9, pp. 893–898, Sept. 2014.

[102] T. H. Cormen, C. E. Leiserson, R. L. Rivest, and C. Stein, *Introduction to Algorithms*, 2nd ed. Cambridge, MA: MIT Press, 2001.

[103] X. Ouyang, O. A. Dobre, Y. L. Guan, and J. Zhao, "Chirp spread spectrum toward the Nyquist signaling rate – orthogonality condition and applications," *IEEE Signal Processing Letters*, vol. 24, no. 10, pp. 1488–1492, Oct. 2017.

[104] R. Bomfin, M. Chafii, and G. Fettweis, "Low-complexity iterative receiver for orthogonal chirp division multiplexing," in *IEEE Wireless Communications and Networking Conference Workshop*, Apr. 2019, pp. 1–6.

[105] P. Zhu, X. Xu, X. Tu, Y. Chen, and Y. Tao, "Anti-multipath orthogonal chirp division multiplexing for underwater acoustic communication," *IEEE Access*, vol. 8, pp. 13 305–13 314, Jan. 2020.

[106] M. S. Omar and X. Ma, "Performance analysis of OCDM for wireless communications," *IEEE Transactions on Wireless Communications*, vol. 20, no. 7, pp. 4032–4043, July 2021.

[107] M. S. Omar and X. Ma, "The effects of narrowband interference on OCDM," in *IEEE 21st International Workshop on Signal Processing Advances in Wireless Communications*, 2020, pp. 1–5.

[108] L. G. de Oliveira, M. B. Alabd, B. Nuss, and T. Zwick, "An OCDM radar-communication system," in *14th European Conference on Antennas and Propagation*, Mar. 2020, pp. 1–5.

[109] L. G. de Oliveira, B. Nuss, M. B. Alabd, Y. Li, L. Yu, and T. Zwick, "MIMO-OCDM-based joint radar sensing and communication," in *15th European Conference on Antennas and Propagation*, Mar. 2021, pp. 1–5.

[110] T. F. Moreira, A. Camponogara, S. Baig, and M. V. Ribeiro, "Data rate and bit error probability in narrowband PLC systems: OCDM versus HS-OFDM," in *39th Brazilian Symposium on Telecommunications and Signal Processing*, Sept. 2021, pp. 1–5.

[111] L. Giroto de Oliveira, B. Nuss, M. B. Alabd, A. Diewald, M. Pauli, and T. Zwick, "Joint radar-communication systems: Modulation schemes and system design," *IEEE Transactions on Microwave Theory and Techniques*, vol. 70, no. 3, pp. 1521–1551, 2022.

[112] L. G. de Oliveira, M. de L. Filomeno, H. V. Poor, and M. V. Ribeiro, "Orthogonal chirp-division multiplexing for power line sensing via time-domain reflectometry," *IEEE Sensors Journal*, vol. 21, no. 2, pp. 955–964, Jan. 2021.

[113] Y. Wang, Z. Shi, X. Ma, and L. Liu, "A joint sonar-communication system based on multicarrier waveforms," *IEEE Signal Processing Letters*, vol. 29, pp. 777–781, 2022.

[114] E. P. Adams and R. L. Hippisley, *Smithsonian mathematical formulae and tables of elliptic functions*. Smithsonian Institution, 1922.

[115] X. Ouyang, C. Antony, F. Gunning, H. Zhang, and Y. L. Guan, "Discrete fresnel transform and its circular convolution," 2015, acessed on: https://arxiv.org/abs/1510.00574.

[116] M. S. Omar and X. Ma, "Spectrum design for orthogonal chirp division multiplexing transmissions," *IEEE Wireless Communications Letters*, vol. 9, no. 11, pp. 1990–1994, Nov. 2020.

[117] X. Ouyang, O. A. Dobre, and J. Zhao, "Unbiased channel estimation based on the discrete fresnel transform for CO-OFDM systems," *IEEE Photonics Technology Letters*, vol. 29, no. 8, pp. 691–694, Apr. 2017.

[118] X. Ouyang, C. Antony, G. Talli, and P. D. Townsend, "Robust channel estimation for coherent optical orthogonal chirp-division multiplexing with pulse compression and noise rejection," *Journal of Lightwave Technology*, vol. 36, no. 23, pp. 5600–5610, Dec. 2018.

[119] R. Zhang, Y. Wang, and X. Ma, "Channel estimation for OCDM transmissions with carrier frequency offset," *IEEE Wireless Communications Letters*, vol. 11, no. 3, pp. 483–487, 2022.

[120] A. Diewald, C. Kurz, P. V. Kannan, M. Giessler, M. Pauli, B. Göttel, T. Kayser, F. Gauterin, and T. Zwick, "Radar target simulation for vehicle-in-the-loop testing," *Vehicles*, vol. 3, no. 2, pp. 257–271, May 2021.

[121] Y. L. Sit, B. Nuss, and T. Zwick, "On mutual interference cancellation in a mimo ofdm multiuser radar-communication network," *IEEE Transactions on Vehicular Technology*, vol. 67, no. 4, pp. 3339–3348, Apr. 2018.

[122] C. Sturm and W. Wiesbeck, "Waveform design and signal processing aspects for fusion of wireless communications and radar sensing," *Proceedings of the IEEE*, vol. 99, no. 7, pp. 1236–1259, July 2011.

APPENDIX A – Waterfilling Algorithm

This appendix briefly describes Algorithm #5, which performs optimal power allocation for maximizing the achievable data rate in a single channel with the waterfilling technique [24]. This algorithm also returns the *Lagrange* multiplier, which is understood as the inverse of the water level.

Algorithm #5: Waterfilling algorithm

Input :

$\overline{\gamma}_k$ is the nSNR for the k^{th} subchannel, $\forall k \in \{1, 2, \ldots, N_{\text{S}}\}$

P_{T} is the total transmission power

Output :

p_k is the power allocated to the k^{th} subchannel, $\forall k \in \{1, 2, \ldots, N_{\text{S}}\}$

λ is the *Lagrange* multiplier

Function $[\{p_k\}, \lambda] = \text{waterfilling}(\{\overline{\gamma}_k\}, P_{\text{T}})$

$C = \{1, 2, \ldots, N_{\text{S}}\}$;

$\text{c} \in C$;

$\Delta = P_{\text{T}} + \sum_{C} \overline{\gamma}_{\text{c}}^{-1}$;

$\lambda = \text{Card}\{C\}/\Delta$;

$q = \arg\min_{C}\{\overline{\gamma}_{\text{c}}\}$;

while $\lambda^{-1} - \overline{\gamma}_q^{-1} < 0$ **do**

$C = C - q$;

$\text{c} \in C$;

$\Delta = P_{\text{T}} + \sum_{C} \overline{\gamma}_{\text{c}}^{-1}$;

$\lambda = \text{Card}\{C\}/\Delta$;

$q = \arg\min_{C}\{\overline{\gamma}_{\text{c}}\}$;

end

$p_k = \max\{\lambda^{-1} - \overline{\gamma}_k^{-1}, 0\}, \forall k \in \{1, 2, \ldots, N_{\text{S}}\}$;

APPENDIX B – Park's Algorithm

This appendix briefly describes Algorithm #6, or Park's algorithm [25], which performs optimal power allocation for minimizing the average bit error probability in a single channel considering any M-ary square QAM. This algorithm also returns the *Lagrange* multiplier.

Algorithm #6: Park algorithm

Input :

$\overline{\gamma}_k$ is the nSNR for the k^{th} subchannel, $\forall k \in \{1, 2, \ldots, N_{\text{S}}\}$

P_{T} is the total transmission power

Mod is the coherent modulation

M is the modulation order

Output :

p_k is the power allocated to the k^{th} subchannel, $\forall k \in \{1, 2, \ldots, N_{\text{S}}\}$

λ is the *Lagrange* multiplier

Function $[\{p_k\}, \lambda] = \text{ParkAlgorithm}(\{\overline{\gamma}_k\}, P_{\text{T}}, Mod, M)$

$C = \{1, 2, \ldots, N_{\text{S}}\}$;

$\text{c} \in C$;

Compute a_M and b_M from Mod and M;

$\lambda_o = \left(P_{\text{T}} - \frac{2}{b_M} \sum_{C} \frac{\ln(\overline{\gamma}_{\text{c}})}{\overline{\gamma}_{\text{c}}}\right) / \sum_{C} \overline{\gamma}_{\text{c}}^{-1}$;

while $e^{-b_M \lambda_o / 2} \geq \min_{C}\{\overline{\gamma}_c\}$ **do**

$\lambda_o = \left(P_{\text{T}} - \frac{2}{b_M} \sum_{C} \frac{\ln(\overline{\gamma}_{\text{c}})}{\overline{\gamma}_{\text{c}}}\right) / \sum_{C} \overline{\gamma}_{\text{c}}^{-1}$;

$q = \arg\min_{C}\{\overline{\gamma}_{\text{c}}\}$;

$C = C - q$;

$\text{c} \in C$;

end

$d_k = \frac{\lambda_o}{\overline{\gamma}_k} + \frac{2}{b_M \overline{\gamma}_k} \ln(\overline{\gamma}_k), \forall k \in \{1, 2, \ldots, N_{\text{S}}\}$;

$p_k = \max\{d_k, 0\}, \forall k \in \{1, 2, \ldots, N_{\text{S}}\}$;

$\lambda = \frac{a_M b_M}{4 N_{\text{S}}} e^{-b_M \lambda_o / 2}$;

APPENDIX C – Minimization of the Sum of Products

Let $\{a_1, a_2, \ldots, a_{N_S}\}$ and $\{b_1, b_2, \ldots, b_{N_S}\}$ be two independent sets, such that $a_k, b_k \in \mathbb{R}$, $\forall k \in \{1, 2, \ldots, N_S\}$. Based on these sets, the summation of the products with permutation allowed can be defined as

$$\sum_k a_k \cdot b_{c_k}, \tag{C.1}$$

with $c_k \in \{1, 2, \ldots, N_S\}$, and $c_1 \neq c_2 \neq \ldots \neq c_{N_S}$. It is desired to obtain the permutation, defined by c_k, that minimizes (C.1).

In order to find the optimal solution, let (C.1) be rewritten as

$$a_i \cdot b_{c_i} + a_j \cdot b_{c_j} + \sum_{k \neq i,j} a_k \cdot b_{c_k}, \tag{C.2}$$

with $i, j \in \{1, 2, \ldots, N_S\}$ and $i \neq j$. Notice that the optimal solution is the one in which any pair of (a_i, b_{c_i}) and (a_j, b_{c_j}) chosen from the original sets yields the lowest possible value, by taken its permutation into account. Mathematically, it means that

$$a_i \cdot b_{c_i} + a_j \cdot b_{c_j} \leq a_i \cdot b_{c_j} + a_j \cdot b_{c_i}. \tag{C.3}$$

By assuming that $a_i \geq a_j$ without loss of generality, one can obtain

$$\begin{aligned} a_i \cdot b_{c_i} + a_j \cdot b_{c_j} &\leq a_i \cdot b_{c_j} + a_j \cdot b_{c_i} \Leftrightarrow & \text{(C.4)} \\ \Leftrightarrow a_i(b_{c_i} - b_{c_j}) &\leq a_j(b_{c_i} - b_{c_j}) \Leftrightarrow & \text{(C.5)} \\ \Leftrightarrow b_{c_i} &\leq b_{c_j}. & \text{(C.6)} \end{aligned}$$

Therefore, if $a_i \geq a_j$, then one should have $b_{c_i} \leq b_{c_j}$ for the sum of the products to be the lowest possible. Moreover, for minimizing (C.1), this condition should be valid for any two pairs taken at a time and, as a consequence, one obtains that the minimum summation is achieved with $b_{c_1} \leq b_{c_2} \leq \ldots \leq b_{c_{N_S}}$ as $a_1 \geq a_2 \geq \ldots \geq a_{N_S}$.

APPENDIX D – List of Publications

The list of papers related to the dissertation published or submitted during the doctoral period is as follows:

- **M. de L. Filomeno**, M. L. R. de Campos, H. V. Poor, and M. V. Ribeiro, "Hybrid power line/wireless systems: an optimal power allocation perspective," *IEEE Transactions on Wireless Communications*, vol. 19, no. 10, pp. 6289-6300, Oct. 2020.

- **M. de L. Filomeno**, M. L. R. de Campos, H. V. Poor, and M. V. Ribeiro, "Hybrid power line/wireless systems: Power allocation for minimizing the average bit error probability," *IEEE Transactions on Communications*, vol. 70, no. 2, pp. 810-821, Feb. 2022.

- **M. de L. Filomeno**, V. J. E. Lima, M. L. R. de Campos, H. V. Poor, and M. V. Ribeiro, "Hybrid power line/wireless systems with optimal subcarrier permutation under uniform or optimal power allocation," *IEEE Internet of Things Journal*, July 2022, early access, doi: 10.1109/JIOT.2022.3188703 .

- **M. de L. Filomeno**, L. G. de Oliveira, Â. Camponogara, A. Diewald, T. Zwick, M. L. R. de Campos, and M. V. Ribeiro, "Joint channel estimation and Schmidl & Cox synchronization for OCDM-based systems," *IEEE Communications Letters*, vol. 26, no. 8, pp. 1878-1882, Aug. 2022.

- **M. de L. Filomeno**, T. F. Moreira, Y. F. Coutinho, Â. Camponogara, M. L. R. de Campos, and M. V. Ribeiro, "Orthogonal chirp-division multiplexing-based hybrid power line/wireless system," in *IEEE Global Communications Conference (GLOBECOM)*, 2022, pp. 1-6.

- **M. de L. Filomeno**, L. G. de Oliveira, Â. Camponogara, T. Zwick, M. L. R. de Campos, and M. V. Ribeiro, "Wide-sense stationary random processes in the discrete-Fresnel domain," Under review.

- M. V. Ribeiro, **M. de L. Filomeno**, Â. Camponogara, T. R. Oliveira, S. Galli, and H. V. Poor, "The synergy between power line and wireless media for empowering connectivity among machines," Under review.

The list of papers non-related to the dissertation published or submitted during the doctoral period is as follows:

- Â. Camponogara, **M. de L. Filomeno**, T. R. Oliveira, L. G. de Oliveira, T. F. A. Nogueira, A. A. M. Picorone, S. A. Souza, and M. V. Ribeiro, "Measurement and characterization of a MV distribution network for data communication," in *Brazilian Symposium on Telecommunications and Signal Processing*, Oct. 2019, pp. 1-6.

- L. de M. B. A. Dib, G. R. Colen, **M. de L. Filomeno**, and M. V. Ribeiro, "Orthogonal chirp division multiplexing for baseband data communication systems," *IEEE Systems Journal*, vol. 14, no. 2, pp. 2164-2174, June 2020.

- L. G. de Oliveira, **M. de L. Filomeno**, H. V. Poor, and M. V. Ribeiro, "Orthogonal chirp-division multiplexing for power line sensing via time-domain reflectometry," *IEEE Sensors Journal*, vol. 21, no. 2, pp. 955-964, Jan. 2021.

- T. F. do A. Nogueira, T. R. Oliveira, A. A. M. Picorone, **M. de L. Filomeno**, Â. Camponogara, A. C. S. Lima, and M. V. Ribeiro, "Measurement campaign of rural overhead MV power distribution networks for PLC systems," in *Brazilian Symposium on Telecommunications and Signal Processing*, Sept. 2021, pp. 1-6.

- V. J. E. de Lima, **M. de L. Filomeno**, Â. Camponogara, and M. V. Ribeiro, "Um símbolo no domínio de Fresnel para utilização de *Schmidl & Cox* em esquemas OCDM," in *Brazilian Symposium on Telecommunications and Signal Processing*, Sept. 2021, pp. 1-2.

- L. G. de Oliveira, **M. de L. Filomeno**, L. F. Colla, H. V. Poor, and M. V. Ribeiro, "Analysis of typical PLC pulses for sensing high-impedance faults based on time-domain reflectometry," *International Journal of Electrical Power & Energy Systems*, vol. 135, p. 107168, Feb. 2022.

- L. G. de Oliveira, **M. de L. Filomeno**, H. V. Poor, and M. V. Ribeiro, "Fault detection and location in power distribution systems: The usefulness of the HS-OFDM scheme for time-domain reflectometry," *Electric Power Systems Research*, vol. 203, p. 107600, Feb. 2022.

- T. F. A. Nogueira, T. R. Oliveira, A. A. M. Picorone, Â. Camponogara, **M. de L. Filomeno**, and M. V. Ribeiro, "Inductive coupling-based narrowband PLC system for MV power distribution networks: New insights," Submitted to *International Journal of Electrical Power & Energy Systems* (second round of review).